Fuel 404 (2026) 136401

Contents lists available at ScienceDirect

Fuel

journal homepage: www.elsevier.com/locate/fuel

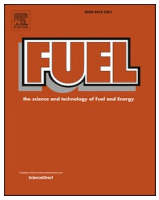

Review article

Computational fluid dynamics (CFD) modelling as a power multiplier tool for the design improvement of gaseous and liquid fuels: current status, challenges and perspectives

Eleana Harkou [a,1], Panayiota Adamou [a,1], S.M. Al-Salem [b], Nikol Atanasova [a], Junwang Tang [c,d,e], George Manos [c], Alberto Villa [f], Nikolaos Dimitratos [g,h,*], Achilleas Constantinou [a,*]

[a] Department of Chemical Engineering, Cyprus University of Technology, 57 Corner of Athinon and Anexartisias, 3036 Limassol, Cyprus
[b] Environment and Life Sciences Research Centre, Kuwait Institute for Scientific Research, Safat 13109, Kuwait
[c] Department of Chemical Engineering, University College London (UCL), WC1E 7JE London, United Kingdom
[d] Industrial Catalysis Centre, Department of Chemical Engineering, Tsinghua University, Beijing 100084, China
[e] Ordos Laboratory, Inner Mongolia 017000, China
[f] Dipartimento di Chimica, Universitá degli Studi di Milano, via Golgi, 20133 Milan, Italy
[g] Department of Industrial Chemistry "Toso Montanari", University of Bologna, viale Risorgimento 4, 40136 Bologna, Italy
[h] Center for Chemical Catalysis – C3, University of Bologna, viale Risorgimento 4, 40136 Bologna, Italy

ARTICLE INFO

Keywords:
CFD
Fuels
H_2
CO_2 hydrogenation
Reactor design

ABSTRACT

Climate change and global warming are urgent concerns, prompting the scientific community to focus on achieving net-zero greenhouse gas (GHG) emissions primarily through renewable energy sources. Carbon capture and utilisation (CCU) technology offers a practical solution by converting carbon dioxide (CO_2) into usable chemicals and fuels, while hydrogen (H_2) presents a highly efficient, zero-emission fuel alternative, despite challenges in its production and storage. The processes for generating these fuels differ, necessitating specific system conditions for each. Computational tools, especially computational fluid dynamics (CFD), have become vital for optimizing these processes. Central to CFD models are kinetic equations that describe the conversion of feedstock and the generation of products. This review discusses the reaction pathways for gaseous and liquid fuel production, along with the proposed kinetic rate equations from existing literature. Additionally, it emphasises the significance of accounting for various factors in CFD models, including catalyst deactivation and competitive reactions, to maintain selectivity for desired products. Accurate physical representations are also crucial for modelling fluid flow, mixing, and heat transport, improving reactor design, optimisation, and scaling processes effectively compared to traditional experiments. The presentation of governing equations varies based on reactor types and flow systems. Ultimately, CFD not only validates experimental results but also aids in discovering optimal reactor designs and parameters for enhanced efficiency and product yields. Its ongoing advancement in predictive modelling and optimization marks it as an essential tool in contemporary research and industrial sectors focused on sustainable fuel production.

1. Introduction

The burning of fossil fuels for different applications and modern technologies concurs to the extensive production of greenhouse gas (GHG) emissions. The increase of the concentration of carbon dioxide (CO_2) and other GHGs are contributing to the global warming and environmental crisis with significant effects to the climate that are more obvious each year. The continuation of emissions of GHGs to the

* Corresponding authors at: Department of Industrial Chemistry "Toso Montanari", University of Bologna, viale Risorgimento 4, 40136 Bologna, Italy. Center for Chemical Catalysis - C3, University of Bologna, viale Risorgimento 4, 40136 Bologna, Italy (N. Dimitratos). Department of Chemical Engineering, Cyprus University of Technology, 57 Corner of Athinon and Anexartisias, 3036 Limassol, Cyprus (A. Constantinou).
E-mail addresses: nikolaos.dimitratos@unibo.it (N. Dimitratos), a.konstantinou@cut.ac.cy (A. Constantinou).
[1] These authors share first authorship.

https://doi.org/10.1016/j.fuel.2025.136401
Received 30 May 2025; Received in revised form 16 July 2025; Accepted 26 July 2025
Available online 31 July 2025
0016-2361/© 2025 The Authors. Published by Elsevier Ltd. This is an open access article under the CC BY-NC-ND license (http://creativecommons.org/licenses/by-nc-nd/4.0/).

atmosphere, CO_2 will triple from the pre-industrial levels by the year 2100 [1]. A critical target implementing new technologies to stabilise the global mean temperature between 1.5 and 2 °C relative to the pre-industrial era by end of this century has been set. To achieve the goal, the global yearly emissions should be net-negative or net-zero [2,3]. To cope with the great energy demand and the depleting of energy sources, the emphasis has shifted towards the renewable energy sources (RES) and greener alternative sources of gaseous and liquid fuels.

In order to decongest the atmosphere from emissions and mitigate the climate change the capture and catalytic conversion of CO_2 emissions through the carbon capture and utilisation (CCU) technology, to gaseous and liquid fuels is promising [4]. Possible utilisation pathways of CO_2 include not only the synthesis of fuels but also, chemicals and materials. Some of the most common products are methane (CH_4), methanol (MeOH), dimethyl ether (DME), formic acid (HCOOH, FA), ammonia (NH_3), polyurethanes, carbonates, higher hydrocarbons and alcohols. The CCU is indeed a rising technology which is still facing particular issues in terms of products selectivity, catalyst activity and stability while the energy consumption and the economic feasibility of the process are also contributing to development of the process in commercial level. The nature of generated products plays a vital role on the emissions from their consumption as in many cases the product can only delay the CO_2 emissions in the atmosphere [5]. In addition, the hydrogen (H_2) industry is producing and consuming about 60 million tons with the feedstock coming from gas, oil and coal through the steam reforming and partial oxidation reaction processes [6]. H_2 is an emission free fuel that has gained the interest of many the recent years, for the higher efficiency prospects of H_2 in comparison to gasoline. The domestic production and the development of fuel cells are some of the potential uses, although, the challenge of its production and storage in pure form is still a major factor [7]. Also, beyond its utilisation in applications as a fuel, it is required in order to perform the CO_2 hydrogenation reactions. The electrolysis of water for green H_2 production, as an alternative scenario is a more expensive route when compared to the production of H_2 from natural gas [6]. However, the storage of H_2 is another issue, as in liquid form, large amounts of energy are required. Therefore, H_2 energy carriers such as liquid organic hydrogen carriers (LOHCs), metal–organic frameworks (MOFs), hydrides and NH_3 can be involved as an intermediate step for the storage of H_2 [8,9].

With the increasing of the complexity of existing and new processes and the cost of manufacturing and operation of developing technologies, the advanced computational modelling tools with an exponentially increasing on the computational capabilities are contributing to the new developments in the field of research. The lower time and cost, are some of the advantages of the computational tools, when compared to carrying out the processes in the lab, while they offer a deeper understanding according to underlying physics and the opportunity for optimisation [10]. Computational fluid dynamics (CFD) modelling coupling all the governing equations, boundary conditions and kinetics can display a wider insight of all the phenomena occurring inside the system that would be very difficult to obtain experimentally. Such phenomena include the reaction efficiency, mass and heat limitations, system configuration limitations, mixing and/or flow behaviour etc. Moreover, CFD modelling could predict the performance of the design system under different operating conditions (temperature, pressure, velocity, mass of the catalyst etc), reactor configurations, feedstock and chemical reactions with ease without carrying out experiments that require consumables, equipment, space and time to perform the studies. The accuracy of the simulated results can be determined by the accuracy of the model and hence the dimensions of the designed model that can vary from one-dimensional (1D), two-dimensional (2D) and three-dimensional (3D). In literature, most of the numerical studies regarding catalytic reactions in reactor units use 1D and 2D models, though 2D models assume axial symmetry. 3D models are the most realistic, but they require the most computing resources [11]. Moreover, in many different studies 1D models are preferred especially in batch reactor simulations as there are no spatial variations of flow, temperature and concentration. In a study of Leonzio and Foscolo [12], a comparison was conducted between 1D and 2D models regarding the CO_2 hydrogenation reaction towards MeOH in a packed bed reactor. The results indicated that both models showed good agreement between them, however the 2D model was evidently more practical for simulating with accuracy the structured packed bed reactor as it can provide important information considering the radial direction.

In the recent years, reviews implementing CFD studies have been published considering the H_2 production from various feedstocks considering safety issues during the production, storage, transport and utilisation chain as well as the investigation regarding the reactor design set-up of the process which provides insightful information for optimisation and validation [10,13,14,15]. Additionally, there is an extensive discussion in literature considering the catalyst advancements and development and mechanistic understanding for both CO_2 hydrogenation and H_2 generation from energy carrier molecules [16,17,18,19,20,21,22]. At the same time, literature reviews are found to focus mainly on the hydrogenation towards MeOH [23,24,25,26,27], while only few provide insightful information from techno-economic and energy analyses [28,29,30]. However, it was observed the lack of completed published surveys in literature, that are focusing in-depth on the CFD modelling and are presenting not only the theoretical investigations, but also indicate the significance of CFD, the equations and kinetics that are implemented in the model development as well as the possibility and opportunity to assess completely different reactor set-ups. Hence, we present a CFD review considering the generation of gaseous and liquid fuels from CO_2 hydrogenation and H_2-storage molecules focusing on validation, optimisation and recent progress. Through the discussion of various investigations, the importance of simulation modelling is highlighted as well as their excelling performance compared to the effort that needs to be put for experiments.

In this work, the focus is to review CFD simulations to produce gas and liquid fuels in different reaction systems including all pathways of processes with the kinetic models and governing equations that are required to be considered in the model development. Moreover, the contribution of the process optimisation emphasising on investigated factors affecting the performance of production rates will be described and how the optimisation has given a practical solution. An in-depth discussion of the different reactor units used for carrying out the simulations will be made as well as future directions will be highlighted and discussed.

2. Production pathways and kinetic mechanisms

The origin and production process of alternative gas and liquid fuels may varies, but they are all generated through clean and sustainable procedures without additional emissions released into the atmosphere [31]. The CO_2 conversion process into value added products is a hydrogenation process where CO_2 reacts with H_2 and is classified into two categories, the methanation reaction and the formation of hydrocarbons through the Fisher-Tropsch (FT) reaction [32]. Fig. 1 presents the possible pathways of CO_2 hydrogenation into value added chemicals and fuels. CO_2 hydrogenation is extensively investigated for providing direct routes for the production of various fuels and chemicals with the catalytic hydrogenation being the a developed and promising technology [33]. On the other hand, the necessity to find a solution for the storage of H_2 which faces safety challenges and limitations, has led to technologies including H_2-lean molecules that act as storage system and with dehydrogenation they release H_2. Such storage molecules can be generated from atmospheric CO_2 with the liquid compounds being FA, NH_3 and alcohols. The other pathway is the LOHCs which undergo fully reversible hydrogenation/dehydrogenation cycles [34]. H_2 generation from hydrogen carriers has several practical applications in the context of green energy systems for the decarbonisation of the power, industry and transportation sectors. It offers on-demand H_2 generation for portable

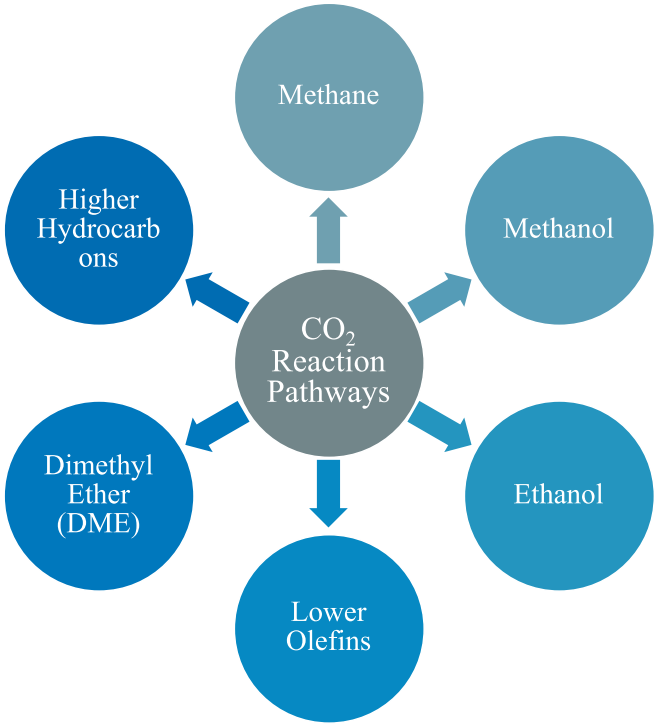

Fig. 1. Schematic illustration of chemical and fuels from CO_2 hydrogenation [37].

systems such as fuel cells and vehicles, and supports supply in areas lacking pipeline infrastructure [35]. Moreover, it provides an alternative option of the traditional power grid because combined with a fuel cell, the electricity can be produced as needed, reducing the need for H_2 storage [36]. In the section herein, a mechanistic description and discussion of the main CO_2 hydrogenation fuel products and H_2 production routes from H_2 storage materials are presented. Different investigated kinetic models are summarised and the kinetic rates are introduced for the first time of different materials and reaction conditions. Kinetic equations implemented in CFD models could be simple power law kinetic expressions as well as kinetics derived from in-depth understanding of reaction mechanisms.

2.1. The main products of CO_2 hydrogenation

2.1.1. Methane

CO_2 methanation was firstly proposed by Paul Sabatier and Jean-Beptiste Senderens in 1902 where CO_2 and H_2 react to produce CH_4, potentially developing a power-to-platform solving the intermittent issue of solar and wind RES and circular economy [38]. The power-to-gas (PtG) technology for renewable electricity generation is considered to be one of the most promising applications among the CO_2 utilisation routes. The CH_4 produced known as synthetic natural gas (SNG) provides a solution in electric energy storage with many pilot scale examples around the world [39,40]. In addition, SNG could be utilised as a fuel or as a feedstock for further synthesis of chemical products such as alcohols or even for biogas upgrading. With biogas consisting mainly CH_4 and CO_2, its upgrading enhances the CH_4 content. However, the techniques for removal of CO_2 from the mixture and its release into the atmosphere are environmentally unfriendly and contributing to the climate crisis. Therefore, the hydrogenation of the existing CO_2 through the methanation reaction improves content of CH_4 [41]. The methanation process reaction is expressed by the catalytic reaction in Eq. (1) [20]:

$$CO_2 + 4H_2 \longleftrightarrow CH_4 + 2H_2O \quad (1)$$

The methanation of CO_2 is an exothermic reaction that is favoured at lower temperatures. The activation of C-O bond is considered as a challenge as it has a high kinetic barrier being an eight-electron process and thus, higher temperatures are required for the reaction activation [42]. There are two possible pathways converting the CO_2 into CH_4, the direct and CO route. The direct methanation is displayed by Eq. (1) as the CO route implements the reverse water–gas shift reaction (RWGS) and CO methanation reaction expressed as [20]:

$$CO_2 + H_2 \longleftrightarrow CO + H_2O \quad (2)$$

$$CO + 3H_2 \longleftrightarrow CH_4 + H_2O \quad (3)$$

The CO production from the RWGS reaction, is dominant especially at high temperatures as well as the coke formation. Many different catalytic materials have been tested for their catalytic activity, production rates and selectivity towards main products. Promising results was shown by metals from the groups of 8, 9 and 10 of the periodic table, including metals such as cobalt (Co), iron (Fe), ruthenium (Ru), molybdenum (Mo) [43]. Also, transition metals such as Rb, Pd, nickel (Ni) and Ru have been all investigated displaying high activity towards the methanation reaction, with Ni-based catalysts being commonly utilised for their low cost and outstanding catalytic performance [44]. A vital challenge is catalyst deactivation that can occur physically or chemically. The catalysts used for the methanation reactions tend to be sensitive and more prone to be poisoned by carbon deposition chlorine compounds, tars, NH_3, sulfur compounds or alkalis [45]. The mechanism of the methanation reaction and its exact route have been in discussion and not agreed upon, as experiments show different pathways at different conditions. The dissociation of CO(s) and the following hydrogenation of CH_x(s) have been suggested as the rate-limiting step between 270 and 400 °C [46]. However, many kinetic models have been proposed for different catalysts through the years, with some of the approaches being based on the simple power law model and others followed more complex models. Table 1 groups validated kinetic models at different ranges of temperatures, pressures and H_2 and CO_2 ratio.

Weatherbee and Bartholomew [47], used a Ni/SiO_2 catalyst to define the kinetic model for the hydrogenation of CO_2. A simple power law approach was not able to describe the kinetic while with the Langmuir-Hinshelwood rate approach the results fitted well. The mechanism involves the dissociative adsorption of CO_2 to CO and atomic oxygen followed by dissociation of adsorbed CO to atomic carbon and atomic oxygen and then CH_4 is generated by the hydrogenation of atomic carbon. Xu and Froment [48], investigated the steam reforming of CH_4 in 1989 using $Ni/MgAl_2O_4$, where the reverse reaction pathway leads to CO_2 and CO methanation. A large number of reaction schemes were proposed with only two being considered for the model discrimination. In most of studies the reaction rates expressed by Xu and Froment are utilised and can predict with accuracy at high temperatures over 300 °C and up to 575 °C and pressures between 3–15 bar [11].

More recent studies occurred to determine the hydrogenation of CO_2 in the presence of catalyst. Onrubia-Calvo et al. [49], performed more than 120 kinetic experiments shifting different parameters such as reaction temperature, total pressure, space velocity and partial pressure of products and reactants in order to define the reaction kinetic rates of CO_2 methanation using a Ni/CeO_2 catalyst. Characterisation studies revealed that two different Ni sites are involved with the one being the reduced Ni for H_2 dissociation and cationic Ni stabilised in the NiO/Ce interface for CO_2 dissociation. For the first time, the Langmuir-Hinshelwood-Hougen-Watson (LHHW) approach was utilised for this catalyst material, considering the formate route to be the rate-limiting step while being effective to predict with accuracy the performance of reaction. The model was found to predict satisfactorily the obtained results from the experiments with the mean absolute deviation which was less than 11 % to be lower than other common models investigated in literature. Moreover, two different active sites where for CO_2 adsorption and H_2 dissociation were considered providing also good

Table 1
Reaction rate equations for CO_2 methanation.

Catalyst	T (°C)	P (bar)	H_2/CO_2	Rate equation	Ref
Ni/SiO_2	227–327	1.4	4	$r_{CH_4} = \frac{\left(\frac{K_1K_2K_{10}k_4k_{11}}{2}\right)^{0.5} L^2 {P_{CO_2}}^{0.5} {P_{H_2}}^{0.5}}{\left[1+\left(\frac{2K_2k_4}{K_1K_{10}k_{11}}\right)^{0.5}\frac{{P_{CO_2}}^{0.5}}{{P_{H_2}}^{0.5}}+\left(\frac{K_1K_2K_{10}k_{11}}{2k_4}\right)^{0.5}{P_{CO_2}}^{0.5}{P_{H_2}}^{0.5}+\frac{P_{CO}}{K_3}\right]^2}$	[47]
$Ni/MgAl_2O_4$	300–575	3–15	–	$r_{CH_4} = \frac{\frac{k_1}{p_{H_2}^{3.5}}\left(p_{H_2}^4 p_{CO_2} - \frac{p_{CH_4}p_{H_2O}^2}{K_{eq,\,CO_2\,Meth.}}\right)}{\left(1+K_{CO}p_{CO}+K_{H_2}p_{H_2}+K_{CH_4}p_{CH_4}+\frac{K_{H_2O}p_{H_2O}}{p_{H_2}}\right)^2}$	[48]
Ni/CeO_2	200–500	–	4	$r_{CH_4} = \frac{kP_{CO_2}{P_{H_2}}^{0.5}\left(1-\frac{P_{CH_4}{P_{H_2O}}^2}{K_{eq}P_{CO_2}{P_{H_2}}^4}\right)}{\left(1+K_{H_2}{P_{H_2}}^{0.5}\right)\left[1+K_{CO_2}P_{CO_2}+K_{H_2O}P_{H_2O}+K_{OH}\left(\frac{P_{H_2O}}{{P_{H_2}}^{0.5}}\right)\right]}$	[49]
Ni/Al_2O_3	315–430	1–6	1–16	$r_{CH_4} = \frac{k{P_{CO_2}}^{0.5}{P_{H_2}}^{0.5}\left(1-\frac{P_{CH_4}{P_{H_2O}}^2}{K_{eq}P_{CO_2}{P_{H_2}}^4}\right)}{\left[1+\sqrt{K_{CO_2}P_{CO_2}}+\sqrt{K_{H_2}P_{H_2}}+K_{OH}\left(\frac{P_{H_2O}}{{P_{H_2}}^{0.5}}\right)\right]^2}$	[50]
Dual-function $Ru\text{-}Na_2CO_3/Al_2O_3$	250–400	1	1	$r_{CH_4} = k\left({P_{CO_2}}^n {P_{H_2}}^{4n} - \frac{{P_{CH_4}}^n {P_{H_2O}}^{2n}}{[K_{eq}(T)]^n}\right)$	[51]
M/NiO-MgO (M=Co, Fe and Cu)	400	–	8	$r_{CH_4} = \frac{\frac{{P_{H_2}}^{0.5}}{\left(1+\frac{1}{k_7}+\frac{1}{k_8}\right)}\left(K_3 - \frac{{P_{H_2}}^{0.5}}{2\left(1+\frac{1}{k_7}+\frac{1}{k_8}\right)k_5}\right)}{\left[1+K_1P_{CO_2}+\left(1+\frac{1}{2\left(1+\frac{1}{k_7}+\frac{1}{k_8}\right)k_4}\right)K_3{P_{H_2}}^{0.5}\right]}$	[52]

results with mean absolute deviation being less than 12 %. In contrast to the first model, in the second the mean absolute deviation might have showed a slight rise, thus the two active sites assumption is physically more realistic.

Quindmil et al. [50], similarly to previous study, have analysed various experiments under different operating conditions to define the mechanism and kinetics of CO_2 methanation reaction of low-loaded Ni/Al_2O_3 catalyst. Even though the reducibility of Ni was found to be as low as less than 10 %, the strong $NiO\text{-}Al_2O_3$ interaction was considered to be stable during the kinetic experiments. 153 experiments were performed and alongside to the DRIFTS results, an H-assisted CO formation route was suggested for the first time. Comparing to other reported routes an improvement in the mean absolute deviation was observed with value of 7 %. The LHHW mechanistic model regards the decomposition of formate species into carbonyls via the proposed route and the further hydrogenation into CHO as the rate-determined step. The results demonstrated that the mechanism and kinetics of CO_2 methanation can accurately describe the intrinsic kinetics. Activity tests were conducted showing poor performance. The low activity and CH_4 selectivity were suggested to be attributed to high interaction between metal and support. At the same time, the stability investigation showed no relevant changes within the stream time period of 48 h, revealing that reduced Ni sites did not suffer from any deactivation mechanism or sintering.

Varun et al. [52], synthesised a M/NiO-MgO nanocomposite (M = Co, Fe and Cu) to comprehend the mechanism and activity of catalyst of methanation reaction. It was observed that uniform particle distribution is achieved for Co/NiO-MgO and Cu/NiO-MgO nanocomposites while a flaky distribution was obtained for Fe/NiO-MgO catalyst as the pore volume is higher compared to the other catalytic materials. Using inputs from temperature programming reduction with H_2 (H_2-TPR) and temperature programming desorption with CO_2 (CO_2-TPD) the mechanism of reaction was explored. The mechanism of reaction was suggested considering the metallic active sites from doped and undoped catalysts as M where the model was found to validate the experimental results well. Considering a pseudo-steady state approximation the reaction rate was developed assuming that both reactants are chemisorbed on the surface of catalyst. The association of adsorbed C and H are regarded as the rate-determining step.

2.1.2. Alcohols

Among the CO_2 hydrogenation products, alcohols and especially C_1 alcohol (MeOH) is one of the most known products as it can be advanced into various chemical products. Higher alcohols (HAs) C_2-C_5 can also be implemented into the transportation section and more specifically into the fuel blends or alone in order to enhance the performance of the engines [53]. Thus, the direct formation of alcohols from CO_2 has gained the interest of scientists to mitigate the stress of environmental crisis [54]. However, the direct CO_2 hydrogenation to HAs is difficult to succeed due to the uncontrollability of the C–C bond coupling path and various complex reaction routes [53,54]. Two possible routes have been proposed, the formate (HCOO) route and the carboxyl (COOH) route, with the first one being regarded as the significant intermediate in the MeOH synthesis as the adsorption of COOH species is much weaker than the HCOO species. The CO_2 hydrogenation to MeOH is expressed as [55]:

$$CO_2 + 3H_2 \longleftrightarrow CH_3OH + H_2O \quad (4)$$

Due to the fact that the formation of CO is comprised in the CO_2 hydrogenation, the synthesis of HAs from CO_2 can be related with the RWGS reaction and CO conversion to HAs. The promotion of C-O bond breaking and the C–C bond coupling while keeping at least one C-O bond intact in the products is the considered the main challenge and thus, the strategy for the catalyst design for HA synthesis is multifunctional [56]. Catalysts with non-dissociative CO activation and insertion and CO dissociative activation and carbon chain propagation were found to be effective for HAs production through the CO pathway [57]. Several different kinetic models have been developed for the hydrogenation of CO_2 to MeOH and HAs. In addition, it was also found that MeOH can be the key intermediate product, where the combination of two molecules of them can lead to the formation of ethanol. Since the CO_2 hydrogenation into HAs is a relatively new research field, the knowledge around the reaction mechanism due to the complexity of reaction pathways, is yet at an early stage with the efforts of computational chemistry to be

significant [58]. Noble metal catalysts are great option for HAs synthesis and especially for ethanol production with strong C=O bond activation and C–C bond coupling. However, their high cost limits their application. Therefore, non-noble metals such as Cu- and Co-based with additional alkali metals as promoters were found to convert CO_2 to a satisfactory extent [48]. Table 2 summarises proposed reaction rates at different ranges of temperatures, pressures and H_2 and CO_2 ratios for MeOH and HAs alcohols.

Lim et al. [59], suggested a kinetic model for the CO_2 hydrogenation into MeOH over $Cu/ZnO/Al_2O_3/ZrO_2$ catalyst. A detailed kinetic mechanism including RWGS pathway through the CO and CO_2 hydrogenation was considered. Between the proposed reaction rates, it is suggested that the rate determined steps were the methoxy species surface reaction for the CO hydrogenation, the formate intermediate HCO_2 hydrogenation for the CO_2 hydrogenation and the formation of a formate intermediate for the RWGS rection. It was found that the direct CO_2 hydrogenation rate is much lower than the CO hydrogenation rate. Also, an investigation for the influence of CO_2 on the reaction rates occurred showing that CO_2 prevents the production of dimethyl ether (DME) from MeOH indirectly through the RWGS reaction.

Li et al. [60], using measured kinetic data developed two reaction kinetic models for the MeOH generation using a commercial $Cu/ZnO/Al_2O_3$ catalyst. Considering a single-active site and a double-active site absorption Langmuir-Hinshelwood mechanisms, both models can describe the experimental results within a relative deviation smaller than 20 %. Moreover, it was found that the average sum of error of CO and CH_3OH in the case of single-site model is higher than that of double-site model and hence the latest can predict the experimental results more accurately.

Similarly, Poto et al. [61], used kinetic models implementing single-site, dual-site and three-site adsorption mechanisms for the CO_2 hydrogenation into MeOH using $Cu/CeO_2/ZrO_2$ catalyst. Different tools were used for model discrimination to understand better the mechanism of the reaction and to identify which model describes better the experimental data. The formation of formate HCOO was found to be the limiting step. The dual-site model developed by Graaf et al. [65], was found to be the best performing kinetic model suggests that one of the O of CO_2 is adsorbed on the O vacancies of CeO_2-ZrO_2 while H_2 is adsorbed and dissociated on the metallic Cu. Through this mechanism the MeOH can be synthesised directly or through the CO pathway and the maximum deviation from the experimental results was around 2 % for both CO_2 conversion and MeOH selectivity.

Calverley and Smith [64], developed a kinetic model that can successfully predict the HAs synthesis over a K_2CO_3-promoted $Cu/ZnO/Cr_2O_3$ assuming that the rate determined step was the C–C bond formation between the two formyl intermediates, while previous models could not describe the observations from this study. On the other hand, the proposed model was found to be consistent with the results of several studies. Both CO and CO_2 contribute to the MeOH production through their adsorption on different sites. Also, it was observed that CO, CO_2 and MeOH can directly converted into HAs.

2.1.3. Higher hydrocarbons

Under specific operating conditions and catalytic materials, CO_2 hydrogenation can contribute to the renewable sources intermittency by storing energy in fuels and chemicals such as liquefied petroleum gas (LPG), lower olefins, gasoline, aromatics etc. [66]. Long-chain hydrocarbons possess higher energy density being appropriate for a wide range of applications. The hydrogenation to hydrocarbons is proceeded through direct and indirect routes, and since the direct route makes the reaction kinetic limited it is not used [67]. The conversion of CO_2 can be achieved indirectly through the MeOH route, in which CO_2 is converted into MeOH (described by Eq. (4)), followed by the hydrogenation of MeOH to C_{2+} compounds including DME, gasoline and light olefins. The MeOH hydrogenation mechanisms to synthesise hydrocarbon products are described [68]:

$$2CH_3OH \longleftrightarrow CH_3OCH_3 + H_2O \quad (5)$$

$$nCH_3OH + H_2 \longleftrightarrow CH_3(CH_2)_{n\text{-}2}CH_3 + nH_2O \quad (6)$$

$$nCH_3OH + H_2 \longleftrightarrow CH_2{=}(CH_2)_{n\text{-}3}CH_3 + nH_2O \quad (7)$$

Another route for the formation of hydrocarbons from CO_2 is the RWGS Fischer – Tropsch (FT) pathway, where CO_2 forms long-chain hydrocarbons through the RWGS reaction (Eq. (2)) resulting CO and

Table 2
Reaction rate equations for CO_2 hydrogenation to methanol.

Methanol synthesis					
Catalyst	T (°C)	P (bar)	H_2/CO_2	Rate equation	Ref
$Cu/ZnO/Al_2O_3/ZrO_2$	250	50	–	$r_{MeOH-CO_2} = \frac{k_{MeOH-CO_2}K_{CO_2,s1}K_{H_2,s2}\frac{\left(P_{CO_2}P_{H_2}{}^3 - \frac{P_{CH_3OH}P_{H_2O}}{K_{CH_3OH-CO_2}}\right)}{P_{H_2}{}^2}}{D_{CH_3OH-CO_2}}$	[59]
$Cu/ZnO/Al_2O_3$	200–300	20	–	$r_{MeOH} = \frac{k_1\left(P_{H_2}^{1.5}P_{CO_2} - \frac{P_{CH_3OH}P_{H_2O}}{K_{eq1}P_{H_2}^{1.5}}\right)}{\left(1+K_{a_1}P_{CO_2}+K_{a_2}P_{CO}+K_{a_3}P_{CO_2}P_{H_2}\right)\left(1+K_{b_1}P_{H_2}^{0.5}+K_{b_2}P_{H_2O}\right)}$	[60]
$Cu/CeO_2/ZrO_2$	200–260	10–40	3–7	$r_{MeOH} = \frac{k_1 b_{CO_2} C}{\left(1+b_{CO}P_{CO}+b_{CO_2}P_{CO_2}\right)\left(P_{H_2}^{0.5}+\frac{b_{H_2O}}{\sqrt{b_{H_2}}}P_{H_2O}\right)}$	[61]
$Cu/ZnO/Al_2O_3$	180–280	1–51	–	$r_{MeOH} = \frac{k_{MeOH-CO_2}K_2{}'K_3K_4K_{H_2O}P_{CO_2}P_{H_2}\left[1-\left(\frac{1}{K^*}\right)\left(\frac{P_{CH_3OH}P_{H_2O}}{P_{CO_2}P_{H_2}{}^3}\right)\right]}{\left(1+\left(\frac{K_{H_2O}}{K_8K_9K_{H_2}}\right)\left(\frac{P_{H_2O}}{P_{H_2}}\right)+\sqrt{K_{H_2}P_{H_2}}+K_{H_2O}P_{H_2O}\right)^3}$	[62]
$Cu/ZnO/Al_2O_3$ Cu/Al_2O_3 Cu/SiO_2	180–220	5 and 20	1	$r_{MeOH} = kP_{CO}{}^{aCO}P_{H_2O}{}^{aH_2O}P_{CO_2}{}^{aCO_2}P_{H_2}{}^{aH_2}P_{tot}{}^{\gamma}\left(1-\frac{P_{CO_2}P_{H_2}}{K_gP_{CO}P_{H_2O}}\right)$	[63]
$Cu/ZnO/Cr_2O_3$	285	–	–	$r_{MeOH} = \left(\frac{AP_{CO}P_{H_2}{}^{3/2}}{(1+BP_M)^2}+\frac{CP_{CO_2}P_{H_2}}{\left(1+D\frac{P_{CO_2}}{P_{CO}}\right)^2}\right)\times\left(1-\frac{P_M}{K_{eq}P_{CO}(P_{H_2})^2}\right)$	[64]
$Cu/ZnO/Cr_2O_3$	285	–	–	$r_{HA} = \left(\frac{P_{CO}P_{H_2}{}^{1/2}}{A+BP_M}+CP_M(P_{H_2})^{-3/2}+\frac{P_{CO_2}(P_{H_2})^{1/2}}{D+E\frac{P_{CO_2}}{P_{CO}}}\right)^2$	[64]

then via the FT synthesis the hydrocarbons are generated by the hydrogenation of CO. Both pathways synthesise a plethora of products where the route is controlled by the catalytic properties and reaction conditions [69]. The first of the two steps of the mechanism includes the RWGS reaction as previously expressed by Eq. (2) and then the CO product reacts via FT mechanisms to synthesise the hydrocarbons [70].

$$CO + 2H_2 \longleftrightarrow -(CH_2)_n- + H_2O \quad (8)$$

The silica-supported Ni and Ru catalysts do not favour the synthesis of long-chain hydrocarbons but CH_4. Conversely, Fe- and Co-based catalysts are known for promoting the FT synthesis to generate C_{2+} hydrocarbons with further enrichment with promoters such as Cu, Mo and alkali metals [70]. Despite the wide spread of applications of Fe-based catalysts in the hydrogenation of CO_2, they suffer from rapid physical and chemical deactivation affecting catalyst active sites [33].

Ghosh et al. [71], performed a kinetic analysis for the CO_2 hydrogenation into hydrocarbons over an In_2O_3/HZSM-5 bifunctional catalyst. The catalyst was preheated at 400 °C which resulted to the formation of oxygen vacancies on the catalyst that were reduced after the hydrogenation reaction. The suggested kinetic model is an integration of models and is following LHHW reaction mechanism for the generation of MeOH as an intermediate product over the In_2O_3 catalyst incorporated with a lump-type model for the transformation of MeOH to hydrocarbons over the HZSM-5 zeolite. Some of the reactions the model were MeOH synthesis, RWGS reaction, methanation reactions, C_2-C_4 olefin production, C_2-C_4 paraffin production, oligomerisation reactions and cracking reactions. DME was not incorporated as an intermediate for the reaction from MeOH to hydrocarbons as it could not be possible to detect DME at the reactor outlet, assuming that the formed DME reacts fast to form the hydrocarbons. It was found that the model could validate the experimental findings allowing a good prediction of the product distribution when pure CO_2 and H_2 were used as feeds [72].

A kinetic model considering the MeOH to CH_4 and individual olefins such as ethylene, propylene and C_{4+} olefins over a SAPO-18 catalyst was proposed by Gayubo et al. [73]. For the development of the model theories considering the synthesis of intermediate active species that are trapped in the catalyst cages were made as well as taking into account the deactivation of the catalyst from zero time on stream due to the active intermediates inactivation. Also, the model was tested and found to be consistent with the obtained results from literature in order to understand the intermediate products nature and determine the operating conditions effect on these intermediates.

Brubach et al. [74], investigated the kinetics considering the RWGS FT pathway over a Fe/K on γ-Al_2O_3 catalyst. The new proposed LHHW type model was obtained from previous elementary reaction steps studies. The reaction rates are based on the H-assisted CO_2 and H-assisted CO dissociation mechanisms. Moreover, the product distribution was modeled for up to C_4 components which represent the average carbon number according to the molar product distribution obtained by the experimental results. However, the model is assumed to be able to consider secondary reactions of light products. In general, a good validation was obtained between experimental and modelling findings with the calculated CO_2 conversion deviation to be less than 5 %.

Pour et al. [75], developed a kinetic model for the FT synthesis reaction yielding hydrocarbons using CO as an intermediate product over an Fe/Cu/La/SiO_2 catalyst. The reduction was obtained to take place in two stages, with the first stage to correspond to the reduction of α-FeO_3 and CuO to Fe_3O_4 and Cu, respectively, while the second stage includes the of Fe_3O_4 to α-Fe. The Cu introduction was suggested that contributes to the reduction of α-FeO_3 to Fe_3O_4. The rate of the reaction relies on the feed components partial pressure and the operating temperature, and the equations follow LHHW and empirical power law form. A total of 16 sets of experimental data occurred for the kinetic investigation. Only three of the several LHHW type rate equations that were developed based on possible reaction mechanisms were found to fit the experimental results (carbide, enolic and combined enol/carbide mechanisms), with the kinetic parameters to be evaluated using the experimental results combined with non-linear regression method to make a refined optimisation. The results demonstrated that the model developed based on the enolic mechanism showed better fitting for the experimental findings when compared to the other two proposed mechanisms.

In a recent work by Saeidi et al. [70], a mechanism considering the RWGS FT reaction was proposed with significant improvement in several predictions compared to previous kinetic models. Different reaction mechanisms were suggested regarding to various elementary reactions and carbon-chain distribution routes. It was considered that H_2 dissociative adsorption is followed by the reaction between a molecular of CO_2 and adsorbed atomic H and was found to be the rate determined step. Thereafter, CO and hydroxyl intermediate are formed by the adsorbed oxygenated intermediate, which next forms molecular H_2O. Between all the suggested mechanisms it was obtained that carbide and enolic contribution was significant in observed mechanisms.

2.2. H_2 sources

2.2.1. Formic acid

As already mentioned, H_2 is essential for performing the CO_2 hydrogenation reactions. H_2-carrier molecules, which constitute a solution on H_2 storage limitations, can be a result from the conversion of captured atmospheric CO_2. The production of H_2 from FA is an attractive approach for room temperature storage and release [76]. Since the process, proceeds slowly and with a low yield in the absence of a catalyst, lots of studies focused on the efficient FA catalytic decomposition [77]. When decomposed, it can follow two reaction routes: dehydrogenation (decarboxylation) and dehydration (decarbonylation) (Eqs. (9) and (10)) [78]. The former breaks FA into H_2 and CO_2 and the later to H_2O and CO. The first reaction path is the reverse reaction process of the hydrogenation of CO_2. Thus, by this cycle, H_2 can be efficiently stored in FA [76].

$$HCOOH \rightleftharpoons CO_2 + H_2 \quad (9)$$

$$HCOOH \rightleftharpoons CO + H_2O \quad (10)$$

Since it is denoted as a promising H_2 carrier, many studies focused on employing it in direct FA fuel cells (DFAFCs) as secondary fuel. However, DFAFCs present significant limitations, while hydrogen fuel cells (HFCs) are a more better-established technology [79]. Therefore, using FA to selectively produce H_2 in powering HFCs is a potential idea with a quick route to market. However, the decomposition of FA is not considered a green technology since energy discharge will lead to a notable mass release in the form of CO_2.

Since there are two reaction routes involved, many studies investigated the mechanisms that are involved. Dehydrogenation is believed to undergo decomposition through the intermediates such as formate (HCOO) or carboxylate (COOH), produced from the activation of O–H or C–H bonds in FA [80], which is also considered the rate-determining step. As for dehydration, besides “formate mechanism”, it can also follow a different mechanism without the participation of formates [81]. The most common studied catalysts for FA decomposition are Pd- and Au-based since they were found to favour the H_2 generation against the production of CO. Incorporating non-noble metals such as Ni and Cu were also found to promote the formate intermediate pathway, generating H_2 [78,82]. However, only a few conducted kinetic studies to determine the reaction rate that describes the reaction and most of these studies investigated the order-dependence on FA concentration, assuming a power-law model. The findings of the studies are summarised in Table 3.

Hinshelwood and Topley [83], examined the decomposition of FA vapour. Their experiments focused on the kinetics of the heterogeneous decomposition on rhodium, gold, palladium and titanium oxide

Table 3
Reaction rate equations for H_2 production from formic acid decomposition.

Catalyst	T (°C)	P (bar)	FA conversion (%)	Rate equation	Ref
Rh, Au, Pd, TiO_2	140–200	2.03	–	$r_{HCOOH} = k \times C_{HCOOH}^{1.00}$	[83]
–	360	253.31	61	$r_{HCOOH} = k \times C_{HCOOH}^{0.94\pm0.18}$	[84]
$Pd_{0.58}Ni_{0.18}Ag_{0.24}/C$	50	–	100	$r_{HCOOH} = k \times C_{HCOOH}^{0/0.5} \times C_{catalyst}^{1} \times C_{promoter}^{0.5}$	[85]
10 wt% Pd/C	85	–	95–99	$r_{HCOOH} = k \times C_{HCOOH}^{0.14}$	[86]
5 wt% Pd/C	30	–	99.9 %	$r_{HCOOH} = k \times C_{HCOOH}^{0.2}$	[87]
Au/Al_2O_3, Pt/Al_2O_3	80	–	–	$r_{HCOOH} = \frac{K_1^{A1} k_2^{A1} P_{HCOOH}}{\left[1 + 2\left(K_1^{A1} {P_{HCOOH}}^{0.5}\right)\right]^2}$	[88]
Au/Al_2O_3, Pt/Al_2O_3	80	–	–	$r_{HCOOH} = \frac{k_1^{A2} P_{HCOOH}}{\left[1 + \frac{k_1^{A2}}{k_2^{A2}} P_{HCOOH} + \left(\frac{2k_1^{A2}}{k_3^{A2}}\right)^{0.5} {P_{HCOOH}}^{0.5}\right]^2}$	[88]
1 wt% Pd/C	175	1.01	71	$r_{HCOOH} = k \times C_{HCOOH}^{1.00}$	[89]
1 wt% Pd/C	175	1.01	71	$r_{HCOOH} = \frac{k \times C_{HCOOH}}{1 + K_{ads} C_{HCOOH}}$	[89]
1 wt% Pd/C	175	1.01	71	$r_{HCOOH} = \frac{k \times C_{HCOOH}}{\left(1 + K_{ads} C_{HCOOH}\right)^2}$	[89]

surfaces. Among the kinetic measurements, they concluded that the reaction rate follows first-order kinetics, making it unlikely for the decomposition of the formate species to be the rate-limiting step. Solymosi and Erdöhelyi [90], examined the decomposition of FA in rhodium-based catalysts with different support systems. In contrast with other monometallic catalytic systems, rhodium catalysts demonstrated a nearly first-order dependence on the concentration of FA as it was also observed by Hinshelwood and Topley [83].

In the late 1990 s, Yu and Savage [84], investigated the thermal decomposition of FA at a temperature range of 320 to 500 °C. The focus of the study was the reaction kinetics of the FA disappearance. By evaluating how the reaction rate is affected by the FA concentration, the global reaction order can be ascertained. Under hydrothermal conditions, the order of the reaction was found to be 0.94 ± 0.18, concluding that first-order kinetics appropriately describes the decomposition of FA, given that the reaction order is close to unity. More recent studies have also considered a first-order dependence [91].

Alloying Pd with other metals can lead to the improvement of catalytic performance by preventing CO deactivation and also reduce the quantity of high-cost Pd. Thus, a PdNiAg catalyst supported on carbon was synthesised by Yurderi et al. [85] and utilised for FA decomposition. Kinetic analysis was performed on the dependence on the concentrations of FA, catalyst and promoter of the reaction, in this case sodium formate. The results showed that the reaction rate is first-order towards the concentration of catalyst and half-order towards the promoter concentration. Regarding the reactant, at low concentrations of FA the rate is zero-order dependent and at high concentrations was found to be half-order.

Vapour phase FA decomposition on different catalytic systems was studied by Bulushev et al. [86]. The Pd/C catalyst exhibited the best performance among the catalysts tested at temperatures below 400 K. The rate of H_2 production was calculated, at low conversion rates, as a function of FA concentration. A very low reaction order (0.14) was found, thus the reaction rate is independent on the FA concentration. Zero-dependence reaction kinetics was also observed by other monometallic catalysts, typically indicating that reactions are inhibited by steps that involve intermediates present at saturation coverages.

Sanchez et al. [87], examined the performance of a 5 wt% palladium on carbon catalyst for the FA decomposition at moderate conditions. After the catalyst exhibited a great selectivity (99.9 %) towards H_2 at 30 °C, studies were conducted for the preferable pathway that the decomposition follows. Based on their studies, the most plausible path is the formates formation, concluding that the H-atoms occurring after the formate decomposition recombine with the H-atoms generated after the dissolution of the O–H bond to yield H_2. DFT calculations on Pd (111) supported also these findings, with an energy profile showing two different paths initiated by O–H (1) and C–H (2) dissociation. Pathway 1 began with the adsorption of trans FA followed by splitting of the O–H bond. Pathway 2 was initiated with a reorientation from trans configuration to cis (slightly more unstable than trans). HCOO was the preferable intermediate leading exclusively to CO_2 and H_2, supporting the experimental very low ppm level concentration of CO observed experimentally. Furthermore, knowing the amount of gas generated, the reaction order was calculated ($n = 0.2$) by plotting the rate against the FA concentration and fitting the data to a power-law model equation.

A study by Ojeda and Iglesia et al. [88], investigated the dehydrogenation of FA in Au- and Pt-based catalysts. Under their experimental conditions the only products were H_2 and CO_2 indicating that dehydration towards CO and H_2O and water gas shift (WGS) do not occur. On Au/Al_2O_3 catalyst the dehydrogenation rate was independent of the FA pressure and on the Pt/Al_2O_3 catalyst the rate initially increased with the FA pressure and then remained constant. Two mechanisms were derived. In the first mechanism (A1), FA decomposes forming formate and H_2 and then the formate dissociates into CO_2 and H_2, while in the second mechanism (A2), the produced formate decomposes in CO_2 and H_2 that needs to be recombined with another H_2 to form H_2. The two proposed reaction rates for each mechanism are presented in Table 3, and it is evident that they are dependent on FA pressure that is present in both the numerator and denominator. In the A1 mechanism the FA decomposition, occurs reversibly and thus, the kinetic constant is symbolised as $K_1(k_1/k_{-1})$.

The kinetics of FA decomposition were studied by Winkler et al. [89], in a lab-scale fixed bed reactor using Pd nanoparticles supported on active carbon. The main products of the reaction were H_2 and CO_2, with very little CO and H_2O present. Three kinetic models were used to explain the experimental findings: first order, simple-adsorption and adsorption-dissociation models. Their results exhibited that the first-order model had the lowest degree of explanation, since it neglects FA adsorption and it does not incorporate the reaction mechanism. The simple-adsorption mechanism considers that FA adsorbs rapidly on the active site and then the products are directly formed and released, while the adsorption-dissociation model is an extension of the simple-adsorption mechanism where the products are formed through intermediates. The reaction rates of these two models described better and reproduced similarly the experimental data.

2.2.2. *Hydrous hydrazine*

Hydrazine (N_2H_4) is a carbon-free molecule with a high H_2 content of 12.5 % [92]. Initially, the decomposition of hydrazine was a part of the photochemically decomposition of NH_3 [93] where hydrazine resulted as an intermediate. Since the reaction gained interest, it was also thermally decomposed where only NH_3 and nitrogen (N_2) were the main

products under these conditions (Eq. (11)). From later studies [94,95] that thermally decomposed hydrazine, H_2 was also obtained based on the reaction below (Eq. (12)).

$$3N_2H_4 \rightarrow N_2 + 4NH_3 \quad (11)$$

$$2N_2H_4 \rightarrow H_2 + N_2 + NH_3 \quad (12)$$

Adams and Stocks [96], experimented with the combustion of hydrazine and discovered that at lower temperatures hydrazine decomposes following Eq. (13) instead of Eq. (12). Thus, when decomposed at lower temperatures, it follows two paths, its complete dehydrogenation where N_2 and H_2 are produced (Eq. (13)) and its incomplete dehydrogenation where N_2 and NH_3 are generated as shown in Eq. (11).

$$N_2H_4 \rightarrow 2H_2 + N_2 \quad (13)$$

Even though it is considered a great H_2 carrier it is extremely flammable and dangerous unless handled in solutions e.g. hydrous hydrazine ($N_2H_4{\cdot}H_2O$, HH). HH has a H_2 content of 7.9 % and is safer to use than the anhydrous form [97]. Even though hydrazine hydrate decomposition is known from the 1950 s, the last two decades has gained interest in the science community. The reaction route is determined by the sequence of N–N bond and N–H bond cleavage. The N–N bond cleavage leads to the production of N_2 and NH_3, while the N–H bond breakage gives N_2 and H_2 [98]. Metals such as Rh, Ir, Ru and Ni are the most efficient candidates for N–H bond activation, exhibiting high activity at ambient conditions, however, with low H_2 selectivity over Ru and Ir catalysts [99,100]. Due to the complexity of the reaction mechanism, different kinetics were proposed with the plethora following a Power-law model (Table 4).

In 1956, one of the first studies on the thermal decomposition of anhydrous hydrazine kinetics was conducted by Smith and Solomon [101]. The first experiment was carried out using an iridium wire as a catalyst and the second with an iridium catalyst supported on alumina. Hydrazine was injected in the flow reactor at standard conditions. Since iridium wire is non-porous, the proposed reaction rate was calculated using the transport-controlled reaction rate theory, considering the hydrazine concentration in the bulk (C_g) and at the surface of the catalyst (C_s). Their experimental results were fitted to a graph with a slope of 1.41, which is the order value with respect to hydrazine. For the alumina supported catalyst, a different reaction rate was obtained with a reaction order of 1.32 with respect to hydrazine.

A study by Dai et al. [102], used a bimetallic Ni-Pt-based catalyst for the decomposition of HH as these catalysts were found to have high surface areas, narrow pore size distributions, and great catalytic properties for H_2 generation from HH. TEM revealed an average particle size of 2.4 nm and XPS studies showed that O 1 s spectra corresponded to the O species in the lattice oxygen of metal oxides and the minor hydroxyl group, which may promote the breakage of the N–H bonds. Based on their experimental observations, they proposed a power-law reaction model to describe the reaction rate, depending on the concentration of the hydrazine solution, catalyst and NaOH. At the beginning of the reaction rate where high HH concentrations prevailed, they suggested that the reaction follows near-zero-order kinetics and afterwards at low HH concentrations, follows fraction-order kinetics. A similar trend was observed for the concentration of NaOH, since at high concentrations there is a near-zero-order dependence, while at lower concentrations there is a fraction of 0.57-order dependence. In relation to the catalyst amount the decomposition proceeds with first-order kinetics.

Mono-, bi- and trimetallic catalysts were developed by Al-Thubaiti and Khan [103], for the investigation of the reaction mechanism of HH decomposition. While all the monometallic catalysts did not exhibit any reactivity towards this process, the bi- and tri-metallic catalysts were active for this reaction with the Ni/Fe/Pd catalyst achieving the best performance. The durability of Ni/Fe/Pd was also evaluated by cycling experiments, where the catalytic activity remained unchanged even after five consecutive kinetic experiments. The great properties of Ni/Fe/Pd could be ascribed due to the synergistic effect of three metals and thus was used for further studies. From the obtained rate-law it is evident that the decomposition reaction has complex kinetics, involving hydrazine, catalyst and hydroxyl concentrations. The complexity mainly derives from the presence of OH^- ions, either from hydrazine or the sodium hydroxide solution that promotes the reaction. The reaction order can vary based on the reactants concentration and the nature of the catalyst. When the catalyst surface is saturated with hydrazine the rate is a zero-order reaction and when at low hydrazine concentrations it follows first-order kinetics, as it was observed under their experimental conditions that the authors used. Thus, they concluded that depending on the experimental conditions it follows complex order kinetics.

Lastly, Bercic and Likozar [104], after a literature review of 23 articles, proposed a power-law model to describe the reaction rate for HH decomposition. Since batch systems are mostly used, a simple reaction rate for batch system can be used depending on the concentrations of HH and catalyst. Depending on the catalyst used, the order dependence for HH varied from 0 to 0.644, with an average value of 0.33. Studies that have investigated the value of order dependence for the catalyst amount found a range of 0.87–1.09, agreeing with the studies above that regarding the catalyst, the rate follows first-order kinetics, which is reasonable since it is expected from a catalyst to influence the activity and yield of reaction.

2.2.3. Ammonia

Another substitute for H_2 carrier is NH_3. Claude Luis Bertholett [105], was one of the first to decompose NH_3 discovering that 1 vol of NH_3 can generate 2.046 volumes of a mixture containing 1.545 volumes and 0.501 of H_2 and N_2 respectively, calculating that NH_3 contains 81.13 % N_2 and 18.87 % H_2, which correspond to modern values of 82.83 % and 17.76 %. Although NH_3 has an exciting potential to contribute to green energy generation, there are still many unanswered questions regarding its sustainability due to its production though the Harber-Bosch process, utilising fossil fuels as the main source [106]. Thus, diverse methods need to be used such as electrocatalytic/photocatalytic/biocatalytic NH_3 synthesis [107].

In the early 1880 s, Ramsay and Young [108], conducted the first studies on the temperature at which NH_3 decomposes and later studies from Perman and Atkinson [109] investigated temperature and pressure effects on the decomposition rate. The decomposition of NH_3 is

Table 4
Reaction rate equations for H_2 production from hydrous hydrazine decomposition.

Catalyst	T (°C)	Pressure (bar)	H_2 selectivity/Yield (%)	Rate equation	Ref
Ir wire	320–427	0.001	–	$r_{N_2H_4} = 6.81 \times 10^8 e^{-\frac{2939 \pm 1079}{T}} C_s^{1.41 \pm 0.44}$	[101]
Ir/Al_2O_3	77–177	0.001	–	$r_{N_2H_4} = 3.00 \times 10^2 c_s^{1.32 \pm 0.95}$	[101]
$Ni_{60}Pt_{40}/CeO_2$	30	–	100	$r_{N_2H_4{\cdot}H_2O} = kC_{N_2H_4{\cdot}H_2O}^{0.52/0.043} C_{NaOH}^{0.57/0} C_{catalyst}^{1.03}$	[102]
Ni/Fe/Pd	40	–	100	$r_{N_2H_4{\cdot}H_2O} = \frac{k_1 K_{ads} C_{OH^-} C_{catalyst} (C_{N_2H_4{\cdot}H_2O})_T}{1 + \frac{K_b}{C_{OH^-}} + K_{ads} (C_{N_2H_4{\cdot}H_2O})_T}$	[103]
–	–	–	–	$r_{N_2H_4{\cdot}H_2O} = kC_{N_2H_4{\cdot}H_2O}^{0/0.644} C_{catalyst}^{0.87/1.09}$	[104]

represented by Eq. (14) as shown below.

$$NH_3 \leftrightarrow \frac{1}{2}N_2 + \frac{3}{2}H_2 \quad (14)$$

NH_3 decomposition has been studied extensively over the years and Ru was found as the most active single-metal catalyst, showing the highest activity due to its optimal metal–nitrogen binding energy, while other noble metals such as Rh, Ir, and Pd and non-noble metals like Ni, Cu and Fe, have also been investigated [17]. Many mechanisms have been established, however, there is an uncertainty regarding the limiting step and the most abundant reactive intermediate. Several kinetic models have been proposed for its decomposition reaction using power-law model and Langmuir Hinshelwood models. Temkin-Pyzhev models were also proposed. Table 5 sums up the proposed reaction rate models.

The Temkin – Pyzhev model is usually utilised to describe the reaction rate for NH_3 synthesis. However, many studies use this kinetic model to describe its decomposition [110]. This model considers that the desorption rate of the chemisorbed N_2 is the rate-determined step and that the inverse reaction of NH_3 synthesis can be neglected. As can be seen in Table 5, the reaction rate is now dependent from the partial pressures of NH_3, H_2 and N_2. The constant β depends on the catalyst characteristics and a range of values has been proposed so far. This reaction model has also been used by many studies throughout the years [117,118,119,120,121,122]. The second term of the reaction signifies the contribution of the inverse reaction [111]. However, the value of this term is virtually zero and therefore can be neglected and the overall rate can be rewritten as a power-law model [111], as can be seen in Table 5, where a and β are the orders for NH_3 and H_2 respectively [123,124].

Tamaru et al. [112], investigated NH_3 decomposition on tungsten surface and transition metals. Based on their experimental data, they concluded that the "tungsten-type" mechanism occurs at higher temperatures and lower H_2 pressures, where no dependency on H_2 pressure is observed, while the Temkin-Pyzhev model prevails at lower temperatures and higher H_2 pressures. As a result, at lower NH_3 pressures the reaction is first order, whereas at higher NH_3 pressures is zero-order. Thus, the transition temperature was investigated, and it was found that a change in the mechanism is responsible for this kinetic behaviour. At high temperatures, the cleavage of N–H bond of the adsorbed NH_3 is the rate-determining step while at low temperatures the rate-limiting step is the recombinative desorption of N-adsorbed species. The simplicity of this model led other authors to use it still today as called Tamaru model [125,126,127,128,129]. The constant m is the reaction order where $0 \leq m \leq 1$.

The Langmuir-Hinshelwood mechanism is often utilised to describe the catalytic NH_3 decomposition reaction rate. In this case, the rate depends on the partial pressure of NH_3 and is limited by the hydrogenation of the chemisorbed N_2 in contrast with the Temkin-Pyzhev model. Papapolymerou and Schmidt [113] investigated this reaction decomposition on different precious metals (Pt, Rh). Based on their experimental data, they proposed a simple Langmuir-Hinshelwood kinetic model. As seen from Table 5, the reaction product is also taken into account (symbolised with the subscript B). The exponent m can have a value of 0.5 for possible dissociative adsorption or other forms of inhibition. Inhibition was much stronger on Pt than on Rh. However, in a simple non-dissociative situation the value of m is equal to 1.

Another study by and Papapolymerou and Bontozoglou [114], examined NH_3 decomposition on polycrystalline wires and foils of Pd and Ir and was compared with the previous study. The reaction rate was reproduced by many of the tested wires and foils in a pressure range of 10^{-3} and 1 Torr at high temperatures (500–1900 K). The Ir catalyst exhibited the best performance among all four precious metals. The reaction rate is only depended by the reactant and based on their findings, they suggested that the rate becomes pressure-independent at low temperatures, while at higher temperatures the rate is first-order. Surface morphology studies showed that Pd and Ir wires altered during reaction, however this change affected reaction kinetics only as an area change, since neither the heats of adsorption nor the activation energies appeared to change.

Itoh et al. [115], examined the thermodynamic and kinetic analysis of NH_3 decomposition over a supported Ru catalyst at low temperatures in a membrane reactor. Ru is known as a highly active catalyst and its characterisation showed that the catalyst had a large surface area of 109 m^2/g, where the Ru particles were well dispersed. Seven reaction rate models based on Langmuir-Hinshelwood kinetic models were proposed each one based on a different limiting step (adsorption, surface reaction and desorption processes). The best fitting model for the experimental results was a desorption-based model where the N-atom was the dominant adsorption specie, and the combinative desorption of N-atoms was the rate-determined step. As it can be seen from Table 5, the reaction rate depends on the partial pressure of both reactant and products. The term K_p denotes the equilibrium constant of pressure.

Main objective of a work conducted by Armenise et al. [116], was the development of mechanistically based kinetic models capable of foreseeing the performance of integral reactors, where nearly full NH_3 conversion and high H_2 concentration at the reactor's exit are crucial. All their proposed kinetic models were based on the Langmuir isotherm, and it was assumed that all the adsorbed species are kinetically relevant, all steps, including slow steps, are partially reversible and that the

Table 5
Reaction rate equations for H_2 production from ammonia decomposition.

Catalyst	T (°C)	Pressure (bar)	NH_3 Conversion (%)	Rate equation	Ref
Fe	–	–	–	$r_{NH_3} = k\left[\left(\frac{P_{NH_3}^2}{P_{H_2}^3}\right)^{\beta} - \frac{P_{N_2}}{K_{eq}^2}\left(\frac{P_{H_2}^3}{P_{NH_3}^2}\right)^{1-\beta}\right]$	[110]
Ru/Al/M	300–700	–	100 (627 °C)	$r_{NH_3} = k' P_{NH_3}^{a} P_{H_2}^{\beta}$	[111]
Tungsten surface	370–550	–	–	$r_{NH_3} = k\frac{P_{NH_3}}{(1 + K_{ads}P_{NH_3})} = k' P_{NH_3}^{m}$	[112]
Rh,Pt	327–1527	1.3×10^{-5}-0.004	<10	$r_{NH_3} = \frac{kK_{ads}P_{NH_3}}{(1 + K_{ads}P_{NH_3} + K_{B,ads}^{m}P_B^{m})}$	[113]
Pd, Ir (foil/wire)	227–1627	1.3×10^{-5}-0.001	5–15	$r_{NH_3} = \frac{kK_{ads}P_{NH_3}}{(1 + K_{ads}P_{NH_3})}$	[114]
Ru/SiO_2	350–450	1–2	>90	$r_{NH_3} = \frac{k_F\left(P_{NH_3}^2 - P_{H_2}^3 P_{N_2}/K_p\right)}{\left(P_{H_2}^{1.5} + \sqrt{K_{ads}P_{NH_3}^2}\right)^2}$	[115]
Ni/Al_2O_3/monolith	300–700	1.01	60–99.5	$r_{NH_3} = \frac{k_A K_{NH_3}^2 P_{NH_3}^2}{\left(K_{H_2}^{1.5}P_{H_2}^{1.5}\left(1 + \sqrt{K_{H_2}P_{H_2}}\right) + K_{NH_3}P_{NH_3}\left(1 + \frac{\sqrt{K_{H_2}P_{H_2}}}{K_3}\left(1 + \frac{\sqrt{K_{H_2}P_{H_2}}}{K_2}\left(1 + \frac{\sqrt{K_{H_2}P_{H_2}}}{K_1}\right)\right)\right)\right)^2}$	[116]

surface is considered ideal. Three different cases were developed based on controlling steps and MARI and when fitted with their experimental data it was found that the recombinative desorption of adsorbed N-atoms is the determining step, thus the best model selected was Case A, even though Case A assumed that all species are kinetically relevant. The terms K_1 K_2 K_3, K_{NH_3} and K_{H_2} are equilibrium constants. Variations of Case A (Case A1 and Case A2) were also capable to predict results of the Temkin-Pyzhev kinetic model which assumes a non-ideal surface.

2.2.4. Ammonia borane

Ammonia borane (AB; NH_3BH_3) has recently gained interest as a novel H_2 storage material with 19.6 wt% H_2 capacity of It is a very simple molecule to handle due to its solubility in polar solvents and stability [130]. Pyrolysis and solvolysis are the two primary processes for its decomposition. Solvolysis is far more promising than pyrolysis since it can release a significant amount of H_2 in milder conditions. Solvolysis can be classified to alcoholysis where MeOH is typically added, and hydrolysis where a metal catalyst or an acid is present at ambient temperatures [130].

Both homogeneous and heterogeneous catalytic systems were studied so far, suggesting that there is a wide range of available catalysts enabling its efficient decomposition towards H_2. Pt, Ru, and Rh are the main noble metal elements, which exhibit excellent performance in catalytic hydrolysis to produce H_2, due to the activation of the breaking of B-H bond [131], while Co and Cu are also good and cheaper candidates. Different studies conducted on the catalytic hydrolysis of AB found that one mole of AB can generate three moles of H_2 at room temperature [132,133,134]. The hydrolysis of AB is described by Eqs.15–16, depending on the pH of the reaction while the general hydrolysis reaction is shown in Eq. (17).

$$NH_3BH_3 + 3H_2O \leftrightarrow NH_3 + B(OH)_3 + 3H_2 \quad (15)$$

$$NH_3BH_3 + 4H_2O \leftrightarrow NH_4^+ + B(OH)_4^- + 3H_2 \quad (16)$$

$$NH3BH3 + 2H2O \leftrightarrow NH4+ + BO2- + 3H2 \quad (17)$$

Even though, it is considered a great H_2 carrier, its reaction is complicated. Studies showed that half of the H_2 produced occurs from the water while the other half from the BH_3 group [135]. However, the dehydrogenation of the NH_3 moiety is very endothermic thus, it is thermodynamically unfavourable, limiting the effective gravimetric H_2 storage capacity. Usually, a Langmuir-Hinshelwood model is used to describe the mechanism of AB decomposition, validated by different catalytic systems (Table 6), assuming that the reaction among the adsorbed water and borane is the rate determining step. However, lot of mechanistic details including the rate-determining step, remain unclear.

Figen et al. [136], examined the synthesis and hydrolysis of AB for H_2 generation. After successfully synthesising AB of 98 % purity, they proceeded with the kinetic experiments using a Co-B catalyst. Zero-, first-order and Langmuir-Hinshelwood kinetic models were utilised to evaluate the kinetic behaviour of the AB decomposition. Their outcomes demonstrated that a zero-order kinetic model is recommended for temperatures above 60 °C, while first-order and Langmuir-Hinshelwood can be used for lower reaction temperatures. The former is recommended for temperatures below 40 °C and the later for temperatures up to 60 °C.

A study carried out by Basu et al. [137], investigated the hydrolysis of AB, catalysed by a commercial Ru catalyst supported on cylindrical carbon pellets (2 mm in diameter), since this form of supported Ru catalyst was found to be more efficient than other forms, such as Ru on alumina pellets, and Ru on carbon granules. Between 16 and 55 °C, the hydrolysis showed reaction orders less than unity. The results were interpreted using a Langmuir-Hinshelwood kinetic model, followed by a study conducted by Zhang et al [143]. The Langmuir-Hinshelwood model was adopted taking into account two important steps: the AB molecules adsorption on the catalytic surface and the reaction of the adsorbed molecules for the formation of H_2. As is evident from the reaction rate, if the term $K_{ads}C_{NH_3BH_3}$ is greater than 1, is a zero-order reaction and if less than 1 is a first-order reaction. Also, in the early stages of the reaction, when the term $K_{ads}C_{NH_3BH_3}$ is significantly larger than 1, the reaction rate is proportional to the mass of catalyst (m_{cat}) and inversely proportional to the volume of the solution (V_{sol}).

A work by Chen et al. [138], proposed a bimolecular Langmuir-Hinshelwood model for the decomposition of AB on a Pt/CNT catalyst since, CNT provide Pt catalysts with an effective electron transfer system toward significantly enhanced H_2 generation rate. Based on their experimental results, the reaction between the adsorbed NH_3BH_2* and H_2O* is the rate-limiting step. The authors also assumed that the adsorbed species of H*, H_2O* and NH_3BH_2* are the dominating surface species. Based on the above, the reaction rate expression is depended on the concentrations of H_2O and AB, the Arrhenius constant (k), reaction equilibrium of step 7 (K_7) which is the reversible reaction of AB with two active sites, H_2O adsorption equilibrium constant (K_{H_2O}), H_2 dissociation constant (K_{H_2}) and on the partial pressure of H_2 (P_{H_2}).

When AB undergoes through solid state decomposition then the Avrami-Erofeev kinetic model is used [139,140,141,142] where the progress of the reaction is expressed by the term a as shown in Table 6. The term a represents the progress of the reaction and is estimated by the difference of the initial mass and mass at a specific time t divided by the difference of the initial and the final mass of the reactant. The constant n can have values of 2, 3 or 4 depending on the growth phenomena. Many studies are based on the Avrami-Erofeev equation by taking into consideration different reaction intermediates that occur during the solid-state of AB decomposition, such as B-cyclodiborazanyl amine borane (BCDB), B-cyclotriborazanyl amine borane (BCTB) cyclotriborazane (CTB) and diammoniate of diborane (DADB).

The kinetic model selection is significant on the model development phase since it describes the evolution of the reaction, and it must be chosen based on the characteristics of catalyst material and the conditions of the reaction. Without appropriate kinetic parameters, such as kinetic constants, adsorption constants and reaction orders, the model may fail to accurately predict conversion rates. The reaction rates along with the governing equations contribute to the solution of the problem. The section below describes in detail the different simulation models

Table 6
Reaction rate equations for H_2 production from ammonia borane decomposition.

Catalyst	T (°C)	Pressure (bar)	H_2 generation rate (ml $min^{-1}g_{cat}^{-1}$)	Rate equation	Ref
Co-B	22–80	–	71.72–5474.80	$r_{NH_3BH_3} = k$	[136]
Co-B	22–80	–	71.72–5474.80	$r_{NH_3BH_3} = kC_{NH_3BH_3}$	[136]
Co-B	22–80	–	71.72–5474.80	$r_{NH_3BH_3} = \frac{K_{ads}C_{NH_3BH_3}}{1+K_{ads}C_{NH_3BH_3}}$	[136]
3 wt% Ru/C	16–55	–	843 (25°C) 8327 (55°C)	$r_{NH_3BH_3} = \frac{m_{cat}}{V_{sol}}k\frac{K_{ads}C_{NH_3BH_3}}{1+K_{ads}C_{NH_3BH_3}}$	[137]
Pt/CNT	20–50	–	–	$r_{NH_3BH_3} = \frac{kK_7K_{H_2O}C_{H_2O}C_{NH_3BH_3}/\sqrt{K_{H_2}P_{H_2}}}{\left(K_{H_2O}C_{H_2O}+1+K_7C_{NH_3BH_3}/\sqrt{K_{H_2}P_{H_2}}\right)^2}$	[138]
–	–	–	–	$[-ln(1-a)]^{\frac{1}{n}} = kt$	[139,140,141,142]

focusing mainly on the development of CFD models presenting the mass and heat balance equations of different systems.

3. Development of simulation models

Computer simulation is a functional tool that can represent a plethora of operating systems to analyse and understand different key parameters under various assumptions and scenarios [144]. Moreover, it contributes to solve problems and in decision making situations with solely concern to be the preciseness of the model. The absolute model validation is costly and time consuming and the amount of accuracy is specified prior to the development [145]. Simulation models in chemical reaction engineering (CRE) field are mainly used to solve differential equations considering fluid flow, diffusion, mass and heat transfer phenomena, reactions etc [146]. However, choosing the most proper software in order to compute the mathematical model is critical [147]. Also, it remains a challenge the model development of industrial scale systems due to the complex phenomena occurring which require an important amount of data and more advanced technologies and measurement techniques that might not be available. Thus, the popularity of compartmental method has raised in recent years with main focus on industrial applications and phenomena [148]. Especially, the hand calculation of such industrial complex problems that include many thousands of equations is impossible, and simulation models are of great value across the spectrum of engineering. Thus, CFD simulation models have gained the interest of the scientific world, and their popularity has risen within the recent years. They are showing superior capabilities on the design, validation and optimisation of chemical processes with different approach [149]. Many efforts have been put to overcome challenges such as the high accuracy especially in multiphase flow systems which is discussed further down in the review.

3.1. CFD simulation models

In the CRE field, the prediction of fluid flow behaviour and reaction and reactor performance are considered as privilege. CFD can resolve different fundamental equations together with conservation equations to offer a solution on various challenges. The past 15–20 years it has been noted an augmentation in the utilisation of CFD modelling to describe several problems as well as the publication of CFD works. The model might not only include chemical processes but also mixing, separation, drying processes that might incorporate except the species and energy balances, equations on electric or magnetic fields and radiation flux for the solution of microkinetic models, multiphase models, population balance models, and thermal and electrochemical models [150]. Additionally, the CRE field plays a vital role on the design and scale-up of the chemical reaction processes. The ability of CFD simulation models to provide insights of the design and the scalability of a system results to less time-consuming and cost-effective procedures in contrast to the actual experimental procedure with expenses of consumables and equipment. Rodriguez and Amores [151], stated that the simultaneous analysis of various phenomena occurring withing the system in a plethora of conditions consist the CFD tools dominant and at the same time inexpensive appropriate for novel investigations and predictions and for optimisation purposes. The continuous development of models contributed to the enhancement and improvement of the computational tools being able to demonstrate in more detail complex problems of multiphase and multiscale systems incorporating multiphysics phenomena with in depth investigation of microkinetics [152]. Some of the most known commercial CFD software are the ANSYS Fluent, CFX and COMSOL Multiphysics being very easy and convenient to use [153].

In order to solve the defined equations in space and time a numerical method should be selected. Many numerical analysis methods exist that convert the differential equations which are continuous functions in a set of algebraic equations at discrete counterparts, whereas this process is also known as discretisation [154]. There are many discretisation methods, but currently the main ones used in CFD models are the finite element method (FEM) and finite volume method (FVM) [155]. The first one divides the solution region into smaller domain-elements based on a piecewise approximation of the solution. This approach has the ability to formulate solutions of each element before assembling all the elements together to describe the problem [156]. In the FVM there is not any transfer between the physical and computational coordinate system as the discretisation takes place in the physical space. Moreover, it is considered more suitable to solve flow problems in more complex geometries having a wide range of applications while its mathematical formula remains simple [157]. It is based on the integration form of partial differential equations (PDEs) to be solved. Every geometry is discretised into finite volumes whereas the governing equations are solved for each volume [155].The ANSYS program is developing and analysing systems using FEM for structural, thermal mechanical, CFD, electromagnetics and other applications. The linear systems solution consists of the most significant step for most of models. Moreover, it has the capability to include direct, pre- and post- frontal solver including linear static analysis, multiple non-linear analysis, modal analysis and other types of analysis [158]. Similarly to the ANSYS program, COMSOL Multiphysics is another FEM and PDE tool finding application in many areas including chemical engineering, AC/DC, acoustics, heat transfer, earth science, structural mechanics etc., with its library consisting a plethora of materials [159].

One of the major concerns, as indicated in the beginning of this section, is the validity of the model and the assurance of the quality of the obtained results. However, rather than finding the reasons that cause the inaccuracy, it is suggested to handle the numerical errors and control them [160] and especially investigate the relation between the error and the mesh. The computational mesh divides the geometry domain into a set of discrete cells with the points to be called grid nodes and are located at the edges of the cells or in the centre of the cell [161]. The mesh generation is also called as grid generation and many of the existing commercial CFD tools have built-in mesh generators and independent grid generation packages. Mainly the mesh cells are hexahedral, tetrahedral, square pyramids or polyhedral [162].

Another important factor to solve the PDEs is to define the boundary conditions (BC) of the model [163]. The most typical BC often used are the no-slip BC, axisymmetric BC, inlet–outlet BC and periodic BC and are applied with main aim to direct the motion of the flow [161]. For macroscopic flow problems it is widely used the no-slip BC at the solid–liquid interface. However, at micro- or nanoscale fluid transport problems the liquid spillage on solid surfaces might be performed as downsizing can affect many parameters such as surface to volume ratio, solid–liquid interface properties etc [164]. Maxwell proposed a velocity slip BC for rarefied gas flows at solid surfaces with the BC being able to predict if a rarefied gas could slide over a surface and what variations in temperatures could enhance the force that makes the gas flow slide over a surface from colder to hotter regions, known as thermal creep [165].

3.2. Equations

A plethora of models has been developed according to the formation of gas and liquid fuels from CO_2 capture and utilisation as well as from other feedstocks resulting pure H_2. The following section summarises the most used modelling equations for different configuration processes. The governing equations along with the kinetic rates and BC are solved using the different softwares to obtain the solution of the designed model. To start with, for a batch reactor configuration, mostly used in lab-scale investigations, it is assumed that is a perfectly mixed system with constant volume where there is no inflow or outflow from the reactor. Moreover, in gas phase the reactants are regarded to be ideal and in liquid phase are considered to be incompressible and ideal. The development of such simple model is performed in 0D with the mass balance equation of species, *i*, to be expressed as:

$$\frac{dc_i}{dt} = R_i \tag{18}$$

where, c_i is the concentration of species, i, and R_i displays the sum of the contribution of each reaction to the reaction rate. The energy balance for the batch configuration is described as:

$$V_r \sum_i c_i C_{p,i} \frac{dT}{dt} = Q + Q_{ext} + V_r \frac{dp}{dt} \tag{19}$$

where, V_r is the volume of the reactor, $C_{p,i}$ is the components molar heat capacity and T and p the temperature and pressure, respectively. Q denotes the heat due to the chemical reaction and Q_{ext} is the external heat.

Continuous flow systems exist also in literature with the most popular configuration to be the packed bed reactor. The CFD model generally consist of many assumptions especially for more complex systems as the continuous flow with some of them being the application of steady or un-steady state, isothermal or non-isothermal conditions, plug or laminar flow, ideal gas behaviour, constant physical properties and transport coefficients and no-slip conditions [14]. 2D or 3D configurations are designed for a packed bed reactor with the mass balance equation, in steady state, of the species inside the packed bed area to be given as:

$$u_x \frac{\delta c_i}{\delta x} = D_{i,A} \frac{\delta^2 c_i}{\delta x^2} + D_{i,T} \frac{\delta^2 c_i}{\delta y^2} - J_i S_b \tag{20}$$

where, D_i is the axial dispersion coefficient in the axial and transverse directions, J_i is the molar flux of fluid in the catalyst and S_b the surface-active specific area of the catalyst. The mass balance equation in unsteady state for the species inside the packed bed reactor is transformed as:

$$\frac{\partial c_i}{\partial t} + \nabla \bullet J_i S_b + u \bullet \nabla c_i = R \tag{21}$$

For heterogeneous chemical reactions that are conducted on the surface or within a catalyst particle it is important to consider the mass balance equation of the species inside the catalyst. The mass balance can be described across the particle shell at r_{dim} with a predefined 1D extra dimension on the normalised radius of the catalyst particle, where $r = r_{dim}/r_{pe}$.

$$4\pi N \left\{ r^2 {r_{pe}}^2 \varepsilon_{pe} \frac{\partial c_{pe,i}}{\partial t} + \nabla \bullet \left(- r^2 D_{i,eff} \nabla c_{pe,i} \right) = r^2 {r_{pe}}^2 R_{pe} \right\} \tag{22}$$

where, N is the number of pellets per unit volume, $D_{i,eff}$ is the effective diffusion coefficient and R_{pe} is the reaction rate term per unit volume of the catalyst particle.

To define the hydrodynamics of the reactor system Navier-Stokes equation is used combined with the continuity equation to demonstrate the conservation of mass and momentum, expressed as:

$$\rho_i \left(\frac{\partial u}{\partial t} + u \bullet \nabla u \right) = \nabla \bullet \left[-PI + \tau \right] + F \tag{23}$$

$$\frac{\partial \rho_i}{\partial t} + \nabla \bullet (\rho_i u) = 0 \tag{24}$$

where, P is the pressure, τ is the viscous stess tensor and F is the volume force vector.

In addition, investigations occurred in coated wall reactors not only for the CO_2 methanation but also for the methanol steam reforming (MSR) for H_2 production [166,167]. In the characteristic design of coated wall configuration, the solid catalyst particles are loaded in a packed layer in contact with the wall of the reactor [168]. Thus, the mass balance equation of species in the unpacked area of the configuration is described as:

$$u_x \frac{\delta c_i}{\delta x} = D_i \left(\frac{\delta^2 c_i}{\delta x^2} + \frac{\delta^2 c_i}{\delta y^2} \right) \tag{25}$$

The energy balance for the continuous reactor systems is expressed as:

$$(\rho C_p)_f u_f \nabla \bullet T_f + k_f \nabla \bullet T_f = Q_f \tag{26}$$

where, $C_{p,f}$ is the specific heat of fluid, k_f is the conductivity of fluid and Q_f is the production of heat in the fluid domain.

Multiphase flow models can also be used to evaluate the interaction of the different phases. These types of models are very significant in heterogeneous catalytic systems where the catalyst is in solid phase and the reactant is either liquid or gas. There are two main approaches for multiphase flow modelling: the Euler-Euler (E-E) model and Euler-Lagrange (E-L) model. The E-E model has been more suitable for simulating complex and large amount of solid particles, where the kinetic theory of granular flow (KTGF) is applied to derive the physical properties of the dispersed phase [169].

In the E-E model, each phase is considered as a continuum and equations for conservations of mass and momentum (Eqs. (27) and (28)) is solved for each phase (gas/liquid and solid), incorporating also the volume fraction α_k, (where $\sum \alpha_k = 1$ and k symbolises the phase), and the interactions between different phases are modelled. It can be used for gas–solid systems and gas–liquid systems where solids, gas bubbles or droplets act as a granular material. In the right-hand side of Eq. (28), the first term symbolises the gravitational body force, the second is the pressure force, third is the stress tensor and the last term represents the external and interaction forces (collision, lift force, drag force etc.) [170].

$$\frac{\partial (\alpha_k \rho_k)}{\partial t} + \nabla \bullet (\alpha_k \rho_k u_k) = 0 \tag{27}$$

$$\frac{\partial (\alpha_k \rho_k u_k)}{\partial t} + \nabla \bullet (\alpha_k \rho_k u_k) = \alpha_k \rho_k g - \alpha_k \nabla p_k + \nabla \bullet (\alpha_k T_k) + F_k^{inter} \tag{28}$$

The energy balance equation is shown in Eq. (29), where H_k is the specific enthalpy, λ_k is the thermal conductivity, and Q_{pk} represents the heat transfer between fluid and particle.

$$\frac{\partial (\alpha_k \rho_k H_k)}{\partial t} + \nabla \bullet (\alpha_k \rho_k u_k H_k) = \nabla (\lambda_k \nabla T_k) + Q_{pk} \tag{29}$$

The species transport equation is given by Eq. (30), where Y_i represents the mass fraction of i th species in the fluid phase [171].

$$\frac{\partial (\alpha_k \rho_k Y_i)}{\partial t} + \nabla \bullet (\alpha_k \rho_k u_k Y_i) = - \nabla (\alpha_k J_i) + \alpha_k R_i \tag{30}$$

The E-L model, also called discrete particle models (DPM), solves one phase with the Eulerian framework (considered continuum), and a Lagrangian framework is considered for all the dispersed phases (solid phase). The velocity of particle is solved according to Newton's second law, which can be written as:

$$\frac{du_p}{dt} = \sum F_p \tag{31}$$

The term on the right-hand side represents all the forces acting on it. Usually, the gravity, buoyancy, drag, virtual mass, lift and pressure gradient forces are usually considered which should be incorporated with the momentum equation of the continuous phase [172].

The energy balance is described according to a Lagrangian approach as:

$$c_p m_p \frac{dT_p}{dt} = Q_p \tag{32}$$

where c_p is the specific heat capacity of the particle, m_p is the particle

mass, T_p is the particle temperature, and Q_p denotes the resulting power of heat source acting on the particle [173].

4. Reactor configurations

Despite the effort to achieve high conversion and selectivity of a desired product within a reactor, downstream separation units are primarily responsible for achieving the desired purity. However, by optimising reactor technology, low-value by-products/waste materials can be reduced and the installation of a downstream separation unit to increase purity might not be needed [174]. Thus, it is evident that reactor design plays a crucial role in the efficient operation of a reaction. The geometric configuration, constructive materials, mass/heat transfer properties and fluid flow characteristics are parameters of significant importance when designing a reactor. Nevertheless, carrying out real-time experiments for the design and optimisation it is time-consuming and not cost-effective [175].

CFD can solve momentum and conservation equations for the visualisation of fluid flow and heat transport phenomena for various chemical, physical and biological processes [176]. Historically, CFD was mainly used for mechanical and aerospace engineering and in many cases CFD simulations studies have been applied to find the best approach for obtaining the optimal structural parameters of aerodynamic shape and automobiles [177]. By solving momentum equations that describe the fluid flow inside the reactor, important information on the reactor geometry can be achieved through the model. For example, based on the flow patterns, the exact position of inlet/outlet and baffles can be found in order to provide efficient mixing and residence time. Dead zones and short-circuiting can be detected and minimised or even eliminated. Regarding energy balances, when incorporated in a model, hot spots can be identified and eliminated by improving temperature distribution.

Computational studies can therefore be implemented for reactor design, coupling robust modelling and accurate kinetic data in order to build a reactor design, giving the possibility of trying different configurations [178]. Many studies also focused on the optimisation of existing reactor systems to maximise the performance of the reactor based on their experimental data. When developing a CFD model, is crucial to consider model fidelity, design practicability and computational cost. For industrial-scale systems where more unit parts are needed for real-life experiments, 3D modelling is more efficient and accurate, while 2D systems despite their limitations can offer valuable insights into flow trends and are very practical for initial design evaluations [178]. However, in some cases where the system is symmetric, a 2D-axisymmetric model can be developed saving computational resources [179,180]. 2D models can also be used when modelling cross-section of reactors.

4.1. Batch reactors

Batch reactors are usually a tank with a capacity ranging from few millilitres to over 100 L, depending on the application and scale. They are preferred due to the simplicity of the system and scalability. Considering the effect of mixing in designing a batch system, many factors are considered such as mixing duration, power draw, impeller capacity and impeller shape/size. Thus, many CFD studies were conducted through the years for the simulation of the mixing pattern in batch systems. Exploiting the relationships between mixing, reaction, operating conditions, and reactor configuration may be more beneficial in determining the ideal reactor set-up and operating parameters [181].

A study by Rosa et al. [182], presented a numerical research aimed at optimising the production of bio-hydrogen (bio-H_2) in an anaerobic sequencing batch reactor (ASBR). CFD modelling was utilised to obtain accurate results on the mass transfer, momentum and kinetics of the associated reactions. The two-phase flow (liquid mixture and gas bubbles) was described by the E-E method. The liquid phase was characterised as a Newtonian fluid, while for the dispersed phase, the properties of biogas were applied. It was also investigated whether the addition of baffles to the bioreactor would offer better mixing. Large vortices were observed in the unrestricted flow, however, when one baffle with a length half of the radius partially obstructs the flow, the flow followed a preferred direction with smaller vortices. It was discovered that the addition of a baffle measuring ¼ of the bioreactor radius, equalised the flow and resulted in the largest increase in turbulent kinetic energy increase with a minimal impact on the pressure drop.

The impact of a reactor's impeller distribution on the flux patterns in a process for bio-H_2 generation was ascertained by Niño-Navarro et al [183]. CFD studies were used to analyse and characterise the flux patterns. Evaluations were conducted on two different mixing systems: radial flow (Rushton) and predominantly axial (pitched blade PB4). The most effective system, as exhibited by CFD modelling, was the PB4 impellers as seen in Fig. 2, where the velocity contours are presented. The flow patterns produced by the PB4 impellers, drive the molecules of bio-H_2 into the headspace and also encourage the passage of dissolved bio-H_2 to the gaseous phase. Besides, the hydrodynamic behaviour, the PB4 impellers enhanced the metabolic process, causing higher cell growth and substrate consumption and thus, increasing bio-H_2 generation.

A thorough modelling approach was used by Maluta et al. [184], to examine a gas–liquid bioreactor for H_2 production through the dark fermentation of organic materials. For the simulation, a two-fluid model was chosen, considering therefore the liquid and gas phase as interpenetrating continua interacting through the interphase transfer terms. The bioreactor operated at both batch and attached growth modes. Two reactor geometric configurations were studied: one designed for an efficient fluid dynamics behaviour where the supports for the attached-growth of bacteria were placed inside the draft tube only, and the other designed to boost the productivity of H_2 where the supports were placed outside the draft tube. Their main difference was the volume and the position of supports. The results indicated that the configuration with the supports outside of the reactor reached steady state quicker due to the higher H_2 generation rate. Overall, the analysis of both configurations mentioned above, showed that the system was able to produce more H_2 when the amount of biomass is increased, but if the interphase mass transfer rate for H_2 stripping from the aqueous to the gas phase, is not quick enough, can lead to significant H_2 supersaturation.

Lefebvre et al. [185], conducted a modelling investigation of an innovative tube bundle reactor (TBR) and a slurry bubble column reactor (SBCR) for catalytic three-phase CO_2 methanation as a component as an aspect of a Power to Gas (PtG) process chain. The model used axial dispersion coefficients for the gas and liquid phase and considered two bubble classes, assuming that large bubbles flow upwards, while small bubbles recirculate with the liquid phase entrained by the large bubble flow. Mass transfer took place between the bubbles and the slurry phase. The heterogeneous flow regime was used to simulate the SBCR to provide a high gas hourly space velocity (GHSV). The reactor was functioning under semi-batch flow conditions, meaning that it did not circulate any new or recycled slurry and it only allowed the gas phase to get through. Compared to SBCR, the TBR allows for significantly higher GHSV during steady-state operation. A sensitivity analysis exhibited that mass transfer limits the SBCR and heat transfer limits the TBR. The SBCR temperature displayed minor changes, and the outlet gas composition complies with high gas quality standards. However, TBR underwent major temperature changes in a short amount of time, leading to unacceptable temperature hot spots and out-of-spec product gas qualities. The transient behaviour of the TBR can be improved by lowering the catalyst concentration in detriment to GSHV, while the GSHV of the SBCR can be improved by increasing the specific interfacial area controlling gas/liquid mass transfer.

In a study by Lašič Jurković et al. [186], the CH_4 dry reforming reaction was investigated under both plasma-only and plasma-catalytic conditions in an atmospheric pressure spark discharge plasma reactor. Two mathematical models were created: a basic batch model and a 3D

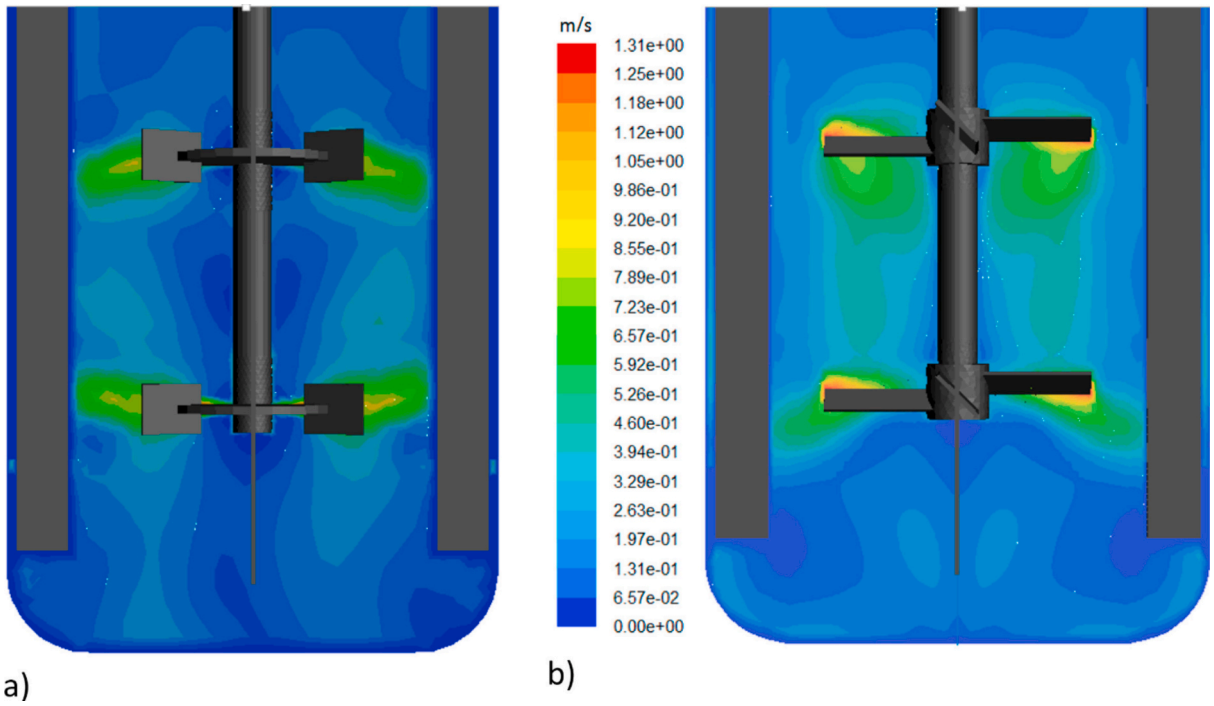

Fig. 2. CFD velocity contours of a) Rushton and b) pitched blade (PB4) impeller [183].

CFD model coupled with kinetics, accounting for the realistic three-dimensional geometry of the reactor. The experimental results demonstrated that the feed mixture of CH_4 and CO_2 was converted into H_2 and CO with great selectivity and conversions of 85 % and 75 % for CH_4 and CO_2 respectively. The CFD model was in a great agreement with the experiments (Fig. 3) due to the utilisation of simple plasma kinetics, which makes it not intensive and useful for scale-up simulations and optimisation. Moreover, by optimising the reactor geometry the coking issue could be significantly reduced.

Adamou et al. [187], simulated a two-neck round bottom flask batch reactor that was tested experimentally for H_2 production from HH decomposition. Aim of the work was to evaluate the velocity and temperature fields as well as the distribution of the reactant and particles in the batch system. From the CFD results it was evident that the small circular geometry of the reactor was sufficient for good mixing after 0.75 s (Fig. 4). Moreover, extra studies on the stirrer were performed in order to find the optimum size where it was shown that a medium size stirrer is more efficient for this system. The simulation was also checked for higher degrees of freedom with no noticeable difference in the results. Lastly, the CFD outcomes were in a great agreement with the experimental results contributing to a better understanding of the kinetics of HH and enhancing the possibility for future optimisation studies.

4.2. CSTR

Continuous Stirred Tank Reactor (CSTR) is considered the classical Chemical Reaction Engineering (CRE) model for a perfectly macromixed reactor [152]. CSTRs are able to achieve better separation between reactants and products due to the continuous flow in and out of the reactor. Moreover, they can handle larger reactant concentrations compared to batch systems [78]. Mixing is an important parameter for an efficient performance of a CSTR. The degree of mixing determines how efficient are heat and mass transfer. In most cases CSTRs use mechanical agitation. CFD methodology can calculate the flow field in the stirred tank and optimise the mechanical stirring as well. Since they are

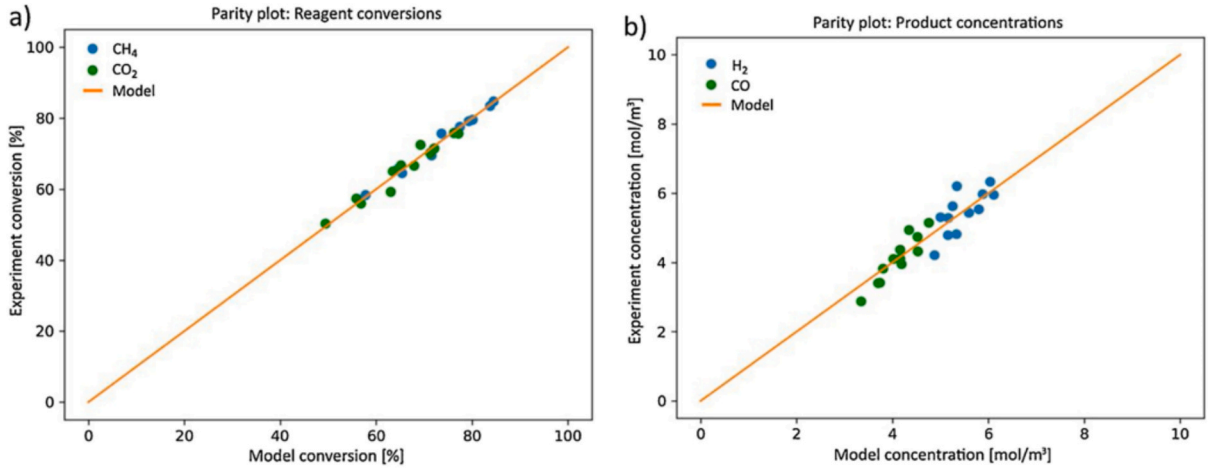

Fig. 3. a) Comparison of experimental and model conversion data and b) Comparison of experimental and model concentration data.

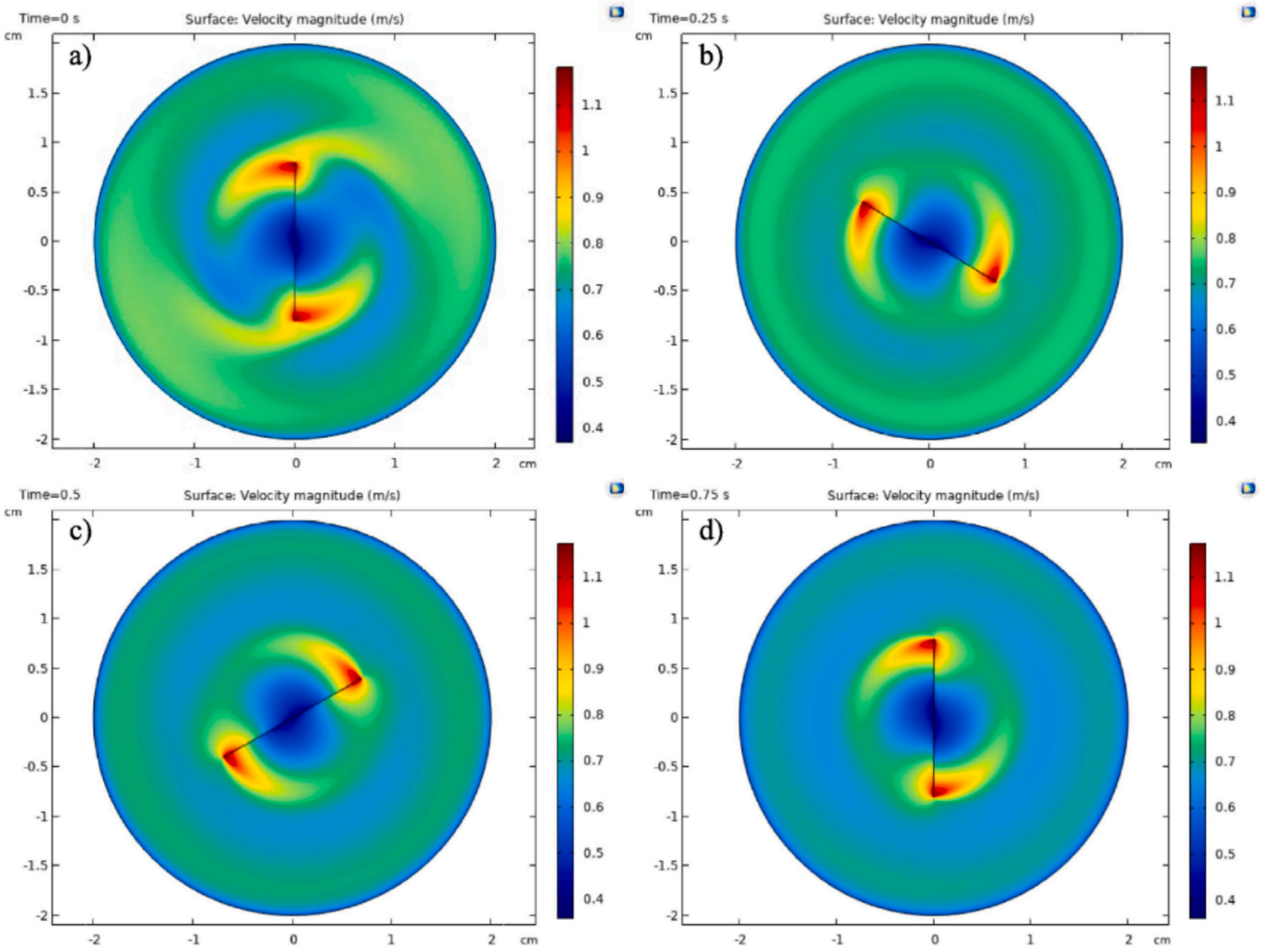

Fig. 4. Velocity field at 1400 rpm in the batch reactor at a) 0 s, b) 0.25 s, c) 0.5 s and d) 0.75 s [187].

preferred for larger-scale applications, scaling-up a reactor system is easier by achieving it computationally first to thoroughly investigate different parameters that affect its performance [152].

An existing gas–liquid CSTR was simulated by Patwardhan et al. [188], utilising CFD studies, in order to analyse the reactor performance and suggest improvement strategies. Gamma ray tomography was also used to measure the gas hold-up distribution. The concentration profiles demonstrated that there is a lack of dissolved reactant in the gas phase in the reactor and more specifically in the upper part of the reactor. Therefore, to improve the performance, different strategies were simulated such as the power input increase to the reactor, an alternative impeller configuration and distributing the gas/liquid feed to the reactor. When the gas and liquid phases were distributed at multiple locations, the total power increased by 75 % and the agitation was enhanced by 50 % at the top part of the reactor. The product quality was also enhanced by 22 %. When the upper impeller diameter was changed and made more uniform, this resulted again in an increase in total power of 75 % and an improvement of 50 % was observed at the power delivered at the top part of the reactor. The product quality was also enhanced by 20 %.

Ding et al. [189], investigated both experimentally and computationally a gas–liquid two-phase lab-scale CSTR for bio-H_2 production, using an E-E multiphase model to describe the flow behaviour of each phase. The mechanisms of the interaction of the phases were the flow resistance modelled by momentum transfer, the phase changes modelled by mass transfer and the heat conduction modelled by energy transfer. The hydrodynamic behaviour of the reactor, comprising the velocity field, turbulent kinetic energy, shear strain rate and biogas volume fraction were portrayed by CFD studies. To improve the hydrodynamic behaviour of the reactor, an optimised impeller was designed. The standard impeller design had a diameter of 100 mm and a blade angle of 45°, while the optimised impeller had a diameter of 120 mm and a blade angle of 45°. It was established that the type and speed of the impeller greatly influenced the flow patterns. The integration of simulation results with experimental observations, states that, when the impeller speed is between 50 and 70 rpm, the optimised impeller generates a better velocity distribution at lower impeller speed. Consequently, a higher H_2 yield is achieved, and a shorter start-up time is needed compared to the standard impeller. A comparison between the experimental and simulated data (RTD over 90 rpm) was conducted for the normal and optimised impeller respectively. It can be seen that there was only a 20 % relative error, indicating that the model describes well the reactor behaviour.

Ri et al. [190], simulated a 3D CFD model of a gas–liquid flow in a horizontal CSTR (HCSTR) for bio-H_2 generation. Main focus was to determine the ideal agitating speed and the appropriate three-phase separator (gas–liquid–solid three phase separations). In this study, drag force and lift force between the continuous phase (liquid) and dispersed phase (gas) were the most important for the simulation of bio-H_2 production. The best performance was achieved at low stirring rates of 40–50 rpm (Fig. 5), indicating that the HCSTR design is better suited for increasing the generation of bio-H_2 due to its comparatively large

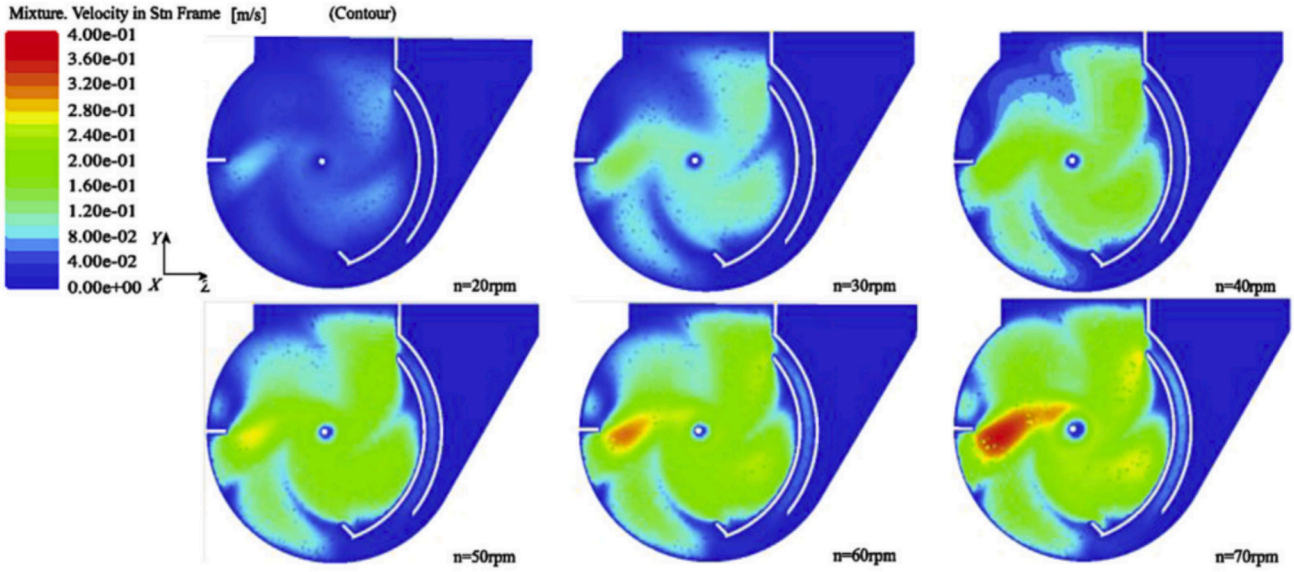

Fig. 5. Velocity contour at different stirring rates [190].

effective working volume with low production and operation expenses. It was also demonstrated how the hydrodynamic properties of bio-H_2 generation reactors influence the biological/chemical reaction within the reactor. Since there was only 21 % relative error between the measured and simulated data, suggesting that the model accurately describes the reactor behaviour, the authors concluded on the significance of the utilisation of CFD-based programs to forecast flow patterns in reactor designs.

A numerical methodology for the prediction of the generation of biogas and bio-H_2 from a horizontal and vertical CSTR (HCSTR, VCSTR) was conducted by Brindhadevi et al [191]. CFD was also applied, investigating the hydraulic retention duration, impeller speed, vortex growth, and pH influence on the bio-H_2 yield rate. Multiple simulations were performed with ideal boundary conditions for optimum biogas and bio-H_2 generation rate. The speed of the impeller was ranging from 40 to 120 rpm, and it was discovered that the rate was increased as the speed was increasing reaching to a maximum plateau at 80 rpm for bio-H_2 and 100 rpm for biogas. Based on the experiments and CFD, VCSTR performed better due to a better velocity distribution in the reactor. Comparing the experimental and simulated data, a low relative error of 8–10 % was discovered due to geometry restrictions and/or boundary conditions. Nevertheless, the error was reduced at 5–7 % by decreasing the mesh size and increasing the interaction steps. Due to the good validation of the results the authors also concluded that CFD can be implemented to any kind of reactor before scaling-up a system.

4.3. Fixed bed

Fixed or packed bed reactors are widely employed for heterogeneous catalysis for gas or liquid phase reactants. The catalytic particles are packed in a bed and are in direct contact with the reactant. The catalyst bed greatly influences the transfer process and thus, is a parameter that must be considered for a practical design and operation of a catalytic fixed bed reactor [192]. Their complex geometry has hindered the comprehensive modelling of their hydrodynamics. However, with the exponential growth of computer power coupled with modern CFD algorithms, realistic flow fields for fixed-bed simulations can now be obtained, even the flow characteristics in the near-wall region that differ from those in the bed centre. This information can be utilised directly in in-depth 3D reactor simulations or in process design modelling [193].

Darfilal et al. [194], used CFD for a packed bed thermochemical receiver/reactor setup for H_2 generation. The momentum, energy, and species transport equations were solved by the CFD model. The local thermal non-equilibrium (LTNE) model was utilised to determine the reactor's solid and fluid phases temperature fields. In this model approach, the solid and fluid phases were spatially coincident and interact between them with regard to heat transfer. Experimental data from literature were used for the validation of the developed model. The outcomes demonstrated a strong correlation between experimental and numerical data. The model, then, was utilised to numerically assess the reaction through the packed bed including packing arrangement, inlet velocity and solar radiation, to predict the thermal behaviour under various conditions. The simulation results showed that the features of porous media and the working conditions have a significant impact on the temperature distribution. It was noteworthy that the configuration of the packing had an interesting impact on the reactor's internal distribution.

The simulation of the anaerobic dark fermentation of biomass in a packed bed continuous plug flow reactor for bio-H_2 production was studied by Wodołazski and Adam Smoliński [195]. The E-L approach was adopted with a two-phase model and the liquid flow was laminar based on Reynolds number general criteria at the inlet. Depending on the conditions the rate of bio-H_2 generation ranged from 0.2 to 0.68 mg/L h. CFD results showed that within 12 days (Fig. 6), the dark fermentation process's maximum rate of bio-H_2 generation employing recirculation flow was reached. After that, the amount of bio-H_2 generated gradually reduced. The challenge of achieving consistent H_2 production may stem from anaerobic homoacetogenic microbes. It was concluded by the authors that CFD was proven useful for evaluating the reactor's performance by examining the reaction rate, interphase H_2 fluxes and other processes occurring inside the reactor.

Harkou et al. [144], examined computationally the performance of four different reactor configurations for CO_2 methanation. The four configurations were a packed bed, a coated wall, a membrane packed bed and a membrane coated wall reactor as shown in Fig. 7. The coated wall reactor performed less than the packed bed reactor (30 %), as it had lower residence time. However, higher conversion values were achieved a lower flow rate, due to the decrease of fluid velocity and thus the increase of residence time. Studies on the optimal bed thickness showed a value of 1 mm. Two different membranes (M1, M2) were then investigated for the separation of the products. M1 indicated the removal of H_2O, while M2 the removal of H_2O, CO_2 and H_2. Even though, the thickness of the two membranes was the same (7 mm), when reduced, the conversion was better with the M2 membrane.

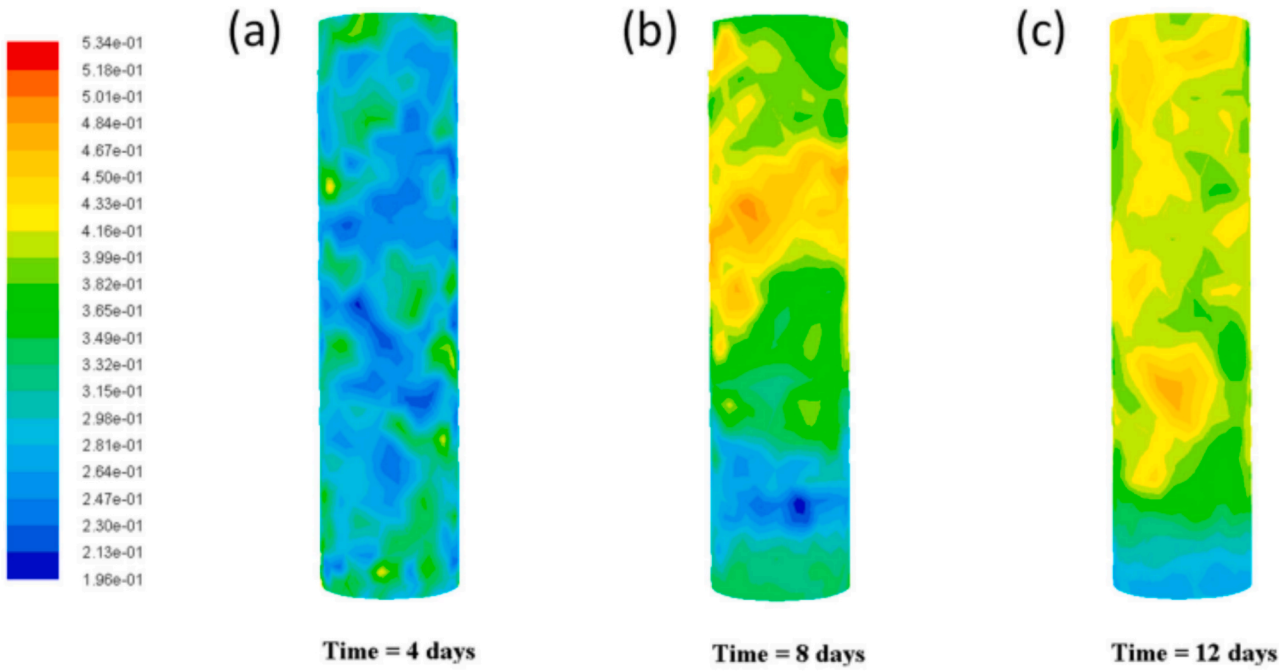

Fig. 6. Bio-H_2 concentration in the packed bed: at: (a) 4 days, (b) 8 days and (c) 12 days [195].

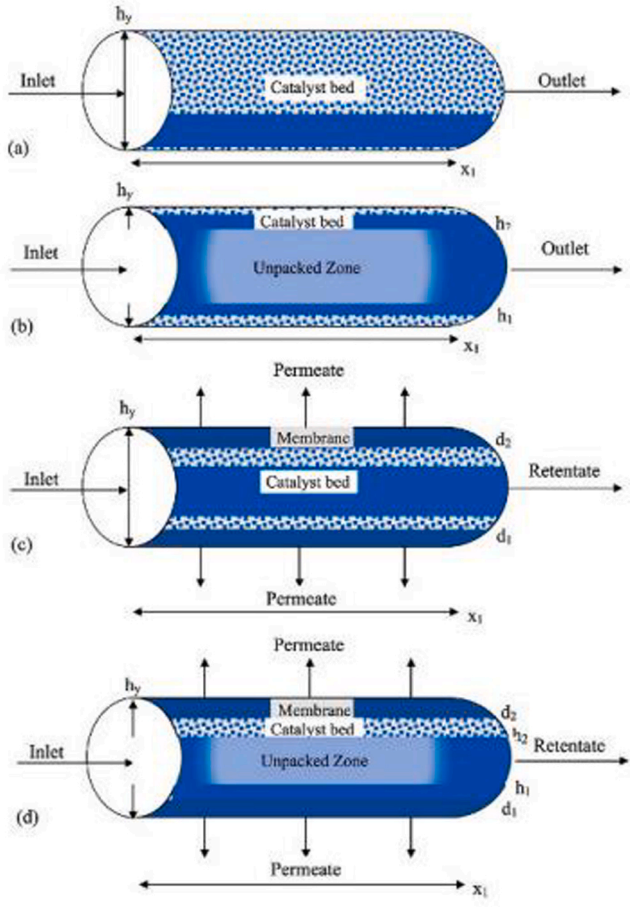

Fig. 7. Configuration of a) packed bed, b) coated wall, c) membrane packed bed and d) membrane coated wall reactor [144].

Nailwal et al. [196], investigated the decomposition of NH_3 using a packed bed catalytic reactor (PBCR) and a single tube packed bed catalytic membrane reactor (PBCMR), both, experimentally and computationally. The PBCMR outperformed the PBCR with a conversion of 93 % at 773 K and 1 bar, compared to 80 % achieved with the PBCR. The developed 2D CFD model was verified by the experimental results with an error within a range of 10 % and thus, 3D simulations were also developed for the parametric optimisation of the PBMCR. Multi-tube PBCMR were designed to demonstrate the impact of membrane tubes on the conversion of NH_3. As the number of tubes increased from 19 to 22, the conversion also increased from 93 to 96 % (Fig. 8), due to a more available permeation area for H_2 promoting the process. Additionally, feed header simulations were run to ensure uniform gas distribution in the reactor at the inlet. The ideal axis ratio for an elliptical head was discovered to be 1.42.

4.4. Fluidised bed

In contrast to fixed bed reactors where the bed is stationary, in fluidised bed reactors the catalytic particles are moving, providing more efficient mixing. Moreover, the temperature distribution is better in a fluidised bed with a good heat exchanged resulting in no hot spots. Also there is better scale-up potential than the fixed bed reactor [197]. Usually, in fluidised bed reactors, particle densities are greater than liquid densities, with typical particle sizes exceeding 150 μm. Thus, an important goal of CFD studies is to simulate the complex hydrodynamics of the fluidised bed reactors that have larger particles [198].

Utilising the multiphase particle-in-cell (MP-PIC) approach, a 3D CFD model was developed in a study by Liu et al. [199], to simulate a dual-fluidised bed biomass gasifier operating at pilot scale. Particle circulation, reaction temperature, and the composition of the production gas were predicted by integrating the momentum, mass and energy transfer equations with the kinetics of homogeneous gas-phase and gas–solid reactions. Gas composition and temperature at 6 locations of the gasifier and combustor were simulated and for all cases investigated, the uncertainties were less than 20 %. It is evident from Fig. 9 that particles are completely fluidised and carried by gases from the separator to the combustor and then returned to the gasifier. Particle accumulation is also observed in the loop-seal at 5 s and continued to grow at

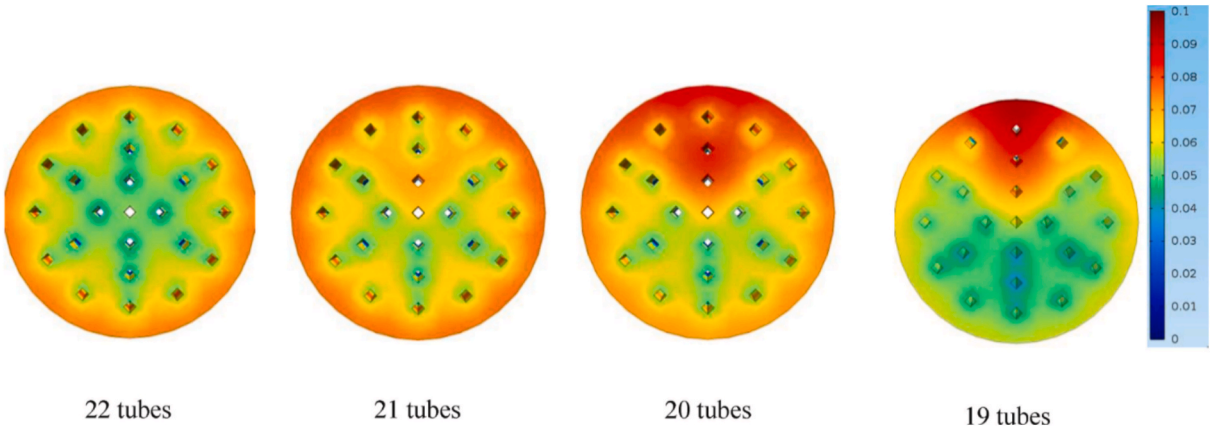

Fig. 8. Effect of number of membrane tubes on H_2 mole fraction [196].

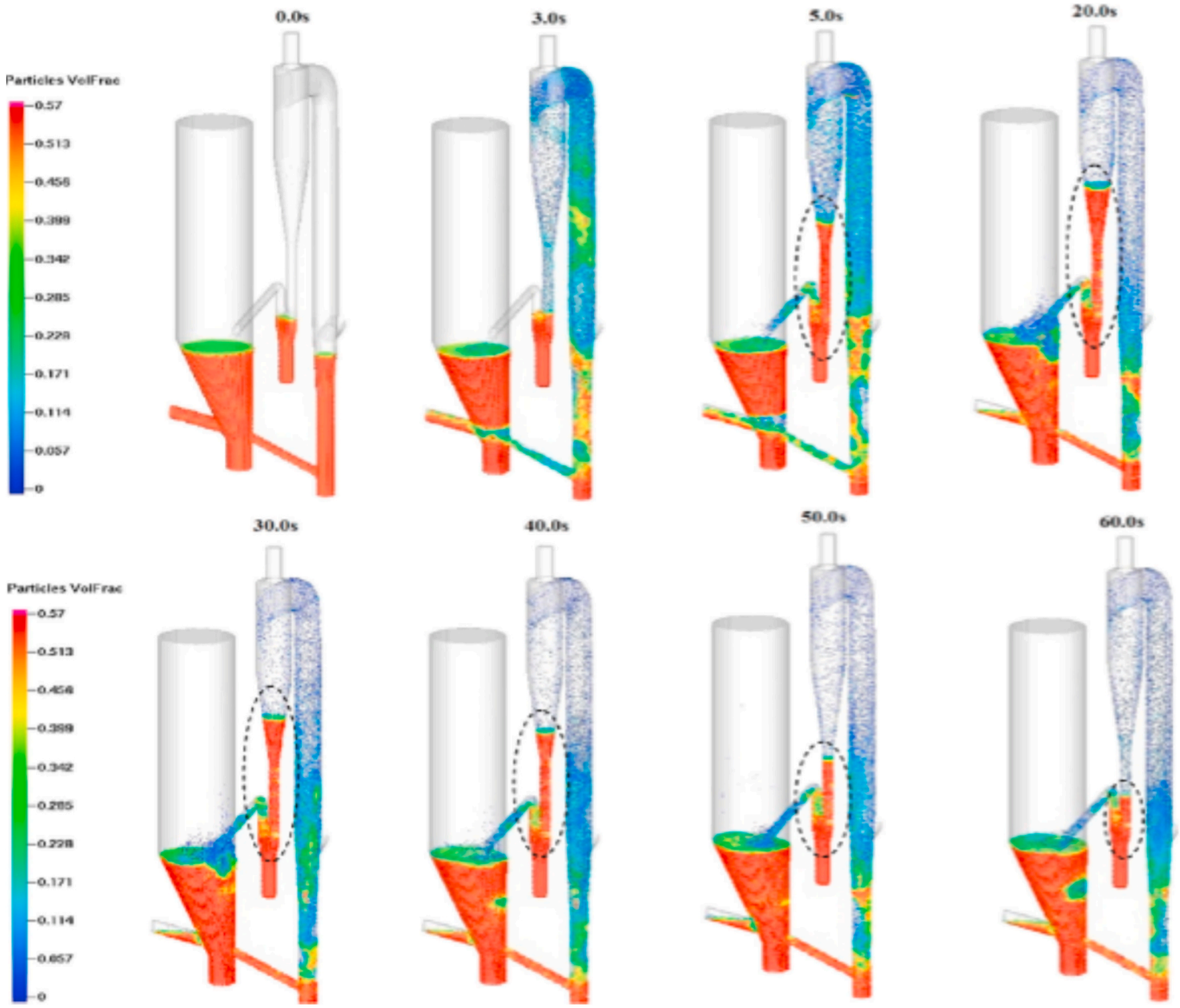

Fig. 9. Particle circulation and accumulation in the dual fluidised-bed system [199].

20 s where it reached the bottom of the cyclone separator. Then, the accumulated particles were sent to gasifier after being progressively removed from the loop-seal over a period of 30 to 60 s. Particle accumulation from CFD modelling was consistent with the observation made experimentally. Also, the CFD model accurately predicted that in the current fluidised bed system, in the presence of steam as sealing gas, neither producer gas nor air leaked to the gasifier.

The development of a CFD-Discrete Element Method (CFD-DEM) simulation of a glucose gasification in a supercritical water fluidised bed reactor was conducted by Zhao and Lu [171]. The fluid phase which was a homogeneous mixture of glucose, water, intermediate and product gases was modelled as a continuum. The solid phase (inert quartz sand) was developed based on particle motions, comprising translational motion and rotational motion, by integrating Newton's equation of motion. The analysis focused on reaction rate profiles, gas composition and particle distribution as well as on the influence of wall temperature, flow rates, bed height and the impact of chemical reactions on flow behaviour. The outcomes of the model indicated that gasification is improved by high starting bed height, low flow rate, and high wall temperature. However, at flow rates below the minimum fluidisation velocity, reduced H_2 output and gasification efficiency were observed. Below the minimum fluidisation velocity the bed is not fluidised. Big bubbles form and the bed height changes at e relatively high flow rate, causing the fluidisation to be intensified. The robustness of this model was demonstrated by the model results, which were in a great agreement with the experimental findings.

A CFD model for small-scale H_2 generation in a fluidised bed membrane reactor, was developed by Foresti et al [200]. The model incorporated two options on the permeate side (sweep gas, vacuum), comprehensive hydrodynamics of the bubble and emulsion phases, and reforming processes. For the vacuum configuration, the simulation was initially evaluated against another well-established simulation; for the sweep gas configuration, experimental findings were employed. The model was then used to evaluate the membrane reactor's performance when it is powered by bioethanol and incorporated into a micro-combined heat and power (m-CHP) system using a PEM fuel cell. The maximum deviation on H_2 output at base-case conditions was 1.15 %. For a fixed membrane area, the difference in H_2 output among the simpler models that do not take into consideration the fluidised bed's hydrodynamics and transport phenomena, ranged from 10 to 55 % for the scenarios when the permeate side had a sweep gas or vacuum, accordingly. The primary cause of this, particularly in the sweep gas case, is the slow gas diffusion in the comparatively thick membrane supports, keeping the partial pressure of H_2 at the membrane interface significantly higher than the majority of the permeate, preventing the sweep gas's intended effect.

CFD simulations were applied for sorption enhanced steam methane reforming (SESMR) in a circulating fluidised bed (CFB) riser by Phuakpunk et al [201]. The E-E model with the KTGF were applied with heterogeneous kinetics of the catalyst and the sorbent in 2D and transient simulation. The main focus of this work was the design of an appropriate pilot-scale CFB riser that generated high-purity H_2 and high flux. The results of 32 runs demonstrated that the SESMR could function in the CFB riser since, in many cases, the H_2 purity could approach 99 % as theoretical equilibrium. First off, compared to the reaction parameters, the design parameters were clearly more efficient. The most important parameters were the velocity of gas, riser's diameter and solid flux which, with the exception of the gas velocity, had positive impact on both H_2 purity and flux. The highest H_2 purity value was 98.58 % obtained by the optimum case. Because of the well-developed axial and radial solid distributions that did not exhibit excessive segregation between the sorbent and catalyst, the hydrodynamics of this ideal scenario demonstrated that SESMR had almost reached completion at 5 m height, therefore the riser's 7 m height was adequate.

Using the MP-PIC approach, the thermodynamic and hydrodynamic properties of the sorption enhanced steam ethanol reforming process in a fluidised bed were explored by Yu et al [202]. Firstly, the model was validated by experimental data. Since the results were in a good agreement, the model approach was used to predict the flow dynamics in the fluidised bed. The findings showed that while the heat transfer coefficient increased with bed height, the solid temperature decreased. H_2 and CO_2 were distributed throughout the bed and primarily were building up in the reactor's upper section. H_2 and CO_2 yields increased as the ratio of H_2O to ethanol was increased. Studies on the particle parameters showed that large particle Reynolds number occurred mostly with a small solid volume percentage and the particle heat transfer coefficient increased with increasing the slip velocity.

4.5. Microreactors

In recent years, microreactors have emerged as a promising alternative technology. It is simple to adjust the size, shape and contact time of the fluid–fluid interphase. Superior mass and heat transfer rates have been observed by microstructured reactors. Due to these characteristics, they are suitable for quick, exothermic and explosive reactions. Moreover, their large surface to volume ratio limit the diffusion length, contributing to their high efficiency [203]. One of the most common methodologies for the investigation of micromixing is the Navier-Stokes equation coupled with the mass transfer equation. By that, CFD can characterise mixing by means of diffusion. Another methodology used by CFD is to solve the momentum and mass transfer equation, giving information regarding flow and concentration [204].

A work by An et al. [205], aimed to investigate, through mathematical modelling, various microreactor configurations to improve overall performance. The study was performed for a square cross-section channel microreactor with eight distinct configurations. The channel geometries were parallel, wavy, pin-hole, oblique fin, serpentine, coiled, coiled with serpentine and coiled with double serpentine as presented in Fig. 10. Experimental results derived by Bond et al. [206] were used for the validation of the model at two different inlet stoichiometric ratios. As can be observed (Fig. 10i), the current simulation closely matched with the experimental outcomes, particularly at higher stoichiometric ratios, whereas the model data by Bond et al. [206] and Canu et al. [207], greatly deviated. This could be due to the fact that the current model, accounted for the fluid characteristic's temperature dependence, another example of the on-going development of CFD modelling. Their results were compared to those of traditional straight microreactor with the same cross-section area. The methane single phase process was investigated for a variety of geometric parameters and Reynolds number and the reaction performance was evaluated based on figure of merit. In comparison to rectilinear reactor designs, coil-based reactors offered better conversion at all Reynolds numbers but with a high pressure drop penalty. Thus, coil-based reactors have substantially lower figures of merit than those of other geometries. Among the tested configurations, the pin-hole design had a great figure of merit with great conversion, offering a great potential for utilisation as a novel microreactor.

The objective of a work by Harkou et al. [208], was the development of a scale-out membrane microreactor for use as a capture system by studying it both experimentally and computationally. The microreactor was designed to examine the velocity profile within each microplate for both gas and liquid flows. The primary goal was the achievement of a uniform flow distribution at each reactor plate. Based on the CFD models, nearly uniform flow distribution was obtained at each layer of the scale-out microreactor. For both gas and liquid flows, the highest variation was less than 6 %. Improved flow distribution was achieved by optimising the inlet/outlet tube's radius. In addition, experimental studies on CO_2 removal with a single-channel reactor were compared to the results of the CFD simulation. Similar to expectations, single and scale-out microreactors did not produce comparable CO_2 removal outcomes. Contrary to the experimental data, which suggested that an uneven flow distribution would be obtained, the CFD models demonstrated a nearly uniform distribution, supporting the theory that the

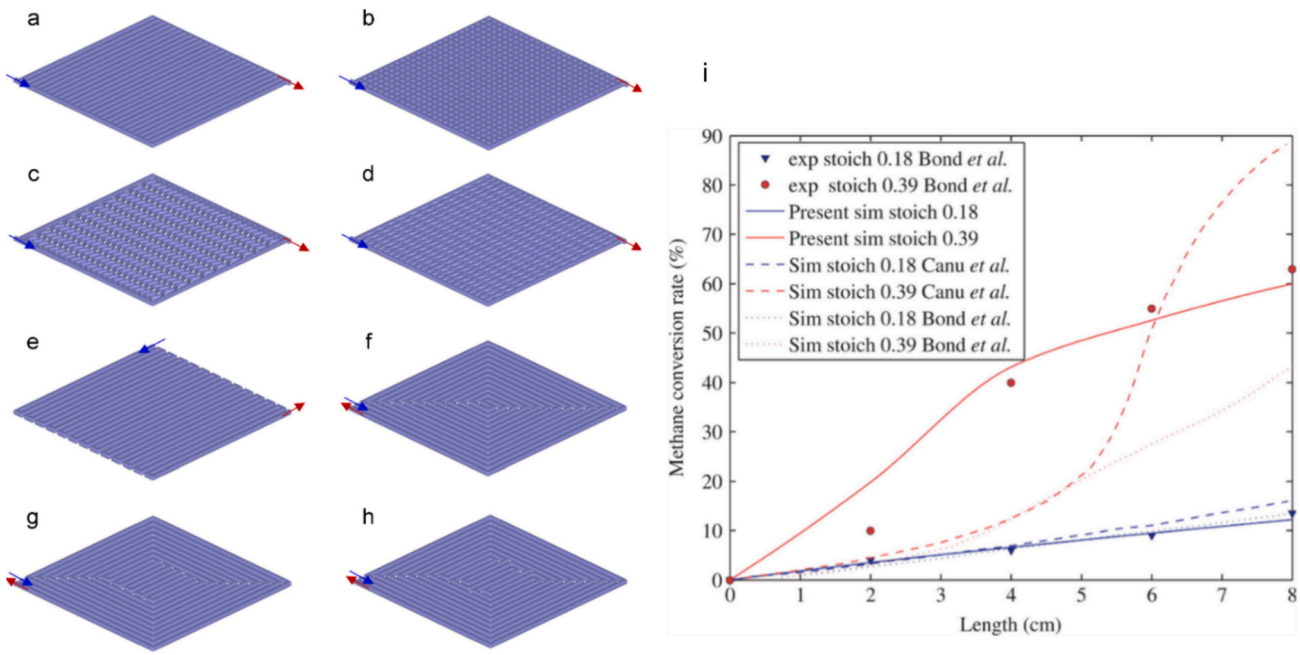

Fig. 10. Configuration of a) parallel, b) pin-hole, c) wavy, d) oblique fin, e) serpentine, f) coiled, g) coiled with serpentine and h) coiled with double serpentine, i) experimental and simulation data comparison at low and high inlet stoichiometry ratio [205].

maldistribution is caused by flaws in the plate fabrication process. Furthermore, the difference between the results could also be explained by phase breakthrough of the liquid into the gas phase or vice versa.

Studies on FA decomposition over a Pd/C catalyst were performed by Hafeez et al. [209], at moderate temperatures using a fixed bed and batch microreactors. A CFD model was also developed to validate the experimental findings. To demonstrate the accuracy of the CFD model, the simulation of the packed bed microreactor was compared with experimental outcomes. CFD was utilised to predict the heterogeneous particle–fluid transport phenomena within the microreactor using finite element methodology. The packed bed microreactor was modelled as 2D under the assumption that mass, temperature, and velocity profiles occur in the radial and axial directions only. As observed in Fig. 11, modelling and experimental results have a strong correlation and thus, the model was used for further studies. It was demonstrated that the packed bed microreactor could achieve slightly higher conversion than the batch microreactor, with less than 10 % difference, indicating that their performance were comparable. The CFD model was also able to predict the catalyst deactivation occurring from the generation of the poisoning species CO. Lastly, the CFD model showed that there were no limitations on external or internal mass transfer. Since all model results were in a great agreement with the experimental findings, the authors concluded that this model can be used to predict FA decomposition in fuel cell applications.

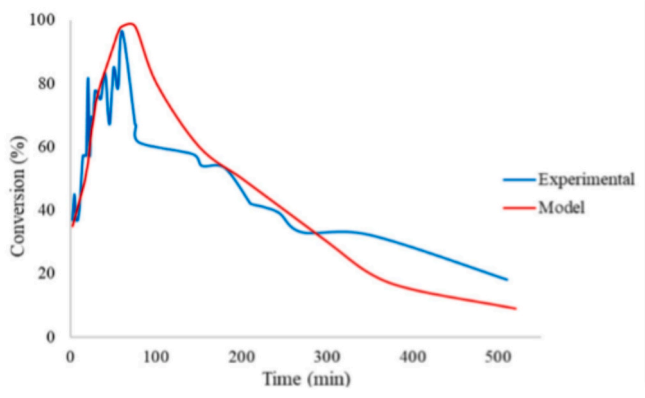

Fig. 11. Experimental data and CFD modelling results comparison for packed bed microreactor [209].

Another study by Hafeez et al. [210], evaluated the efficacy of three microreactor configurations consisting of packed bed, coated wall and membrane microreactors (Fig. 12) for H_2 generation. Before investigating different parameters, the robustness of the model was determined by comparing the CFD outcomes with the experimental work (Fig. 12d). The outcomes showed that there was a comparable performance between the packed bed and coated wall microreactors, both experimentally and computationally. In contrast to the other microreactors, the membrane microreactor demonstrated noticeably better performance. Previous research using CFD, revealed that the generation of the poisonous species CO, was the reason for the catalyst's loss of catalytic activity in the packed bed microreactor. In the case of membrane microreactor, CO is continuously removed from the process, extending the catalytic activity, leading to an increase in H_2 production. Due to the great permeability of the membrane, it was found that increasing its thickness has no influence on the conversion of FA. Subsequent analysis showed that all configurations had negligible mass transfer limitations.

Similar reactor configurations were investigated by Harkou et al. [211], for FA decomposition. A packed bed, a single membrane and double membrane were evaluated. The investigated parameters were temperature, reactant flow rate, porosity and concentration. Although, the packed bed design achieved high conversion, the catalytic activity gradually declined as a result of CO poisoning. The same trend was observed for the membrane microreactors. However, the double membrane microreactor outperformed the other two microreactors. Conversions over 80 % were attained, and despite the fact the deactivation reduced the conversion during the first hour of the reaction, the membranes' selective removal of CO, caused a subsequent increase in conversion. The authors concluded that a microreactor's efficiency is increasing with the addition of membranes to the CO separation system.

Summing up, using CFD is crucial for analysing and optimising different reactor configurations. CFD allows detailed simulations of fluid flow, heat transfer, and chemical reaction within the reactor, providing insights into complex phenomena that are challenging to study

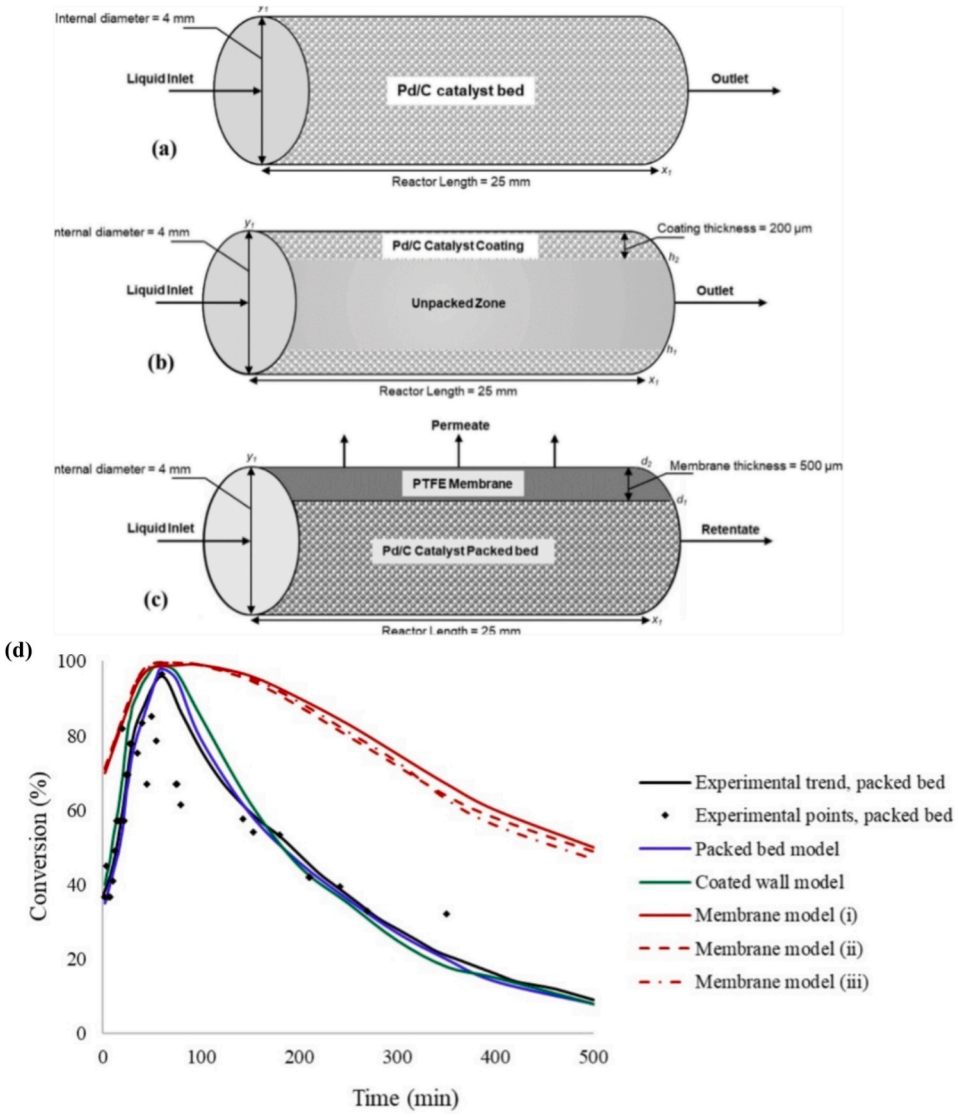

Fig. 12. Configurations of a) fixed bed, b) coated wall and c) membrane microreactors, d) experimental and CFD results of the conversion of formic acid over time [210].

experimentally. For different reactor designs, such as batch, CSTR, packed bed, fluidised and microreactors, CFD enables the assessment of reactor performance under various conditions, identification of hot-spots, and prediction of mixing and mass transfer efficiency. This can later help in scaling up processes from lab scale to industrial scale, improving efficiency and product quality.

5. Process optimisation/effect of factors on the performance

CO_2 hydrogenation process to methanol, ethanol, higher alcohols or higher hydrocarbons involves catalytic reactors designed to control temperature and pressure since these parameters affect significantly product yield/selectivity. In contrast, for H_2 generation from hydrogen storage materials, pressure is not a key parameter since the process is typically conducted under atmospheric pressure. However, temperature plays a crucial role. In continuous flow systems, flow rate is also an important parameter that affects heat/mass transfer in both CO_2 hydrogenation and H_2 generation processes. These parameters can be incorporated in CFD studies and once the results are accurately validated, then optimisation can be carried out to effectively implement and scale up the process, avoiding cost-effective experimental analysis. In the case of CO_2 hydrogenation CFD studies, it is also a challenge to address competing reactions and catalyst poisoning from CO formation that are influenced through the experimental conditions. However, with the appropriate reaction kinetics and deactivation parameters these challenges can be eliminated resulting in robust models. This section explains the effect of the above-mentioned factors on the performance of liquid and gaseous fuels production through experimental studies and CFD simulations.

5.1. *Effect of temperature*

Fu et al. [212], studied the CO_2 conversion to MeOH in a packed bed reactor model, evaluating the influence of the inlet temperature on the MeOH production. The experiment occurred in a range of 475 K to 555 K, at different pressure, using $CuO/ZnO/Al_2O_3$ as catalyst. Eq. (4) was examined in their study. The CO_2 conversion at 475 K, 498 K, and 555 K was found to be 18.18 %, 22.97 % and 23.02 %, respectively. This showed that the temperature increase led to an increase of CO_2 conversion to MeOH. Although, temperatures above 498 K did not significantly affect the MeOH production, (increase in conversion between 498 K and 555 K was only 0.05 %) concluding that there is a minimal benefit from further temperature increase. However, its highest value was reached at a shorter distance from the entrance of the reactor,

meaning a shorter packed bed can achieve the same conversion. Based on the computational results, the size of the packed bed can be altered for real-life experiments.

Hafeez et al. [210], examined the H_2 generation from FA using commercial 5 wt% Pd/C catalyst in a packed bed, coated wall, and membrane microreactors using CFD simulations. Coated wall and membrane microreactors were used to examine the impact of temperature on FA conversion. To determine the validity of the model, CFD results and experimental data were compared, and the uncertainty was found to be less than 3 %, confirming the accuracy of the model. Thus, parametric CFD studies were conducted varying the temperature at 30, 40 and 60 ℃, while the other parameters remained constant. Researchers found that the conversion of FA is increasing when the temperature also increases for both microreactors. According to them, this was anticipated according to Arrhenius equation, which generates 39 kJ/mol activation energy with Pd/C catalyst for this reaction. However, at very high temperatures poisonous species CO can occur, promoting the catalyst deactivation. Their study concluded that the deactivation of the catalyst and thus the FA conversion depend on temperature.

A tubular reactor was developed for CO_2 methanation-based biogas upgrading, utilising the disk and doughnut concept by Soto et al. [213]. A 2D axisymmetric single tube model was developed to confirm the accuracy of the chosen kinetic models based on the operating conditions from Gruber et al. [214]. Interaction between phases was included through source terms that account for momentum, energy and mass transfer. Based on the comparison plot below (Fig. 13), it is evident that the experimental temperature profile and the findings obtained with the chosen kinetic model are in a good agreement. At the tube inlet and hot spot, the largest deviation between the experimental and simulated data is 20 % and 5 %, respectively. It is also observed that the temperature rose rapidly until the hot spot, which is located 0.8 cm from the inlet and afterwards, the temperature dropped until it reached the outlet temperature. Since the kinetic model validated the experimental results, parametric studies were performed afterwards, using molten salts and thermal oil for four different coolant flow rates.

Multiphase heat transfer in reacting gas-catalyst bed, reacting gas-reactor tube, and reactor tube-coolant in a shell-and-tube reactor were simulated by Zhang et al. [215], aiming to develop a technology to detect the appearance of hotspots in a CO_2 methanation reactor. To verify the behaviour of the solver, the reaction rate of methanation was considered. Since many reaction rate models were developed throughout the years, only three were selected to be included in this study. Despite the fact that these models were created for different catalysts, they are useful in simulations to confirm that the model is applicable. Out of the three models, simulation results from model A were consistent with the experimental data, after its scaling to 1/8 of the original rate. The simulated catalyst bed temperature and the gas temperature vary significantly between the centre and near the reactor tube. In contrast, due to the high specific heat capacity of the coolant and high heat conductivity of the wall, the temperatures of the reactor tube and coolant fluctuate slightly.

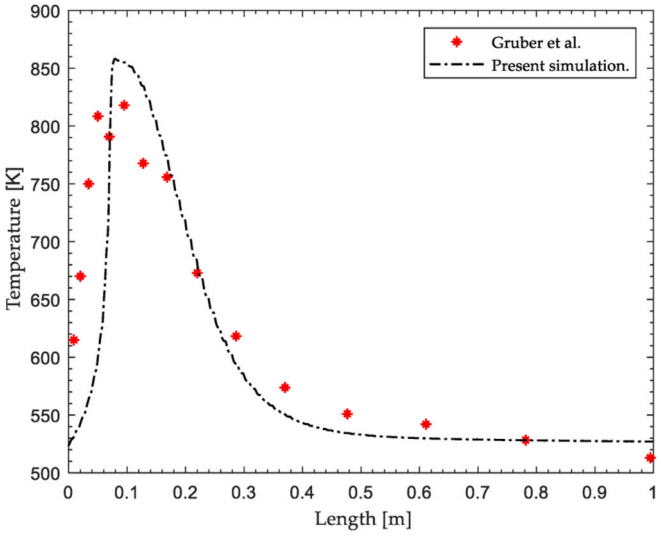

Fig. 13. Temperature profile between experimental [214] and computational results [213].

Ni catalysts supported on sol–gel produced Pr-doped CeO_2 were tested by Tsiotsias et al. [216], for CO_2 methanation. Catalytic tests were performed under three experimental protocols. CFD simulations were utilised for the prediction of the catalytic performance using COMSOL Multiphysics at a temperature range of 200 to 450 °C for the protocols #1 and #2. Fig. 14 depicts the comparison among the experimental data and CFD findings, where the model's validity is evident with errors of less than 12 %.

5.2. *Effect of pressure*

Pavlišič et al. [217], examined MeOH generation via CO_2 hydrogenation using a $Cu/ZnO/Al_2O_3$ catalyst with CFD modelling. Researchers aim was to optimise the process studying temperature and pressure impact on the MeOH production. A range between 1 and 40 bar was examined, which showed that MeOH selectivity increased as the pressure increased due to Le Chatelier's principle, as expected from STANJAN calculations, the equilibrium of which either maximised the gas mixture's entropy or minimised its suitable properties. CO_2 conversion and pressure showed parabolic relation, obtaining maximum MeOH production at 10 bar, as can be seen in Fig. 15, upon attaining the equilibrium, due to the constant GHSV, meaning the reactor length is insufficient to achieve a complete thermodynamic conversion at either high concentrations due to high pressure or high linear velocities due to low pressure. The agreement between the experimental and CFD results, demonstrates the feasibility to model real system processes with a fully computational approach.

Nailwal et al. [196], studied H_2 generation via NH_3 decomposition in a packed bed catalytic membrane reactor (PBCMR) and without membrane (PBCR). A CFD model was used, and the impact of various parameters were examined aiming to optimise the process. Experimental results showed that an increase in outlet pressure decreased NH_3 conversion (from 78.2 % at 1 bar to 42.2 % at 1.3 bar). The decreased conversion is due to the inverse relationship between pressure and reaction rate. In addition, the NH_3 decomposition reaction produced a greater number of product atoms than the number of atoms consumed in the reaction. Thus, when the pressure increased, the reaction shifted to the left (backwards) according to Le Chatelier's Principle resulting in a lower conversion rate. The H_2 flux also decreased with pressure increase. However, a rise in pressure led to increased H_2 permeation through the membrane. Researchers found that at 773 K and 1 bar 93 % NH_3 conversion was obtained in PBCMR, while in PBCR the achieved conversion was 80 %. Based on these results, simulation optimisation studies were conducted with the optimum pressure value of 1 bar, feed velocity of 0.00025 m/s, reactor wall temperature of 660 K, feed temperature of 523 K, bed porosity of 0.3 and with 22 membrane tubes, NH_3 conversion of 96 % was achieved.

CFD studies for CO_2 methanation reaction in a cooled reactor were performed by Di Nardo et al. [218]. The validity of the model was established by available experimental data in literature. After adjusting for pressure variations, an effectiveness factor of 0.14 was found, giving a good match between the experimental and numerical data. This value was also consistent with what other authors have obtained. Both experimental and CFD data showed that by increasing the pressure, conversion was also increased, since the Sabatier's reaction is favoured at higher pressures. Upon validation of the results, further studies were carried out using two different coolants (N_2 and oil cooling), aiming to find feasible options that retain high conversion rates and low

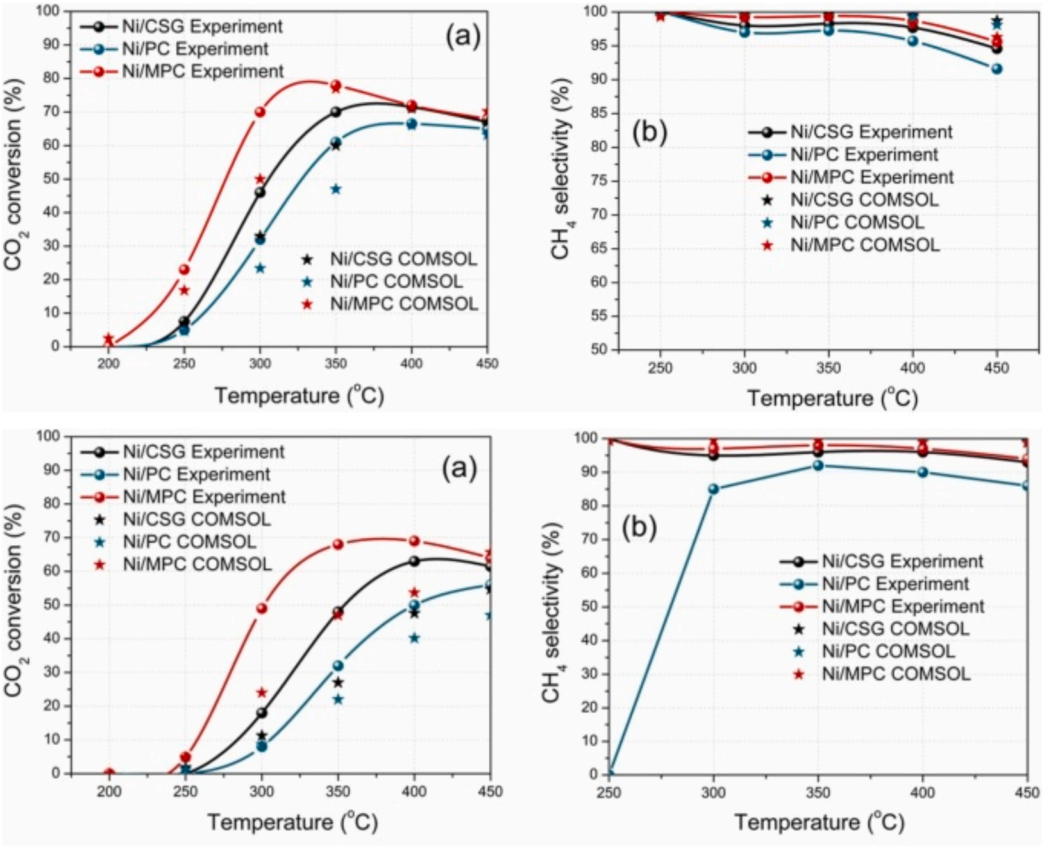

Fig. 14. Experimental and CFD results for (a) CO_2 conversion and (b) CH_4 selectivity vs temperature (Experimental Protocol #1). Experimental and CFD model results. (a) CO_2 conversion and (b) CH_4 selectivity vs temperature (Experimental Protocol #2) [216].

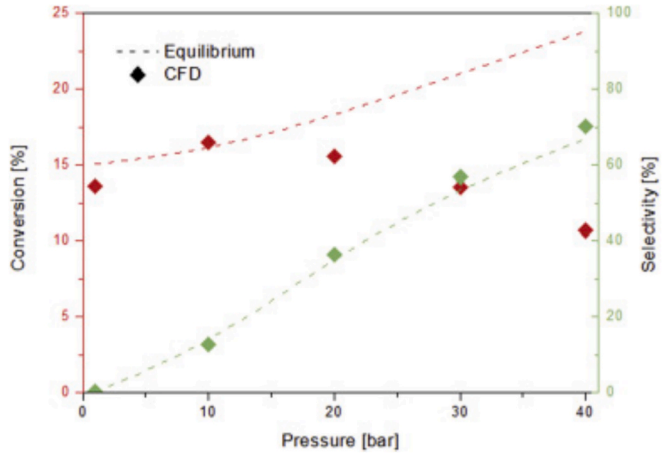

Fig. 15. Effect of pressure on CO_2 conversion and methanol selectivity at 240 °C and 12,030 h^{-1} GHSV [217].

temperature levels. Oil cooling performed better, leaving the possibility of updating the experimental setup using the CFD simulations as it was concluded by the authors.

5.3. Effect of flow rate

Jamshidi et al. [219], studied computationally how gas streams behave in the tube side of a packed bed reactor for MeOH synthesis. Before investigating the effect of different parameters, the model was first validated by experimental data of a petrochemical industrial plant. Overall, the data were in a great agreement excluding the content of H_2O. A possible reason is the chosen Graaf kinetics that were employed, which operate at 15–50 bar pressure range, in contrast of the operating pressure of the industrial plant (80 bar). Following the numerical results' validation the impact of several parameters on MeOH production rate were examined by CFD simulations. The effect of inlet flow was one parameter tested. CFD studies revealed that a rise in the inlet flow rate (originally 0.027 kg/s) increased the MeOH production about 4 times with a slight decrease (by 2 %) of the mass fraction of MeOH. The influence of flow rate was also investigated on CO conversion. The results demonstrated that when the flow rate was increased, space velocity also increased, leading to a decrease in average residence time.

In a study published by Hafeez et al. [220], FA decomposition was studied in a batch and packed bed reactor, both theoretically and experimentally. The CFD model was in great agreement with the

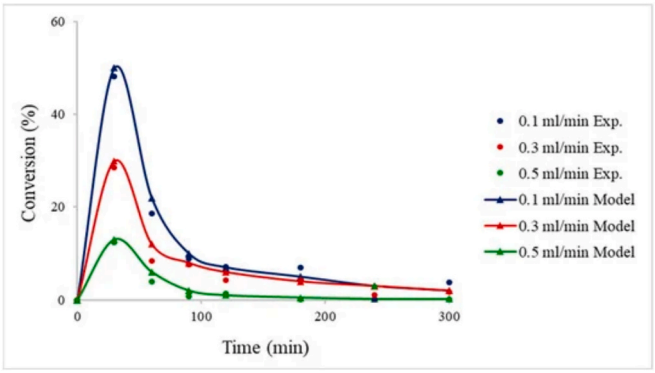

Fig. 16. Experimental and CFD results of formic acid decomposition over time at different inlet flow rates [220].

experimental results and in the case of the packed bed the model precisely predicted the deactivation that takes place from the CO species. One of the parameters tested was the inlet flow rate. As is evident from Fig. 16 below, the conversion is increased at lower flow rates. This can be explained by the residence time dependence; due to the reduced velocity, FA remains in the reactor for a longer period of time, resulting in larger conversions. The optimum flow rate was 0.1 mL/min, obtained from both experiments and CFD simulations.

A numerical study was carried out in a fluidised bed methanation reactor by Liu and Hinrichsen [221], by coupling the E-E gas–solid model with methanation reaction kinetics. The computational findings were compared with experimental data from literature, where the measured values near the end of the bed were in good agreement with the simulated axial species concentrations. Thus, the models were utilised to evaluate the effects of various operating conditions. The impact of inlet gas velocity is presented in Fig. 17a. It is observed that CH_4 concentration declines and H_2 concentration is increased, as the inlet gas rate is increased. Fig. 17b shows how the catalyst concentration is more diluted due to the greater gas input rate. Higher gas inlet rates cause the formation of big bubbles. The volumetric interfacial regions are severely reduced under these conditions. Additionally, the reactant gases' residence time in the bed is shortened by the higher gas velocity with this catalyst amount. Larger reactant input, however, is more interesting from an industrial perspective because it guarantees high volumetric productivity. As a result, when adding more feedstock, the catalyst needs to be modified accordingly.

5.4. Effect of mass transfer

Wang et al. [222], enhanced the CO_2 hydrogenation using Fe-based catalyst through 3D printing technology (direct ink writing (DIW)) optimising the mass and heat transfer, which affect the catalytic stability and product selectivity. It was revealed that the products and intermediate coverage is minimised by the spiral-structured channels of the Fe catalyst, while the usage of active sites is maximised archiving the carbon chain expansion in a specific time. This happens consequently upon the optimised mass transfer method, which also extends the catalyst life preventing unwanted effects, such as the active site accumulation and deposition of carbon. The study involves the experiment analysis of the catalysts in 3D printed monoliths and in powder form. Scientists evaluated the catalyst ability through conversion rate and product distribution using different channel setups, finding that the mass transfer optimisation improved the reaction productivity, stability, and selectivity. Analytically, using CFD simulations, they made three different setups channels of Na-Fe@C-3D (staggered, straight and spiral), evaluating pressure drop and gas flow within the catalyst. The model was solved through the non-isothermal flow module by coupling the solid/fluid heat transfer modules with the laminar flow module. The straight channel structure eased the gas flow, while the staggered channels impeded it. The spiral channel was the best option, providing balance and improving mass transfer. Non-3D printed catalysts were also examined, but they demonstrated low mass transfer efficiency in comparison to 3D printing catalysts. It was concluded that the optimisation of the mass transfer favours the conversion rates of CO_2, prevents the posterior hydrogenation and the extreme growth of carbon chain. In addition, catalyst is essential for mass transfer performance.

Hafeez et al. [210], examined the H_2 production from FA with a CFD packed bed microreactor model. Internal and external mass transfer resistances were studied. The internal pore diffusion limitations were studied within catalyst pores, while the external mass transfer resistance was examined from the difference in concentration of the catalyst particle and the concentration of the bulk fluid. The study of the effect of mass transfer is important in finding ways to improve the process. The difference between concentrations within the catalyst pellets is found to be fewer than 5 %. Considering the above and calculating the Thiele Modulus (F), which was found less than one, is determined that the internal mass transfer limitations are negligible, and the reaction is surface limited. Similarly, the external mass transfer limitations are negligible in the used microreactor due to the minor differences in the concentration of the catalyst particle surface and the concentration of the bulk fluid.

For on-board H_2 generation, NH_3 decomposition over CoCeAlO catalyst was investigated and simulated on a flat-plate microreactor by Maleki et al. [223]. The effect of temperature and NH_3 flow rate was examined through a series of kinetic experiments and on the basis of the conversion data, two kinetic rate expressions were developed (models I and II) and added to the CFD model. The kinetic models accurately predicted the responding flow parameters along the microchannel, and the simulated results exhibited good accuracy in comparison to the experimental data. The distribution of NH_3 concentration in the porous zone and bulk fluid phase at four axial points from the microreactor inlet are presented in Fig. 18a. The concentration gradients are relatively small, sharper though, near the inlet, demonstrating that the microreactor's entry has higher mass transfer rates, and most of the conversion occurs within this region. According to further mass transfer analysis, the optimal operating conditions for the microreactor occur in the region where the Damköhler II (Da_{II}) and Péclet (Pe) numbers are less than 1 (Fig. 18b). Therefore, it can be assumed that the system operates within the kinetic controlled zone without mass transfer limitations and that the microreactor aspect ratios are ideal for this reaction.

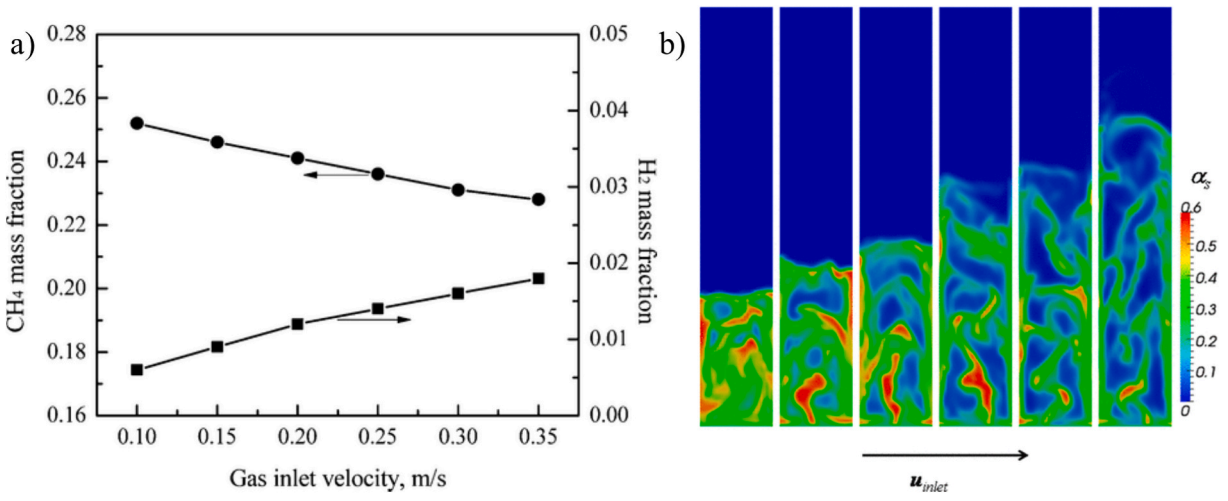

Fig. 17. Effect of inlet gas velocity on a) CH_4 and H_2 mass fractions and b) solid volume fraction [221].

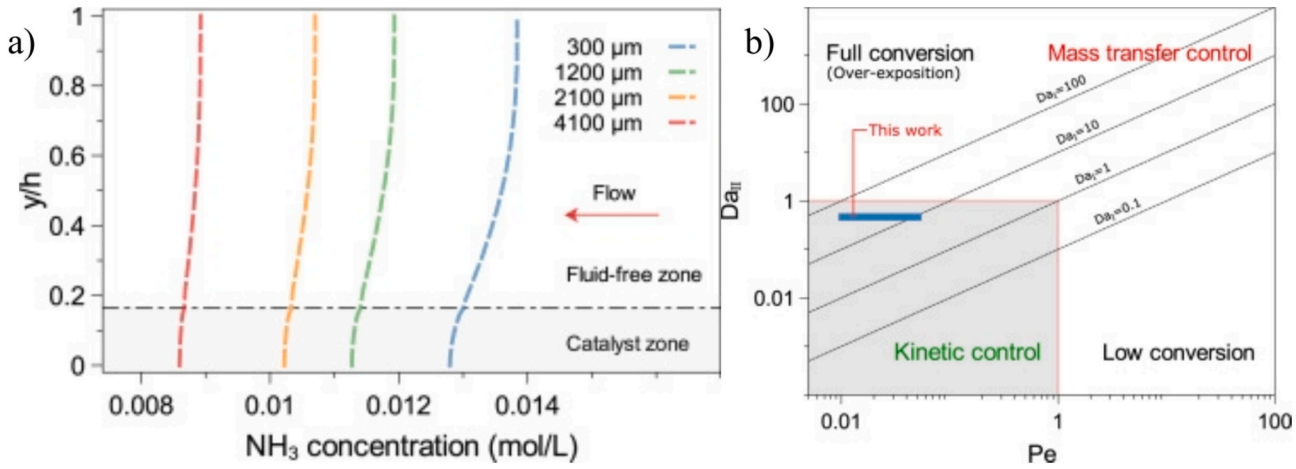

Fig. 18. a) Profile of NH_3 concentration in the dimensionless channel height, y/h at different axial x locations (based on model II), b) Damköhler II vs. Péclet diagram defining the mass transport (grey area) and kinetic controlled regions (top-right area) [223].

In a work by Chiuta et al. [224], a microreactor was evaluated using an integrated experimental and CFD modelling for H_2 generation by NH_3. After a series of experiments with different temperature values and NH_3 flow rates, Temkin-Pyzhev kinetics were employed, utilising a model-based approach with parameter estimation and refinement. This kinetic model provided the reaction source team which was used for the CFD simulations for a deeper understanding of the transfer phenomena inside the microreactor. Comparing the concentration gradients for lower temperature and higher temperature, it was evident that they differ, confirming the lower NH_3 conversion at lower temperatures. As it was also observed by Maleki et al. [223], most of the decomposition process takes place near the entrance for high-temperature operation.

Summarising, using the proper kinetic data and equations, CFD can accurately predict and validate experimental data and improve the understanding behind a reaction process. By varying experimental conditions e.g. temperature, pressure, and flow rate computationally, saves time and money from real-time experiments, enabling simulation try-outs for large ranges of values. Also, CFD enables precise control and prediction of fluid behaviour, investigating mass transport phenomena. Thus, upon validation, optimisation studies can be carried out for all kinds of process systems. In that way, CFD parametric studies, offer invaluable insights for engineers and scientists, leading to an improved system performance and the development of innovative industrial systems.

6. Future prospects in modelling

The role of computational studies is of great importance since they offer a wide range of advantages compared to conducting experiments in laboratories. The less time needed to carry out investigation with the potential of prediction with accuracy as well as the lower cost from not using consumables for experimental studies constitute the basis of the reason for which the computational studies are preferred. However, there is still room for improvement in the speed of computing, in the accuracy and in the development of more friendly in use softwares that can be used by non-specialist engineers for less complex models. The main limitation is the high computer sources that are required to run the simulations in less time, especially for complex geometries that implement complex phenomena. So far, the model development has been excessively utilised in aerospace and generally in the engineering fields. There is a great potential in expanding its employment in various applications beyond the usual ones, such as food processing, biomedical, environmental, buildings ventilation, fire safety, and energy efficiency etc.

The validation of the model is significant during the development. A prototype model should be able to validate experimental results in terms of species mass fractions with the accuracy between the simulated and experimental results to be considered as a challenge. The well quality of the mesh could potentially inhibit numerical problems during the simulation, but increasing the number of elements of the mesh by creating more complex domains this will not only lead to precise results but will also increase the computational time. Therefore, it is important to lower the cost of the simulations in large-scale analyses by reducing the computational time, at the same time without affecting the efficiency, using the optimum mesh-grid for the study to give accurate results.

It is enormous the effect of artificial intelligence (AI) in our everyday life which has also debuted in the computational field gaining popularity. The application of AI in CFD was firstly started in 2015 focusing on aerodynamic and turbulence modelling. Many scientists are applying AI algorithms in order to improve their hardware (computers etc) and to process a large amount of data. Additionally, they are capable to offer solution with high accuracy, efficiency and better process understanding due to their engineering database. The machine learning algorithms use a plethora of base models in order to solve the problem with high accuracy. Their implementation in various simulations is growing swiftly the recent years offering preciseness and reliability on the designed models. They have made their appearance in chemical engineering field and more specifically in the material synthesis field for heterogenous catalysts for significant reactions with intermediates [225]. In the most recent study of Miyazaki et al. [226], the assessment of new additive metals carried out to improve the MeOH selectivity via CO_2 hydrogenation using the SISSO AI-assisted model with main aim to understand the underlying catalytic mechanisms that leads to products generation. It is important to utilise the appropriate AI tools in the CFD modelling for their implementation to a wider range of catalytic systems.

7. Conclusions

The present review aims to highlight the significance of CFD modelling in terms of validation, optimisation and prediction. Simulation studies using computational modelling tools is one of the most convenient, inexpensive and time-saving ways to investigate various systems with an advantageous approach compared to the experimental work. More specifically, CFD modelling employing all the reaction rates, BC and governing equations contribute to the better understanding and optimisation of various parameters that might be the temperature, pressure, velocity, catalyst properties and weight, reactor set-up design and feedstock composition that can be predicted with high accuracy. Nowadays with the climate crisis we face the CCU technology along with

the hydrogenation of CO_2 provide an alternative route for fuel and chemical synthesis. In addition, among the alternatives fuels the H_2 consists one of the most efficient energy sources without burdening the atmosphere with emitted pollutants. CFD modelling tools can contribute to the exploration of existing and new reaction systems for the generation of gaseous and liquid fuels offering a solution to the global warming we face due to the utilisation of conventional fuels. In this review we present the reaction pathways considering the production of these gaseous and liquid fuels that has been extensively investigated in literature with many proposed kinetic mechanisms and hence kinetic rate equations. The kinetic rates consist of key factors for the deployment of CFD models as they represent the evolution of product species and the consumption of the feedstock. The catalyst can affect the reaction mechanism and the rate-determined step as well as the proposed reaction rate. There are many key factors that must be considered in order to inhibit common phenomena such as the catalyst deactivation due to CO poisoning and the competitive reaction of the non-desirable pathway leading to lower selectivity of the preferred product. Another important factor for the CFD design is to incorporate the appropriate physics, with the implementation of the different mass and heat balances to describe all the phenomena occurring inside the system. Moreover, to study the microkinetics of a reaction system using lab experiments is very difficult and time-consuming procedure in contrast to the CFD work that can exhibit such phenomena of reaction efficiency, mass and heat limitations, system configuration limitations, mixing and/or flow behaviours with an ease. Additionally, the goal of CFD optimisation studies is to discover the optimum parameters and conditions for the efficient operation of the reaction system as it's a more affordable approach compared to the experimental work. The optimum reactor design is one of the most significant factors that could contribute to the high efficiency of the operation and to the low manufacturing cost. To achieve that a validated model with experimental results could predict with high accuracy the performance of each reactor configuration and the mass fraction of species at the outlet of the reactor. The enrolment of mesh quality and computational time must be considered on the results accuracy. Lastly, the expansion of numerical modelling into various fields is important for efficiency reasons as well as the integration with AI algorithms that contain a huge engineering database offering better understanding on problems while providing information regarding the optimum operating conditions and solving them with high accuracy.

CRediT authorship contribution statement

Eleana Harkou: Writing – review & editing, Writing – original draft, Software, Resources, Data curation. **Panayiota Adamou:** Writing – review & editing, Writing – original draft, Methodology, Investigation, Formal analysis, Data curation. **S.M.Al- Salem:** Writing – review & editing. **Nikol Atanasova:** Writing – review & editing, Investigation. **Junwang Tang:** Writing – review & editing. **George Manos:** Writing – review & editing. **Alberto Villa:** Writing – review & editing. **Nikolaos Dimitratos:** Writing – review & editing, Visualization, Supervision, Methodology. **Achilleas Constantinou:** Writing – review & editing, Writing – original draft, Visualization, Supervision, Resources, Methodology, Investigation.

Declaration of competing interest

The authors declare the following financial interests/personal relationships which may be considered as potential competing interests: Nikolaos Dimitratos reports was provided by University of Bologna. Nikolaos Dimitratos reports a relationship with University of Bologna that includes: employment. If there are other authors, they declare that they have no known competing financial interests or personal relationships that could have appeared to influence the work reported in this paper.

Data availability

Data will be made available on request.

References

[1] Panda R, Maity M. Global warming and climate change on earth: duties and challenges of human beings. Int J Res Eng Sci Manag 2021;4(1):122–5.
[2] DeAngelo J, et al. Energy systems in scenarios at net-zero CO2 emissions. Nat Commun 2021;12(1):6096.
[3] Mikulčić H, et al. Flexible Carbon Capture and utilization technologies in future energy systems and the utilization pathways of captured CO2. Renew Sustain Energy Rev 2019;114:109338.
[4] Gao P, Zhang L, Li S, Zhou Z, Sun Y. Novel heterogeneous catalysts for CO2 hydrogenation to liquid fuels. ACS Cent Sci 2020;6(10):1657–70. https://doi.org/10.1021/acscentsci.0c00976.
[5] Anwar MN, et al. CO2 utilization: turning greenhouse gas into fuels and valuable products. J Environ Manage 2020;260:110059. https://doi.org/10.1016/j.jenvman.2019.110059.
[6] Preuster P, Papp C, Wasserscheid P. Liquid organic hydrogen carriers (LOHCs): toward a hydrogen-free hydrogen economy. Acc Chem Res 2017;50(1):74–85. https://doi.org/10.1021/acs.accounts.6b00474.
[7] Pareek A, Dom R, Gupta J, Chandran J, Adepu V, Borse PH. Insights into renewable hydrogen energy: recent advances and prospects. Mater Sci Energy Technol 2020;3:319–27. https://doi.org/10.1016/j.mset.2019.12.002.
[8] Peschel A. Industrial perspective on hydrogen purification, compression, storage, and distribution. Fuel Cells 2020;20(4):385–93. https://doi.org/10.1002/fuce.201900235.
[9] Filippov SP, Yaroslavtsev AB. Hydrogen energy: development prospects and materials. Russ Chem Rev 2021;90(6):627.
[10] Shen R, Jiao Z, Parker T, Sun Y, Wang Q. Recent application of Computational Fluid Dynamics (CFD) in process safety and loss prevention: a review. J Loss Prev Process Ind 2020;67:104252. https://doi.org/10.1016/j.jlp.2020.104252.
[11] Scharl V, Fischer F, Herrmann S, Fendt S, Spliethoff H. applying reaction kinetics to Pseudohomogeneous methanation modeling in fixed-bed reactors. Chem Eng Technol 2020;43(6):1224–33. https://doi.org/10.1002/ceat.201900535.
[12] Leonzio G, Foscolo PU. Analysis of a 2-D model of a packed bed reactor for methanol production by means of CO2 hydrogenation. Int J Hydrogen Energy 2020;45(18):10648–63. https://doi.org/10.1016/j.ijhydene.2020.01.248.
[13] Calabrese M, et al. Hydrogen safety challenges: a comprehensive review on production, storage, transport, utilization, and CFD-based consequence and risk assessment. Energies 2024;17(6). https://doi.org/10.3390/en17061350.
[14] Ghasem N. A review of the CFD modeling of hydrogen production in catalytic steam reforming reactors. Int J Mol Sci 2022;23(24). https://doi.org/10.3390/ijms232416064.
[15] Kassi AH, Al-Hattab TA. A review: membrane reactor for hydrogen production: modeling and simulation. Eng Chem 2023;4:17–31. https://doi.org/10.4028/p-XakNe1.
[16] Fan T, Liu H, Shao S, Gong Y, Li G, Tang Z. Cobalt Catalysts Enable Selective Hydrogenation of CO2 toward Diverse Products: recent Progress and Perspective. J Phys Chem Lett 2021;12(43):10486–96. https://doi.org/10.1021/acs.jpclett.1c03043.
[17] Sun S, et al. Ammonia as hydrogen carrier: advances in ammonia decomposition catalysts for promising hydrogen production. Renew Sustain Energy Rev 2022;169:112918. https://doi.org/10.1016/j.rser.2022.112918.
[18] Al-Nayili A, Majdi HSh, Albayati TM, Saady NMC. Formic acid dehydrogenation using noble-metal nanoheterogeneous catalysts: towards sustainable hydrogen-based energy. Catalysts 2022;12(3). https://doi.org/10.3390/catal12030324.
[19] Chu C, Wu K, Luo B, Cao Q, Zhang H. Hydrogen storage by liquid organic hydrogen carriers: catalyst, renewable carrier, and technology – a review. Carbon Resour Convers 2023;6(4):334–51. https://doi.org/10.1016/j.crcon.2023.03.007.
[20] Fan WK, Tahir M. Recent trends in developments of active metals and heterogenous materials for catalytic CO2 hydrogenation to renewable methane: a review. J Environ Chem Eng 2021;9(4):105460. https://doi.org/10.1016/j.jece.2021.105460.
[21] Shao S, Cui C, Tang Z, Li G. Recent advances in metal-organic frameworks for catalytic CO2 hydrogenation to diverse products. Nano Res 2022;15(12):10110–33. https://doi.org/10.1007/s12274-022-4576-z.
[22] Ye R, et al. Design of catalysts for selective CO2 hydrogenation. Nat Synth 2025;4(3):288–302. https://doi.org/10.1038/s44160-025-00747-1.
[23] Ren M, Zhang Y, Wang X, Qiu H. Catalytic hydrogenation of CO2 to methanol: a review. Catalysts 2022;12(4). https://doi.org/10.3390/catal12040403.
[24] Sen R, Goeppert A, Surya Prakash GK. Homogeneous hydrogenation of CO2 and CO to methanol: the renaissance of low-temperature catalysis in the context of the methanol economy. Angew Chem Int Ed 2022;61(42):e202207278. https://doi.org/10.1002/anie.202207278.
[25] Darji HR, Kale HB, Shaikh FF, Gawande MB. Advancement and State-of-art of heterogeneous catalysis for selective CO2 hydrogenation to methanol. Coord Chem Rev 2023;497:215409. https://doi.org/10.1016/j.ccr.2023.215409.
[26] San X, et al. Comprehensive insight into Cu-based catalysts for CO2 hydrogenation to methanol. Sustain Mater Technol 2025;45:e01437. https://doi.org/10.1016/j.susmat.2025.e01437.

[27] Bai S-T, et al. Homogeneous and heterogeneous catalysts for hydrogenation of CO 2 to methanol under mild conditions. Chem Soc Rev 2021;50(7):4259–98.
[28] Yousaf M, Mahmood A, Elkamel A, Rizwan M, Zaman M. Techno-economic analysis of integrated hydrogen and methanol production process by CO2 hydrogenation. Int J Greenhouse Gas Control 2022;115:103615. https://doi.org/10.1016/j.ijggc.2022.103615.
[29] Atsbha TA, Yoon T, Seongho P, Lee C-J. A review on the catalytic conversion of CO2 using H2 for synthesis of CO, methanol, and hydrocarbons. J CO2 Util 2021;44:101413.
[30] Cuevas-Castillo GA, Michailos S, Akram M, Hughes K, Ingham D, Pourkashanian M. Techno economic and life cycle assessment of olefin production through CO2 hydrogenation within the power-to-X concept. J Clean Prod 2024;469:143143. https://doi.org/10.1016/j.jclepro.2024.143143.
[31] Stančin H, Mikulčić H, Wang X, Duić N. A review on alternative fuels in future energy system. Renew Sustain Energy Rev 2020;128:109927. https://doi.org/10.1016/j.rser.2020.109927.
[32] Fan WK, Tahir M. Recent developments in photothermal reactors with understanding on the role of light/heat for CO2 hydrogenation to fuels: a review. Chem Eng J 2022;427:131617. https://doi.org/10.1016/j.cej.2021.131617.
[33] Saeidi S, et al. Recent advances in CO2 hydrogenation to value-added products — current challenges and future directions. Prog Energy Combust Sci 2021;85:100905. https://doi.org/10.1016/j.pecs.2021.100905.
[34] Zheng J, et al. Current research progress and perspectives on liquid hydrogen rich molecules in sustainable hydrogen storage. Energy Storage Mater 2021;35:695–722. https://doi.org/10.1016/j.ensm.2020.12.007.
[35] Li R, Kawanami H. A recent review of primary hydrogen carriers, hydrogen production methods, and applications. Catalysts 2023;13(3):3. https://doi.org/10.3390/catal13030562.
[36] Dai S, Shen P, Deng W, Yu Q. Hydrogen energy in electrical power systems: a review and future outlook. Electronics 2024;13(17):17. https://doi.org/10.3390/electronics13173370.
[37] Hafeez S, et al. Hydrogenation of carbon dioxide (CO 2) to fuels in microreactors: a review of set-ups and value-added chemicals production. React Chem Eng 2022;7(4):795–812.
[38] Tan CH, Nomanbhay S, Shamsuddin AH, Park Y-K, Hernández-Cocoletzi H, Show PL. Current developments in catalytic methanation of carbon dioxide—a review. Front Energy Res 2022;9:795423.
[39] Beniwal A, Bagaria A, Chen T-Y, Bhalothia D. Advancements in CO2 conversion technologies: a comprehensive review on catalyst design strategies for high-performance CO2 methanation. Sustainable Energy Fuels 2025;9(9):2261–86. https://doi.org/10.1039/D5SE00167F.
[40] Rönsch S, et al. Review on methanation – from fundamentals to current projects. Fuel 2016;166:276–96. https://doi.org/10.1016/j.fuel.2015.10.111.
[41] Sanz-Martínez A, Durán P, Mercader VD, Francés E, Peña JÁ, Herguido J. Biogas upgrading by CO2 methanation with Ni-, Ni–Fe-, and Ru-based catalysts. Catalysts 2022;12(12):1. https://doi.org/10.3390/catal12121609.
[42] Li L, Zeng W, Song M, Wu X, Li G, Hu C. Research progress and reaction mechanism of CO2 methanation over Ni-based catalysts at low temperature: a review. Catalysts 2022;12(2). https://doi.org/10.3390/catal12020244.
[43] Esa YAM, Sapawe N. A short review on carbon dioxide (CO2) methanation process. Mater Today Proc 2020;31:394–7.
[44] Shen L, Xu J, Zhu M, Han Y-F. Essential role of the support for nickel-based CO2 methanation catalysts. ACS Catal 2020;10(24):14581–91.
[45] Mebrahtu C, Krebs F, Abate S, Perathoner S, Centi G, Palkovits R. Chapter 5 - CO2 methanation: principles and challenges. Methanation: principles and challenges 2019;vol. 178:85–103. https://doi.org/10.1016/B978-0-444-64127-4.00005-7.
[46] Schmider D, Maier L, Deutschmann O. Reaction kinetics of CO and CO2 methanation over nickel. Ind Eng Chem Res 2021;60(16):5792–805. https://doi.org/10.1021/acs.iecr.1c00389.
[47] Weatherbee GD, Bartholomew CH. Hydrogenation of CO2 on group VIII metals: II. Kinetics and mechanism of CO2 hydrogenation on nickel. J Catal 1982;77(2):460–72. https://doi.org/10.1016/0021-9517(82)90186-5.
[48] Xu J, Froment GF. Methane steam reforming, methanation and water-gas shift: I. Intrinsic kinetics. AIChE J 1989;35(1):88–96. https://doi.org/10.1002/aic.690350109.
[49] Onrubia-Calvo JA, et al. Kinetics, model discrimination, and parameters estimation of CO2 methanation on highly active Ni/CeO2 Catalyst. Ind Eng Chem Res 2022;61(29):10419–35. https://doi.org/10.1021/acs.iecr.2c00164.
[50] Quindimil A, et al. Intrinsic kinetics of CO2 methanation on low-loaded Ni/Al2O3 catalyst: Mechanism, model discrimination and parameter estimation. J CO2 Util 2022;57:101888. https://doi.org/10.1016/j.jcou.2022.101888.
[51] Bermejo-López A, Pereda-Ayo B, González-Marcos JA, González-Velasco JR. Modeling the CO2 capture and in situ conversion to CH4 on dual function Ru-Na2CO3/Al2O3 catalyst. J CO2 Util 2020;42:101351. https://doi.org/10.1016/j.jcou.2020.101351.
[52] Varun Y, Sreedhar I, Singh SA. Highly stable M/NiO–MgO (M = Co, Cu and Fe) catalysts towards CO2 methanation. Int J Hydrogen Energy 2020;45(53):28716–31. https://doi.org/10.1016/j.ijhydene.2020.07.212.
[53] Xu D, Wang Y, Ding M, Hong X, Liu G, Tsang SCE. Advances in higher alcohol synthesis from CO2 hydrogenation. Chem 2021;7(4):849–81.
[54] Cui G, Lou Y, Zhou M, Li Y, Jiang G, Xu C. Review of mechanism investigations and catalyst developments for CO2 hydrogenation to alcohols. Catalysts 2024;14(4). https://doi.org/10.3390/catal14040232.
[55] Zhang S, et al. A short review of recent advances in direct CO2 hydrogenation to alcohols. Top Catal 2021;64(5):371–94. https://doi.org/10.1007/s11244-020-01405-w.
[56] Nie X, Li W, Jiang X, Guo X, Song C. Chapter Two - recent advances in catalytic CO2 hydrogenation to alcohols and hydrocarbons. In: Song C, editor. Advances in Catalysis, vol. 65. Academic Press; 2019. p. 121–233. https://doi.org/10.1016/bs.acat.2019.10.002.
[57] Witoon T, et al. Enhanced CO2 hydrogenation to higher alcohols over K-Co promoted In2O3 catalysts. Chem Eng J 2022;431:133211. https://doi.org/10.1016/j.cej.2021.133211.
[58] Latsiou AI, Charisiou ND, Frontistis Z, Bansode A, Goula MA. CO2 hydrogenation for the production of higher alcohols: Trends in catalyst developments, challenges and opportunities. Catal Today 2023;420:114179. https://doi.org/10.1016/j.cattod.2023.114179.
[59] Lim H-W, Park M-J, Kang S-H, Chae H-J, Bae JW, Jun K-W. Modeling of the kinetics for methanol synthesis using Cu/ZnO/Al2O3/ZrO2 catalyst: influence of carbon dioxide during hydrogenation. Ind Eng Chem Res 2009;48(23):10448–55. https://doi.org/10.1021/ie901081f.
[60] Li H-X, et al. CO2 hydrogenation to methanol over Cu/ZnO/Al2O3 catalyst: kinetic modeling based on either single- or dual-active site mechanism. Catal Lett 2022;152(10):3110–24. https://doi.org/10.1007/s10562-021-03913-0.
[61] Poto S, Vico van Berkel D, Gallucci F, Fernanda Neira d'Angelo M. Kinetic modelling of the methanol synthesis from CO2 and H2 over a CuO/CeO2/ZrO2 catalyst: the role of CO2 and CO hydrogenation. Chem Eng J 2022;435:134946. https://doi.org/10.1016/j.cej.2022.134946.
[62] Bussche KV, Froment GF. A steady-state kinetic model for methanol synthesis and the water gas shift reaction on a commercial Cu/ZnO/Al2O3Catalyst. J Catal 1996;161(1):1–10.
[63] Ovesen C, et al. A microkinetic analysis of the water–gas shift reaction under industrial conditions. J Catal 1996;158(1):170–80.
[64] Calverley EM, Smith KJ. Kinetic model for alcohol synthesis over a promoted copper/zinc oxide/chromium oxide (Cr2O3) catalyst. Ind Eng Chem Res 1992;31(3):792–803.
[65] Graaf GH, Stamhuis E, Beenackers A. Kinetics of low-pressure methanol synthesis. Chem Eng Sci 1988;43(12):3185–95.
[66] Yang H, et al. A review of the catalytic hydrogenation of carbon dioxide into value-added hydrocarbons. Cat Sci Technol 2017;7(20):4580–98.
[67] Li W, et al. A short review of recent advances in CO 2 hydrogenation to hydrocarbons over heterogeneous catalysts. RSC Adv 2018;8(14):7651–69.
[68] Ye R-P, et al. CO2 hydrogenation to high-value products via heterogeneous catalysis. Nat Commun 2019;10(1):5698. https://doi.org/10.1038/s41467-019-13638-9.
[69] Cui L, Liu C, Yao B, Edwards PP, Xiao T, Cao F. A review of catalytic hydrogenation of carbon dioxide: from waste to hydrocarbons. Front Chem 2022;10:1037997.
[70] Saeidi S, et al. Mechanisms and kinetics of CO2 hydrogenation to value-added products: a detailed review on current status and future trends. Renew Sustain Energy Rev 2017;80:1292–311. https://doi.org/10.1016/j.rser.2017.05.204.
[71] Ghosh S, Sebastian J, Olsson L, Creaser D. Experimental and kinetic modeling studies of methanol synthesis from CO2 hydrogenation using In2O3 catalyst. Chem Eng J 2021;416:129120. https://doi.org/10.1016/j.cej.2021.129120.
[72] Ghosh S, Olsson L, Creaser D. Methanol mediated direct CO2 hydrogenation to hydrocarbons: experimental and kinetic modeling study. Chem Eng J 2022;435:135090. https://doi.org/10.1016/j.cej.2022.135090.
[73] Gayubo AG, Aguayo AT, Alonso A, Bilbao J. Kinetic modeling of the methanol-to-olefins process on a Silicoaluminophosphate (SAPO-18) catalyst by considering deactivation and the formation of individual olefins. Ind Eng Chem Res 2007;46(7):1981–9. https://doi.org/10.1021/ie061278o.
[74] Brübach L, Hodonj D, Pfeifer P. Kinetic analysis of CO2 hydrogenation to long-chain hydrocarbons on a supported iron catalyst. Ind Eng Chem Res 2022;61(4):1644–54. https://doi.org/10.1021/acs.iecr.1c04018.
[75] Pour AN, Housaindokht MR, Zarkesh J, Irani M, Babakhani EG. Kinetics study of CO hydrogenation on a precipitated iron catalyst. J Ind Eng Chem 2012;18(2):597–603. https://doi.org/10.1016/j.jiec.2011.11.080.
[76] Wang X, et al. Recent progress in hydrogen production from formic acid decomposition. Int J Hydrogen Energy 2018;43(14):7055–71. https://doi.org/10.1016/j.ijhydene.2018.02.146.
[77] Sanni SE, et al. Strategic examination of the classical catalysis of formic acid decomposition for intermittent hydrogen production, storage and supply: a review. Sustainable Energy Technol Assess 2021;45:101078. https://doi.org/10.1016/j.seta.2021.101078.
[78] Hafeez S, et al. Review on recent progress and reactor set-ups for hydrogen production from formic acid decomposition. Mater Today Chem 2022;26:101120.
[79] Eppinger J, Huang K-W. Formic Acid as a Hydrogen Energy Carrier. ACS Energy Lett 2017;2(1):188–95. https://doi.org/10.1021/acsenergylett.6b00574.
[80] Schlussel S, Kwon S. A review of formic acid decomposition routes on transition metals for its potential use as a liquid H2 carrier. Korean J Chem Eng 2022;39(11):2883–95. https://doi.org/10.1007/s11814-022-1276-z.
[81] Sadovskaya EM, Chesalov YA, Goncharov VB, Sobolev VI, Andrushkevich TV. Formic acid decomposition over V-Ti oxide catalyst: Mechanism and kinetics. Mol Catal 2017;430:54–62. https://doi.org/10.1016/j.molcata.2016.12.010.
[82] Wang B, Yang S, Yu Z, Zhang T, Liu S. Performance modulation strategies of heterogeneous catalysts for formic acid dehydrogenation: a review. Mater Today Commun 2022;31:103617.
[83] Hinshelwood CN, Topley B. CXV.—The energy of activation in heterogeneous gas reactions with relation to the thermal decomposition of formic acid vapour. J Chem Soc Trans 1923;123:1014–25.
[84] Yu J, Savage PE. Decomposition of formic acid under hydrothermal conditions. Ind Eng Chem Res 1998;37(1):2–10. https://doi.org/10.1021/ie970182e.

[85] Yurderi M, Bulut A, Zahmakiran M, Kaya M. Carbon supported trimetallic PdNiAg nanoparticles as highly active, selective and reusable catalyst in the formic acid decomposition. Appl Catal B 2014;160–161:514–24. https://doi.org/10.1016/j.apcatb.2014.06.004.

[86] Bulushev DA, Beloshapkin S, Ross JRH. Hydrogen from formic acid decomposition over Pd and Au catalysts. Catal Today 2010;154(1):7–12. https://doi.org/10.1016/j.cattod.2010.03.050.

[87] Sanchez F, Motta D, Roldan A, Hammond C, Villa A, Dimitratos N. Hydrogen generation from additive-free formic acid decomposition under mild conditions by Pd/C: experimental and DFT studies. Top Catal 2018;61(3):254–66. https://doi.org/10.1007/s11244-018-0894-5.

[88] Ojeda M, Iglesia E. Formic acid dehydrogenation on Au-based catalysts at near-ambient temperatures. Angew Chem 2009;121(26):4894–7. https://doi.org/10.1002/ange.200805723.

[89] Winkler T, et al. Catalytic decomposition of formic acid in a fixed bed reactor – an experimental and modelling study. Catal Today 2022;387:128–39. https://doi.org/10.1016/j.cattod.2021.10.022.

[90] Solymosi F, Erdöhelyi A. Decomposition of formic acid on supported Rh catalysts. J Catal 1985;91(2):327–37. https://doi.org/10.1016/0021-9517(85)90346-X.

[91] Singh S, Li S, Carrasquillo-Flores R, Alba-Rubio AC, Dumesic JA, Mavrikakis M. Formic acid decomposition on Au catalysts: DFT, microkinetic modeling, and reaction kinetics experiments. AIChE J 2014;60(4):1303–19. https://doi.org/10.1002/aic.14401.

[92] Singh SK, Xu Q. Nanocatalysts for hydrogen generation from hydrazine. Cat Sci Technol 2013;3(8):1889. https://doi.org/10.1039/c3cy00101f.

[93] Elgin JC, Taylor HS. The photosensitized and photochemical decomposition of hydrazine. J Am Chem Soc 1929;51(7):2059–82. https://doi.org/10.1021/ja01382a013.

[94] Askey PJ. The thermal decomposition of hydrazine. J Am Chem Soc 1930;52(3):970–4. https://doi.org/10.1021/ja01366a019.

[95] Gilbert M. The hydrazine flame. Combust Flame 1958;2(2):137–48. https://doi.org/10.1016/0010-2180(58)90004-X.

[96] Adams GK, Stocks GW. The combustion of hydrazine. Symp (Int) Combust 1953;4(1):239–48. https://doi.org/10.1016/S0082-0784(53)80030-5.

[97] Singh SK, Xu Q. Complete conversion of hydrous hydrazine to hydrogen at room temperature for chemical hydrogen storage. J Am Chem Soc 2009;131(50):18032–3. https://doi.org/10.1021/ja908037t.

[98] He L, Liang B, Huang Y, Zhang T. Design strategies of highly selective nickel catalysts for H2 production via hydrous hydrazine decomposition: a review. Natl Sci Rev 2018;5(3):356–64. https://doi.org/10.1093/nsr/nwx123.

[99] Adamou P, et al. Recent progress for hydrogen production from ammonia and hydrous hydrazine decomposition: a review on heterogeneous catalysts. Catal Today 2023;423:114022. https://doi.org/10.1016/j.cattod.2023.01.029.

[100] Zhou L, Luo X, Xu L, Wan C, Ye M. Pt-Ni nanoalloys for H2 generation from hydrous hydrazine. Catalysts 2020;10(8):8. https://doi.org/10.3390/catal10080930.

[101] Smith OI, Solomon WC. Kinetics of hydrazine decomposition on iridium surfaces. Ind Eng Chem Fund 1982;21(4):374–8. https://doi.org/10.1021/i100008a010.

[102] Dai H, Dai H-B, Zhong Y-J, Kang Q, Sun L-X, Wang P. Kinetics of catalytic decomposition of hydrous hydrazine over CeO2-supported bimetallic Ni–Pt nanocatalysts. Int J Hydrogen Energy 2017;42(9):5684–93. https://doi.org/10.1016/j.ijhydene.2016.10.160.

[103] Al-Thubaiti KS, Khan Z. Trimetallic nanocatalysts to enhanced hydrogen production from hydrous hydrazine: the role of metal centers. Int J Hydrogen Energy 2020;45(27):13960–74. https://doi.org/10.1016/j.ijhydene.2020.03.093.

[104] Berčič G, Likozar B. Analysis and recompilation of kinetic data about the hydrogen production by the catalytic decomposition of hydrous hydrazine. Int J Hydrogen Energy 2022;47(68):29348–57. https://doi.org/10.1016/j.ijhydene.2022.06.282.

[105] Lemay P, Oesper RE. Claude Louis Berthollet (1748-1822). J Chem Educ 1946;23(4):158. https://doi.org/10.1021/ed023p158.

[106] Smith C, Hill AK, Torrente-Murciano L. Current and future role of Haber–Bosch ammonia in a carbon-free energy landscape. Energ Environ Sci 2020;13(2):331–44. https://doi.org/10.1039/C9EE02873K.

[107] Bora N, et al. Green ammonia production: Process technologies and challenges. Fuel 2024;369:131808. https://doi.org/10.1016/j.fuel.2024.131808.

[108] Ramsay W, Young S. XIV.—The decomposition of ammonia by heat. J Chem Soc Trans 1884;45:88–93. https://doi.org/10.1039/CT8844500088.

[109] Perman EP, Atkinson GAS, Ramsay W. The decomposition of ammonia by heat. Proc R Soc Lond 1905;74(497–506):110–7. https://doi.org/10.1098/rspl.1904.0091.

[110] Temkin MI. Kinetics of ammonia synthesis on promoted iron catalysts. Acta physiochim URSS 1940;12:327–56.

[111] Armenise S, Cazaña F, Monzón A, García-Bordejé E. In situ generation of COx-free H2 by catalytic ammonia decomposition over Ru-Al-monoliths. Fuel 2018;233:851–9. https://doi.org/10.1016/j.fuel.2018.06.129.

[112] Tamaru K. A 'new' general mechanism of ammonia synthesis and decomposition on transition metals. Acc Chem Res 1988;21(2):88–94. https://doi.org/10.1021/ar00146a007.

[113] Papapolymerou GA, Schmidt LD. Unimolecular reactions of nitrogen oxides (NO, N2O, NO2) and ammonia on rhodium and platinum. Langmuir 1985;1(4):488–95. https://doi.org/10.1021/la00064a015.

[114] Papapolymerou G, Bontozoglou V. Decomposition of NH3 on Pd and Ir Comparison with Pt and Rh. J Mol Catal A Chem 1997;120(1):165–71. https://doi.org/10.1016/S1381-1169(96)00428-1.

[115] Itoh N, Oshima A, Suga E, Sato T. Kinetic enhancement of ammonia decomposition as a chemical hydrogen carrier in palladium membrane reactor. Catal Today 2014;236:70–6. https://doi.org/10.1016/j.cattod.2014.02.054.

[116] Armenise S, García-Bordejé E, Valverde JL, Romeo E, Monzón A. A Langmuir–Hinshelwood approach to the kinetic modelling of catalytic ammonia decomposition in an integral reactor. PCCP 2013;15(29):12104–17. https://doi.org/10.1039/C3CP50715G.

[117] Kim S, Song J, Lim H. Conceptual feasibility studies of a COX-free hydrogen production from ammonia decomposition in a membrane reactor for PEM fuel cells. Korean J Chem Eng 2018;35(7):1509–16. https://doi.org/10.1007/s11814-018-0037-5.

[118] Zhang Z, Liguori S, Fuerst TF, Way JD, Wolden CA. Efficient Ammonia Decomposition in a Catalytic Membrane Reactor to Enable Hydrogen Storage and utilization. ACS Sustain Chem Eng 2019;7(6):5975–85. https://doi.org/10.1021/acssuschemeng.8b06065.

[119] Wang B, Kong H, Wang H, Wang Y, Hu X. Kinetic and thermodynamic analyses of mid/low-temperature ammonia decomposition in solar-driven hydrogen permeation membrane reactor. Int J Hydrogen Energy 2019;44(49):26874–87. https://doi.org/10.1016/j.ijhydene.2019.08.175.

[120] Abashar MEE. Ultra-clean hydrogen production by ammonia decomposition. J King Saud Univ – Eng Sci 2018;30(1):2–11. https://doi.org/10.1016/j.jksues.2016.01.002.

[121] Di Carlo A, Vecchione L, Del Prete Z. Ammonia decomposition over commercial Ru/Al2O3 catalyst: an experimental evaluation at different operative pressures and temperatures. Int J Hydrogen Energy 2014;39(2):808–14. https://doi.org/10.1016/j.ijhydene.2013.10.110.

[122] Shlyapin DA, Borisov VA, Temerev VL, Iost KN, Fedorova ZA, Snytnikov PV. Ammonia synthesis and decomposition in the presence of supported ruthenium catalysts. Kinet Catal 2023;64(6):815–25. https://doi.org/10.1134/S0023158423060137.

[123] Brunauer S, Love KS, Keenan RG. Adsorption of nitrogen and the mechanism of ammonia decomposition over iron catalysts. J Am Chem Soc 1942;64(4):751–8. https://doi.org/10.1021/ja01256a005.

[124] Kiełbasa K, Pelka R, Arabczyk W. Studies of the kinetics of ammonia decomposition on promoted nanocrystalline iron using gas phases of different nitriding degree. Chem A Eur J 2010;114(13):4531–4. https://doi.org/10.1021/jp9099286.

[125] Arabczyk W, Zamlynny J. Study of the ammonia decomposition over iron catalysts. Catal Lett 1999;60(3):167–71. https://doi.org/10.1023/A:1019007024041.

[126] Li L, Zhu ZH, Wang SB, Yao XD, Yan ZF. Chromium oxide catalysts for COx-free hydrogen generation via catalytic ammonia decomposition. J Mol Catal A Chem 2009;304(1):71–6. https://doi.org/10.1016/j.molcata.2009.01.026.

[127] Chiuta S, Everson RC, Neomagus HWJP, Le Grange LA, Bessarabov DG. A modelling evaluation of an ammonia-fuelled microchannel reformer for hydrogen generation. Int J Hydrogen Energy 2014;39(22):11390–402. https://doi.org/10.1016/j.ijhydene.2014.05.146.

[128] Dasireddy VDBC, Likozar B. CO*x*-free hydrogen generation *via* decomposition of ammonia over copper and zinc-based catalysts. Fuel 2017;196:325–35. https://doi.org/10.1016/j.fuel.2017.01.117.

[129] Santhana Krishnan P, et al. COx-free hydrogen generation via decomposition of ammonia over al, Ti and Zr−Laponite supported MoS2 catalysts. Int J Hydrogen Energy 2020;45(15):8568–83. https://doi.org/10.1016/j.ijhydene.2020.01.062.

[130] Wu H, et al. Metal-catalyzed hydrolysis of ammonia borane: Mechanism, catalysts, and challenges. Int J Hydrogen Energy 2020;45(55):30325–40. https://doi.org/10.1016/j.ijhydene.2020.08.131.

[131] Liu M, Zhou L, Luo X, Wan C, Xu L. Recent advances in noble metal catalysts for hydrogen production from ammonia borane. Catalysts 2020;10(7):7. https://doi.org/10.3390/catal10070788.

[132] Graham T, et al. Catalytic solvolysis of ammonia borane. Angew Chem Int Ed 2010;49:8708–11. https://doi.org/10.1002/anie.201003074.

[133] Li P-Z, Aijaz A, Xu Q. Highly dispersed surfactant-free nickel nanoparticles and their remarkable catalytic activity in the hydrolysis of ammonia borane for hydrogen generation. Angew Chem Int Ed 2012;51(27):6753–6. https://doi.org/10.1002/anie.201202055.

[134] Coşkuner Filiz B, Kantürk Figen A, Pişkin S. The remarkable role of metal promoters on the catalytic activity of Co-Cu based nanoparticles for boosting hydrogen evolution: ammonia borane hydrolysis. Appl Catal B 2018;238:365–80. https://doi.org/10.1016/j.apcatb.2018.07.031.

[135] Demirci UB. Ammonia borane, a material with exceptional properties for chemical hydrogen storage. Int J Hydrogen Energy 2017;42(15):9978–10013. https://doi.org/10.1016/j.ijhydene.2017.01.154.

[136] Kantürk Figen A, Pişkin MB, Coşkuner B, İmamoğlu V. Synthesis, structural characterization, and hydrolysis of Ammonia Borane (NH3BH3) as a hydrogen storage carrier. Int J Hydrogen Energy 2013;38(36):16215–28. https://doi.org/10.1016/j.ijhydene.2013.10.033.

[137] Basu S, et al. Chemical kinetics of Ru-catalyzed ammonia borane hydrolysis. J Power Sources 2009;188(1):238–43. https://doi.org/10.1016/j.jpowsour.2008.11.085.

[138] Chen W, et al. Reaction mechanism and kinetics for hydrolytic dehydrogenation of ammonia borane on a Pt/CNT catalyst. AIChE J 2017;63(1):60–5. https://doi.org/10.1002/aic.15389.

[139] Gangal AC, Kale P, Edla R, Manna J, Sharma P. Study of kinetics and thermal decomposition of ammonia borane in presence of silicon nanoparticles. Int J Hydrogen Energy 2012;37(8):6741–8. https://doi.org/10.1016/j.ijhydene.2012.01.017.

[140] Gangal AC, Sharma P. Kinetic analysis and modeling of thermal decomposition of ammonia borane. Int J Chem Kinet 2013;45(7):452–61. https://doi.org/10.1002/kin.20781.
[141] Roy B, Hajari A, Kumar V, Manna J, Sharma P. Kinetic model analysis and mechanistic correlation of ammonia borane thermolysis under dynamic heating conditions. Int J Hydrogen Energy 2018;43(22):10386–95. https://doi.org/10.1016/j.ijhydene.2018.04.124.
[142] Kumar V, Roy B, Sharma P. Kinetics of borazine formation from ammonia borane dehydrocoupling reaction through Ab initio analysis. Int J Hydrogen Energy 2019;44(39):22022–31. https://doi.org/10.1016/j.ijhydene.2019.06.172.
[143] Zhang JS, Delgass WN, Fisher TS, Gore JP. Kinetics of Ru-catalyzed sodium borohydride hydrolysis. J Power Sources 2007;164(2):772–81. https://doi.org/10.1016/j.jpowsour.2006.11.002.
[144] Rozinat A, Mans RS, Song M, van der Aalst WMP. Discovering simulation models. Inf Syst 2009;34(3):305–27. https://doi.org/10.1016/j.is.2008.09.002.
[145] Sargent RG. Verification and validation of simulation models. In: Proceedings of the 2010 winter simulation conference; 2010. p. 166–83. https://doi.org/10.1109/WSC.2010.5679166.
[146] Davis ME. Numerical methods and modeling for chemical engineers. Courier Corporation; 2013.
[147] Velten K, Schmidt DM, Kahlen K. Mathematical modeling and simulation: introduction for scientists and engineers. John Wiley & Sons; 2024.
[148] Jourdan N, et al. Compartmental modelling in chemical engineering: a critical review. Chem Eng Sci 2019;210:115196. https://doi.org/10.1016/j.ces.2019.115196.
[149] Bezzo F, Macchietto S, Pantelides CC. A general framework for the integration of computational fluid dynamics and process simulation. Comput Chem Eng 2000;24(2):653–8. https://doi.org/10.1016/S0098-1354(00)00372-0.
[150] Fletcher DF. The future of computational fluid dynamics (CFD) simulation in the chemical process industries. Chem Eng Res Des 2022;187:299–305. https://doi.org/10.1016/j.cherd.2022.09.021.
[151] Rodríguez J, Amores E. CFD modeling and experimental validation of an alkaline water electrolysis cell for hydrogen production. Processes 2020;8(12). https://doi.org/10.3390/pr8121634.
[152] Fox RO. CFD Models for analysis and design of chemical reactors. In: Marin GB, editor. Advances in Chemical Engineering, vol. 31. Academic Press; 2006. p. 231–305. https://doi.org/10.1016/S0065-2377(06)31004-6.
[153] Ao R, Lu R, Leng G, Zhu Y, Yan F, Yu Q. A review on numerical simulation of hydrogen production from ammonia decomposition. Energies 2023;16(2). https://doi.org/10.3390/en16020921.
[154] Bates PD, Lane SN, Ferguson RI. Computational fluid dynamics: applications in environmental hydraulics. John Wiley & Sons; 2005.
[155] Jeong W, Seong J. Comparison of effects on technical variances of computational fluid dynamics (CFD) software based on finite element and finite volume methods. Int J Mech Sci 2014;78:19–26. https://doi.org/10.1016/j.ijmecsci.2013.10.017.
[156] Huebner KH, Dewhirst DL, Smith DE, Byrom TG. The finite element method for engineers. John Wiley & Sons; 2001.
[157] Moukalled F, Mangani L, Darwish M. The finite volume method. In: Moukalled F, Mangani L, Darwish M, Eds. The finite volume method in computational fluid dynamics: an advanced introduction with OpenFOAM® and Matlab, Cham: Springer International Publishing; 2016, p. 103–35. doi: 10.1007/978-3-319-16874-6_5.
[158] Poole G, Liu Y-C, Mandel J. Advancing analysis capabilities in ANSYS through solver technology. Electron Trans Numer Anal 2003;15:106–21.
[159] Pryor RW. Multiphysics modeling using COMSOL®: a first principles approach. Jones & Bartlett Publishers; 2009.
[160] Habashi W, Dompierre J, Bourgault Y, Fortin M, Vallet M-G. Certifiable computational fluid dynamics through mesh optimization. AIAA J 1998;36(5):703–11.
[161] Zawawi MH, et al. A review: fundamentals of computational fluid dynamics (CFD). AIP Conf Proc 2018;2030(1):020252. https://doi.org/10.1063/1.5066893.
[162] Lintermann A. Computational meshing for CFD simulations. In: Inthavong K, Singh N, Wong E, Tu J, editors. Clinical and biomedical engineering in the human nose: a computational fluid dynamics approach. Singapore: Springer Singapore; 2021. p. 85–115. https://doi.org/10.1007/978-981-15-6716-2_6.
[163] Massoudi M. Boundary conditions in mixture theory and in CFD applications of higher order models. Comput Math Appl 2007;53(2):156–67. https://doi.org/10.1016/j.camwa.2006.02.016.
[164] Wang R, et al. A review on slip boundary conditions at the nanoscale: recent development and applications. Beilstein J Nanotechnol 2021;12:1237–51. https://doi.org/10.3762/bjnano.12.91.
[165] Lockerby DA, Reese JM, Emerson DR, Barber RW. Velocity boundary condition at solid walls in rarefied gas calculations. Phys Rev E—Statist Nonlinear Soft Matter Phys 2004;70(1):017303.
[166] Hafeez S, Aristodemou E, Manos G, Al-Salem SM, Constantinou A. Modelling of packed bed and coated wall microreactors for methanol steam reforming for hydrogen production. RSC Adv 2020;10(68):41680–92.
[167] Harkou E, et al. Different reactor configurations for enhancement of CO2 methanation. Environ Res 2023;236:116760. https://doi.org/10.1016/j.envres.2023.116760.
[168] Bravo J, Karim A, Conant T, Lopez GP, Datye A. Wall coating of a CuO/ZnO/Al2O3 methanol steam reforming catalyst for micro-channel reformers. Chem Eng J 2004;101(1):113–21. https://doi.org/10.1016/j.cej.2004.01.011.
[169] Hu G, Li T, Long J, Du W, Qian F. Numerical simulation of the gas–solid two-phase flow-reaction process in a maximizing Isoparaffin process reactor. ACS Omega 2020;5(45):29043–54. https://doi.org/10.1021/acsomega.0c03525.
[170] Parekh J, Rzehak R. Euler–Euler multiphase CFD-simulation with full Reynolds stress model and anisotropic bubble-induced turbulence. Int J Multiph Flow 2018;99:231–45. https://doi.org/10.1016/j.ijmultiphaseflow.2017.10.012.
[171] Zhao L, Lu Y. Hydrogen production by biomass gasification in a supercritical water fluidized bed reactor: a CFD-DEM study. J Supercrit Fluids 2018;131:26–36. https://doi.org/10.1016/j.supflu.2017.07.022.
[172] Li L, Li X, Zhu Z, Li B. Numerical modeling of multiphase flow in gas stirred ladles: from a multiscale point of view. Powder Technol 2020;373:14–25. https://doi.org/10.1016/j.powtec.2020.06.028.
[173] Murer M, Formica G, Milicchio F, Morganti S, Auricchio F. A coupled multiphase Lagrangian-Eulerian fluid-dynamics framework for numerical simulation of Laser Metal Deposition process. Int J Adv Manuf Technol 2022;120(5):3269–86. https://doi.org/10.1007/s00170-022-08763-7.
[174] Winterbottom JM, King M. Reactor design for chemical engineers. CRC Press; 1999.
[175] Ansoni JL, Seleghim P. Optimal industrial reactor design: development of a multiobjective optimization method based on a posteriori performance parameters calculated from CFD flow solutions. Adv Eng Softw 2016;91:23–35. https://doi.org/10.1016/j.advengsoft.2015.08.008.
[176] Khan MJH, Hussain MA, Mansourpour Z, Mostoufi N, Ghasem NM, Abdullah EC. CFD simulation of fluidized bed reactors for polyolefin production – a review. J Ind Eng Chem 2014;20(6):3919–46. https://doi.org/10.1016/j.jiec.2014.01.044.
[177] Wu B. Advances in the use of CFD to characterize, design and optimize bioenergy systems. Comput Electron Agric 2013;93:195–208. https://doi.org/10.1016/j.compag.2012.05.008.
[178] Egedy A, Kummer A, Leveneur S, Varga T, Chován T. Cfd modeling of spatial inhomogeneities in a vegetable oil carbonation reactor. Processes 2020;8(11):1356.
[179] Mertsoy EY. Comparison of 2D and 3D numerical simulation of woody biomass combustion in fluidized bed reactor. Biomass Convers Biorefin 2025:1–20.
[180] Versteeg HK. An introduction to computational fluid dynamics the finite volume method, 2/E. Pearson Education India; 2007.
[181] Zhang J, Smith R. Design and optimisation of batch and semi-batch reactors. Chem Eng Sci 2004;59(2):459–78. https://doi.org/10.1016/j.ces.2003.10.004.
[182] Rosa L, Pederiva L, Maurina G, Beal L, Torres A, Sousa M. CFD Analysis of the effect of baffle plates on the fluid flow in an anaerobic sequencing batch reactor. Chem Eng Trans 2014;38:133–8. https://doi.org/10.3303/CET1438023.
[183] Niño-Navarro C, Chairez I, Torres-Bustillos L, Ramírez-Muñoz J, Salgado-Manjarrez E, Garcia-Peña EI. Effects of fluid dynamics on enhanced biohydrogen production in a pilot stirred tank reactor: CFD simulation and experimental studies. Int J Hydrogen Energy 2016;41(33):14630–40. https://doi.org/10.1016/j.ijhydene.2016.06.236.
[184] Maluta F, Paglianti A, Montante G. Modelling of biohydrogen production in stirred fermenters by Computational Fluid Dynamics. Process Saf Environ Prot 2019;125:342–57. https://doi.org/10.1016/j.psep.2018.09.020.
[185] Lefebvre J, Bajohr S, Kolb T. Modeling of the transient behavior of a slurry bubble column reactor for CO2 methanation, and comparison with a tube bundle reactor. Renew Energy 2020;151:118–36. https://doi.org/10.1016/j.renene.2019.11.008.
[186] Lašič Jurković D, Liu J-L, Pohar A, Likozar B. Methane dry reforming over Ni/Al2O3 catalyst in spark plasma reactor: linking computational fluid dynamics (CFD) with reaction kinetic modelling. Catal Today 2021;362:11–21. https://doi.org/10.1016/j.cattod.2020.05.028.
[187] Adamou P, et al. Hydrous hydrazine decomposition over Rh/Al2O3 catalyst: Experimental and CFD studies. Chem Eng J 2024;493:152715. https://doi.org/10.1016/j.cej.2024.152715.
[188] Patwardhan AW, Joshi JB, Fotedar S, Mathew T. Optimization of gas–liquid reactor using computational fluid dynamics. Chem Eng Sci 2005;60(11):3081–9. https://doi.org/10.1016/j.ces.2004.12.034.
[189] Ding J, Wang X, Zhou X-F, Ren N-Q, Guo W-Q. CFD optimization of continuous stirred-tank (CSTR) reactor for biohydrogen production. Bioresour Technol 2010;101(18):7005–13. https://doi.org/10.1016/j.biortech.2010.03.146.
[190] Ri P-C, Ren N-Q, Ding J, Kim J-S, Guo W-Q. CFD optimization of horizontal continuous stirred-tank (HCSTR) reactor for bio-hydrogen production. Int J Hydrogen Energy 2017;42(15):9630–40. https://doi.org/10.1016/j.ijhydene.2017.02.035.
[191] Brindhadevi K, Shanmuganathan R, Pugazhendhi A, Gunasekar P, Manigandan S. Biohydrogen production using horizontal and vertical continuous stirred tank reactor- a numerical optimization. Int J Hydrogen Energy 2021;46(20):11305–12. https://doi.org/10.1016/j.ijhydene.2020.06.155.
[192] Andrigo P, Bagatin R, Pagani G. Fixed bed reactors. Catal Today 1999;52(2):197–221. https://doi.org/10.1016/S0920-5861(99)00076-0.
[193] Dixon AG, Nijemeisland M. CFD as a design tool for fixed-bed reactors. Ind Eng Chem Res 2001;40(23):5246–54. https://doi.org/10.1021/ie001035a.
[194] Darfilal D. Solar hydrogen production by thermochemical reaction: development of a packed-bed reactor. J Therm Eng 2020;6(2):2. https://doi.org/10.18186/thermal.729318.
[195] Wodołażski A, Smoliński A. Bio-hydrogen production in packed bed continuous plug flow reactor—CFD-multiphase modelling. Processes 2022;10(10):10. https://doi.org/10.3390/pr10101907.
[196] Nailwal BC, et al. Ammonia decomposition for hydrogen production using packed bed catalytic membrane reactor. Int J Hydrogen Energy 2024;49:1272–87. https://doi.org/10.1016/j.ijhydene.2023.09.229.

[197] Warnecke R. Gasification of biomass: comparison of fixed bed and fluidized bed gasifier. Biomass Bioenergy 2000;18(6):489–97. https://doi.org/10.1016/S0961-9534(00)00009-X.
[198] Panneerselvam R, Savithri S, Surender GD. CFD simulation of hydrodynamics of gas–liquid–solid fluidised bed reactor. Chem Eng Sci 2009;64(6):1119–35. https://doi.org/10.1016/j.ces.2008.10.052.
[199] Liu H, Cattolica RJ, Seiser R. CFD studies on biomass gasification in a pilot-scale dual fluidized-bed system. Int J Hydrogen Energy 2016;41(28):11974–89. https://doi.org/10.1016/j.ijhydene.2016.04.205.
[200] Foresti S, Di Marcoberardino G, Manzolini G, De Nooijer N, Gallucci F, van Sint Annaland M. A comprehensive model of a fluidized bed membrane reactor for small-scale hydrogen production. Chem Eng Process - Process Intesif 2018;127:136–44. https://doi.org/10.1016/j.cep.2018.01.018.
[201] Phuakpunk K, Chalermsinsuwan B, Putivisutisak S, Assabumrungrat S. Parametric study of hydrogen production via sorption enhanced steam methane reforming in a circulating fluidized bed riser. Chem Eng Sci 2018;192:1041–57. https://doi.org/10.1016/j.ces.2018.08.042.
[202] Yu H, Sun H, Bao G, Liu H, Hu J, Wang H. Computational fluid dynamics study of hydrogen production by sorption enhanced steam ethanol reforming process in fluidized bed. Fuel 2023;344:128043. https://doi.org/10.1016/j.fuel.2023.128043.
[203] Yao X, Zhang Y, Du L, Liu J, Yao J. Review of the applications of microreactors. Renew Sustain Energy Rev 2015;47:519–39. https://doi.org/10.1016/j.rser.2015.03.078.
[204] Zhendong L, Yangcheng L, Jiawei W, Guangsheng L. Mixing characterization and scaling-up analysis of asymmetrical T-shaped micromixer: Experiment and CFD simulation. Chem Eng J 2012;181–182:597–606. https://doi.org/10.1016/j.cej.2011.11.105.
[205] An H, Li A, Sasmito AP, Kurnia JC, Jangam SV, Mujumdar AS. Computational fluid dynamics (CFD) analysis of micro-reactor performance: effect of various configurations. Chem Eng Sci 2012;75:85–95. https://doi.org/10.1016/j.ces.2012.03.004.
[206] Bond TG, Noguchi BA, Chou C-P, Mongia RK, Chen J-Y, Dibble RW. Catalytic oxidation of natural gas over supported platinum: Flow reactor experiments and detailed numberical modeling. Symp (Int) Combust 1996;26(1):1771–8. https://doi.org/10.1016/S0082-0784(96)80403-6.
[207] Canu P. Simulation and interpretation of catalytic combustion experimental data. Catal Today 2001;64(3):239–52. https://doi.org/10.1016/S0920-5861(00)00528-9.
[208] Harkou E, Hafeez S, Manos G, Constantinou A. CFD study of the numbering up of membrane microreactors for CO2 capture. Processes 2021;9(9):9. https://doi.org/10.3390/pr9091515.
[209] Hafeez S, et al. Decomposition of additive-free formic acid using a Pd/C catalyst in flow: experimental and CFD modelling studies. Catalysts 2021;11(3):3. https://doi.org/10.3390/catal11030341.
[210] Hafeez S, et al. Computational investigation of microreactor configurations for hydrogen production from formic acid decomposition using a Pd/C catalyst. Ind Eng Chem Res 2022;61(4):1655–65.
[211] Harkou E, et al. Computational studies on microreactors for the decomposition of formic acid for hydrogen production using heterogeneous catalysts. Molecules 2023;28(14):14. https://doi.org/10.3390/molecules28145399.
[212] Fu J, et al. Process simulation of methanol production via carbon dioxide hydrogenation. Case Stud Therm Eng 2024;54:103975.
[213] Soto V, Ulloa C, Garcia X. A CFD design approach for industrial size tubular reactors for SNG production from biogas (CO2 Methanation). Energies 2021;14(19):6175.
[214] Gruber M, et al. Power-to-Gas through thermal integration of high-temperature steam electrolysis and carbon dioxide methanation-Experimental results. Fuel Process Technol 2018;181:61–74.
[215] Zhang W, Machida H, Takano H, Izumiya K, Norinaga K. Computational fluid dynamics simulation of CO2 methanation in a shell-and-tube reactor with multi-region conjugate heat transfer. Chem Eng Sci 2020;211:115276.
[216] Tsiotsias AI, et al. Enhancing CO2 methanation over Ni catalysts supported on sol-gel derived Pr2O3-CeO2: an experimental and theoretical investigation. Appl Catal B 2022;318:121836.
[217] Pavlišič A, Huš M, Prašnikar A, Likozar B. Multiscale modelling of CO2 reduction to methanol over industrial Cu/ZnO/Al2O3 heterogeneous catalyst: linking ab initio surface reaction kinetics with reactor fluid dynamics. J Clean Prod 2020;275:122958. https://doi.org/10.1016/j.jclepro.2020.122958.
[218] Di Nardo A, Calchetti G, Bassano C, Deiana P. CO2 methanation in a shell and tube reactor CFD simulations: high temperatures mitigation analysis. Chem Eng Sci 2021;246:116871.
[219] Jamshidi S, Sedaghat MH, Amini A, Rahimpour MR. CFD simulation and sensitivity analysis of an industrial packed bed methanol synthesis reactor. Chem Eng Process-Proce Intensif 2023;183:109244.
[220] Hafeez S, et al. Formic acid decomposition using palladium-zinc preformed colloidal nanoparticles supported on carbon nanofibre in batch and continuous flow reactors: experimental and computational fluid dynamics modelling studies. Nanomaterials 2023;13(23):2993.
[221] Liu Y, Hinrichsen O. CFD simulation of hydrodynamics and methanation reactions in a fluidized-bed reactor for the production of synthetic natural gas. Ind Eng Chem Res 2014;53(22):9348–56.
[222] Wang Y, et al. Boosting CO2 hydrogenation of Fe-based monolithic catalysts via 3D printing technology-induced heat/mass-transfer enhancements. Appl Catal B 2024;340:123211.
[223] Maleki H, Fulton M, Bertola V. Kinetic assessment of H2 production from NH3 decomposition over CoCeAlO catalyst in a microreactor: Experiments and CFD modelling. Chem Eng J 2021;411:128595.
[224] Chiuta S, Everson RC, Neomagus HW, Bessarabov DG. Hydrogen production from ammonia decomposition over a commercial Ru/Al2O3 catalyst in a microchannel reactor: Experimental validation and CFD simulation. Int J Hydrogen Energy 2016;41(6):3774–85.
[225] Ojelade OA. CO2 hydrogenation to gasoline and aromatics: mechanistic and predictive insights from DFT, DRIFTS and machine learning. ChemPlusChem 2023;88(9):e202300301. https://doi.org/10.1002/cplu.202300301.
[226] Miyazaki R, Belthle KS, Tuysuz H, Foppa L, Scheffler M. Materials genes of CO2 hydrogenation on supported cobalt catalysts: an artificial intelligence approach integrating theoretical and experimental data. J Am Chem Soc 2024;146(8):5433–44.